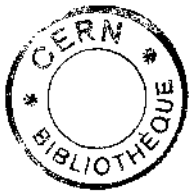

EUROPEAN ORGANIZATION FOR NUCLEAR RESEARCH

CERN-EP/89-72
LBL 26014
DPhPE 88-12
6 June 1989

THE NUMBER OF NEUTRINO SPECIES

D. Denegri, CERN, Geneva, Switzerland
and DPHPE, CEN–Saclay, Gif-sur-Yvette, France

B. Sadoulet, Center for Particle Astrophysics, Department of Physics and
Lawrence Berkeley Laboratory, University of California, Berkeley, USA

M. Spiro, DPhPE, CEN–Saclay, Gif-sur-Yvette, France

ABSTRACT

We discuss the methods used to determine the number of neutrino species N_ν, or an upper limit on this number, within the framework of the Standard Model. The astrophysical limit based on the neutrino burst from SN1987A is discussed first. Next we proceed with the discussion of the cosmological constraint based on the observed He/H abundance ratio. Finally, we discuss the particle physics methods based on single-photon production in e^+e^- collisions, on the production of monojets in $p\bar{p}$ collisions, and on the determination of N_ν from the ratio of the $W \to \ell\bar{\nu}$ to $Z \to \ell\bar{\ell}$ partial cross-sections in $p\bar{p}$ collisions. The various sources of uncertainty and the experimental backgrounds are presented, as well as an idea of what may be expected on this subject in the future. There is remarkable agreement between the various methods, with central values for N_ν between 2 and 3 and with upper limits $N_\nu < 6$. The consistency between the laboratory determinations of N_ν and those from the supernova SN1987A or cosmology represents an astounding success for the Standard Model and for the current description of stellar collapse and of the Big Bang primordial nucleosynthesis. Combining all determinations, we obtain a central value $N_\nu = 2.1^{+0.6}_{-0.4}$ for $m_t = 50$ GeV and $N_\nu = 2.0^{+0.6}_{-0.4}$ if $m_t \geq m_W$. At present, $N_\nu = 3$ is perfectly compatible with all data. Although the consistency is significantly worse, four families still provide a reasonable fit. In the framework of the Standard Model, a fifth light neutrino is, however, unlikely.

(Submitted to Rev. Mod. Phys.)

1. INTRODUCTION

With the discovery of the W and Z bosons at the CERN Super Proton Synchrotron (SPS) Collider (Arnison et al., 1983a,b,c,d; Banner et al., 1983; Bagnaia et al., 1983) and the measurements of their properties, production rates, and decay features, the SU(3) × SU(2) × U(1) Standard Model of electroweak and strong interactions is on a firm footing. The model, however, does not predict the number of fermion generations or their masses.

The quarks and leptons observed so far can be organized into three families (or generations) of weak isodoublets (for left-handed states), as follows:

u	c	t	
			quark doublets
d′	s′	b′	
ν_e	ν_μ	ν_τ	
			lepton doublets
e	μ	τ	

Each leptonic doublet contains a distinct type of neutrino, labelled ν_e, ν_μ, and ν_τ. One of the basic questions is, Are there more families than the three observed so far? In view of the regularity prevailing in the first three generations, counting the number of neutrino types may also mean counting the number of fundamental fermion generations.

Until now, the direct detection of neutrinos has been achieved only for the neutrinos ν_e and ν_μ. The third generation ν_τ has not yet been detected directly through its characteristic interactions with matter. The evidence for ν_τ as an independent species, with the same (universal) Fermi coupling to its third-generation charged-lepton partner τ as is the case for the two lighter generations, is indirect . It is obtained from the τ lifetime (Hitlin, 1987; Braunschweig et al., 1988), or from the tests of e–μ–τ universality based on the W partial production cross-section ratios $\sigma(W \to e\nu)/\sigma(W \to \mu\nu)/\sigma(W \to \tau\nu)$ measured at the SPS Collider by the UA1 Collaboration (Albajar et al., 1987a). Whilst the τ lifetime tests the hypothesis of universality of weak charged currents at a low $Q^2 \leq m_\tau^2$, the Collider results test it at $Q^2 \approx m_W^2$.

Information on the number of light neutrino species N_ν (or an upper limit on N_ν) can be obtained from various fields: astrophysics, cosmology, and particle physics. It should be noted that particle physics' limits apply to a much wider range of neutrino masses ($m_\nu < m_Z/2$) than the limits from astrophysics and cosmology, which apply to neutrinos lighter than a few MeV. However, we will show that the limits are comparable, demonstrating an astounding consistency of our current understanding of diverse phenomena. [For a brief discussion, see Cline et al. (1987).]

The astrophysical and cosmological methods rely on the equipartition of energy between the relativistic degrees of freedom at temperatures of a few MeV at stellar-collapse time or primordial-nucleosynthesis time, respectively. Thermal equilibrium is established through weak neutral-current interactions of the type $e^+e^- \leftrightarrow Z \leftrightarrow \nu_i\,\bar{\nu}_i$. The astrophysical limit on N_ν is based on the observation of antineutrinos emitted by the supernova SN1987A, and is obtained by comparison with the expected neutron-star binding energy (Ellis and Olive, 1987; Schaeffer et al., 1987; Krauss, 1987). This astrophysical limit is discussed in Section 2. The cosmological results are based on the

comparison of the observed cosmological He/H abundance ratio with Big Bang Model calculations (Steigman et al., 1986; Ellis et al., 1986). The cosmological upper limit on N_ν is discussed in detail in Section 3. The laboratory particle physics results from e^+e^- and $p\bar{p}$ colliders are based on the fact that, in the Standard Model, all neutrino species ν_i are universally coupled to the Z boson. Each neutrino species contributes to the Z total width Γ^Z_{tot} with a partial rate $\delta\Gamma^Z = \Gamma^Z_{\nu\bar{\nu}}$ which is given by

$$\Gamma^Z_{\nu\bar{\nu}} = \frac{G_F}{12\pi\sqrt{2}} \; m_Z^3 \; ,$$

where G_F is the Fermi constant and m_Z is the Z mass. For m_Z = 91.9 GeV, which is obtained from the Standard Model prediction $m_Z = (38.68 \pm 0.03 \text{ GeV})/\sin\theta_w \cos\theta_w$ [including electroweak radiative corrections (Marciano, 1987)] and the latest world average for $\sin^2\theta_w = 0.230 \pm 0.005$ (Amaldi et al., 1986; Costa et al., 1988), this partial width amounts to $\approx$ 170 MeV. The above expression is valid for neutrino masses $m_\nu \ll m_Z/2$. The various particle physics methods employed to obtain N_ν all amount to either an (indirect) measurement of the Z total width, or a measurement of the partial width corresponding to the sum over all neutrino species $\Sigma\Gamma^Z_{\nu\bar{\nu}}$. More generally, these results can be interpreted as a limit on the Z partial decay rate into non-interacting particles, as for example, $Z \to \tilde{\nu}\bar{\tilde{\nu}}$. The most significant accelerator experiment limits or values for N_ν, obtained until now, are from searches for $e^+e^- \to \gamma + Z \to \gamma\nu\bar{\nu}$ (Z off-shell) at PEP and PETRA (Ford et al., 1986; Hearty et al., 1987; Behrend et al., 1988), from results on $p\bar{p} \to Z (\to \nu_i\bar{\nu}_i)$ + jet (Z on-shell) (Albajar et al., 1987b), and from the measured ratio of partial W to Z production rates $\sigma(W \to \ell\bar{\nu})/\sigma(Z \to \ell\bar{\ell})$ from the CERN $p\bar{p}$ Collider (Albajar et al., 1987d; Ansari et al., 1987a; Colas et al., 1988). In Sections 4, 5, and 6 we discuss each of these results in turn.

In Section 7 we conclude with an overview of the various results on N_ν.

2. NUMBER OF NEUTRINO SPECIES FROM SUPERNOVA SN1987A

On 23 February 1987, the optical and the neutrino flashes resulting from the ultimate collapse of a star (SN1987A) were detected by astronomers and elementary particle physicists. A supernova exploded in the Large Magellanic Cloud (LMC), which is 154,000 $\pm$ 10,000 light years away. This is the first supernova ever detected through neutrinos. The most significant numbers of detected neutrino events, almost free of background, appeared in two large water-Cherenkov detectors, one at the Kamioka Mine nucleon decay experiment (Kamiokande) and the other at the Irvine-Michigan-Brookhaven (IMB) experiment, which were initially designed for proton lifetime measurements. A less significant signal has also been detected with scintillator detectors at Baksan and possibly in the Mont Blanc tunnel, although not at the same time in the latter case.

These events, as discussed below, were most likely due to $\bar{\nu}_e$ interactions on protons:

$$\bar{\nu}_e + p \to n + e^+ \; .$$

Figure 1 shows the spike (< 13 s) of events, which is the time signature of the burst in Kamiokande (Hirata et al., 1987). Tables 1a and 1b give the information collected on the 11 events detected by Kamiokande and the 8 events detected by the IMB experiment (Bionta et al., 1987).

Figures 2a and 2b show the time sequence and the energy spectrum of events. Most of the events are concentrated in the first few seconds. This is precisely what is expected for a stellar collapse. The proximity in time to the visual observation of SN1987A, the difficulty in finding an alternative interpretation of the short burst of events in the observed low-energy range, and the approximate time coincidence for observations in several detectors, make it most plausible to attribute these events to neutrinos originating in a stellar collapse. In the following we show how the number of species of neutrinos N_ν can be derived from this information. First we will briefly discuss the mechanism leading to stellar collapse.

2.1 Star evolution until collapse

A supernova explosion corresponds to the ultimate phase of stellar evolution. A massive star ($> 8\,M_\odot$) evolves with time following the now well-known scenario.

i) At the beginning, a cloud of gas (mostly hydrogen) contracts under gravitation and radiation losses (infrared protostar stage). The central temperature increases until the onset of thermonuclear fusion, where ultimately four hydrogen nuclei fuse into helium:

$$4p + 2e^- \rightarrow {}^4He + 2\nu_e \ .$$

ii) The star reaches a steady state (main sequence phase) when the heat produced by the thermonuclear fusion of hydrogen in the centre of the star compensates for the radiation losses at the surface. At the centre, a ^4He core gradually develops. Higher Z elements cannot yet be synthetized owing to Coulomb barriers which cannot yet be overcome.

iii) The ^4He core becomes more massive while the thermonuclear reactions with ^4He are not yet effective in the core, and at a certain moment the He core can no longer sustain the gravitational implosive pressure. This is the first collapse, which takes place less than 10^8 years after the formation of the star, for stars more massive than $8\,M_\odot$. The temperature of the collapsing He core increases abruptly, allowing the onset of ^4He burning into C nuclei.

iv) The He burning lasts for less than 10^6 years. Subsequent collapses will then take place, allowing C, N, O, ... and ultimately Si burning, giving an onion-shell structure to the star. As Fe is the nucleus with the highest binding energy, this sequence of fusion reactions must end with the development of an iron core at the centre of the star. This growing iron core is responsible for the inevitable ultimate collapse of the star. Since all fusion reactions of Fe are endothermic, there are no more thermonuclear reactions with Fe that could provide energy to resist the collapse. The final collapse will then give birth to a new state of matter, either a neutron star or a black hole.

2.2 Ultimate collapse of the iron core

The iron core collapses when the degenerate electron-gas pressure cannot sustain the gravitational pressure any longer, that is, when its mass reaches the Chandrasekhar limit. Let us recall the basic mechanism.

The density of the iron core before collapse is $\varrho \approx 4 \times 10^9$ g/cm^3, and the radius is $R \approx 500$ km. The gas is an almost relativistic gas of degenerate Fermi-Dirac electrons (the pressure is

dominated by the degeneracy, and the Fermi energy is greater than 1 MeV). The pressure p is not temperature-dependent: $p = K \varrho^{\gamma}$, with $\gamma = 5/3$ for a non-relativistic, degenerate gas, whilst $\gamma = 4/3$ for a relativistic, degenerate one. The restoring forces are respectively $F = dp/dR = K M^{5/3}/R^6$ and $F = dp/dR = K M^{4/3}/R^5$. In the iron core, we then have $\gamma = 4/3 + \epsilon/3$, with $0 < \epsilon \ll 1$, whilst the implosive force from gravitation is $F \approx G_N M^2/R^5$ ($F \approx G_N \varrho M/R^2$, with $\varrho \approx M/R^3$) where G_N is the gravitational constant, and M and R are the mass and radius of the iron core.

In the non-relativistic case, the restoring force due to pressure, and the gravitational force, have a different power-law variation with radius. Thus the star can adjust its radius to bring the two forces into equilibrium. In the relativistic case, however, the two forces depend on the same power of the radius, but not on the same power of the mass. Hence, there exists a limiting mass, the Chandrasekhar mass M_{Ch} for which the two forces balance. It can be shown that $M_{Ch} = 5.7 \times Y_e^2$ $M_\odot \approx 1.3\ M_\odot$ (Hillebrandt, 1987), where $Y_e = e/(n+p)$ is the ratio of number densities for electrons and nucleons. For masses M smaller than M_{Ch}, the star expands until the density decreases enough for the outer parts to become non-relativistic and to reach the equilibrium. If M is larger than M_{Ch}, the gravitational force exceeds the pressure force and the radius decreases. The collapse then begins. As the density and temperature increase, a new phenomenon takes place—electron capture by nuclei:

$$Fe + e^- \rightarrow Co + \nu_e; \text{ more generally: } p + e^- \rightarrow n + \nu_e\ .$$

The electron pressure now decreases very suddenly with increasing density. The star collapses in almost free fall until the core reaches a new state of matter. This is associated with the type II supernova explosion, with a shock wave and neutrino emission (see, for instance, Weaver and Woosley, 1980; Burrows, 1987).

2.3 Energy released by the ultimate collapse of a star

2.3.1 Neutron star final state

Below 8 $M_\odot$, the above mechanism does not occur because the star never develops a massive enough iron core.

For stars with a mass between 8 $M_\odot$ and 50 $M_\odot$, the predictions are that about 1.4 $M_\odot$ of iron collapses to form a neutron star (all electrons and protons have combined to give neutrons and escaping neutrinos), of roughly the same mass. However, owing to possible rotation, convection, or accretion, the predictions of the mass ranges involved extend from 1.2 to 1.8 $M_\odot$.

The density, temperature, and the radius of neutron stars can be predicted from the equation of state of nuclear matter. Various computations have been made (Pandharipande, 1971; Malone et al., 1975). They all converge towards nearly the same values: $\varrho \approx 3 \times 10^{14}$ g/cm^3, $T \approx 10$ MeV, and $R \approx 10$ km. The energy that is expected to be released in the collapse is directly related to the difference of gravitational binding energies between the initial and final states:

$$\Delta E \approx G_N M^2 \left(\frac{1}{R_{\text{neutron star}}} - \frac{1}{R_{\text{iron core}}} \right) \approx \frac{G_N M^2}{R_{\text{neutron star}}}\ .$$

The predicted values extend from 1.5×10^{53} to 4×10^{53} erg for masses varying from 1.2 $M_\odot$ to 1.8 $M_\odot$ and the acceptable equations of state.

The masses of a few neutron stars—members of binary systems—have been measured experimentally. The results are shown in Fig. 3 (Trimble, 1987). The range of observed masses is indeed in agreement with theoretical expectations.

Supporting evidence for this picture is also provided by the gravitational red shift. The surface gravitational red shift is proportional to $G_N M/R$ and is predicted to be 0.25 ± 0.1; this is in good agreement with available experimental measurements (Schaeffer et al., 1987; Fujimoto et al., 1986). By measuring the rate at which the rotation of a neutron star slows down, and from the total radiated energy, one can also derive the moment of inertia of such an object. This has been done for the remnant neutron star of the Crab nebula and the result agrees fairly well with expectations (Schaeffer, 1984).

In conclusion, therefore, all available experimental data agree with the expectations from this neutron star formation scenario.

2.3.2 Black hole formation

For very massive stars (> 50 $M_\odot$), one expects the collapse to end with the formation of a black hole. Would this mean an energy release much superior to the one resulting from neutron star formation? From computations given in Woosley et al. (1986), this does not seem to be the case, unless we are dealing with ultramassive stars (> 150 $M_\odot$). In the 50 to 150 $M_\odot$ range, however, the energy released is expected to be in the range 3 to 4×10^{53} erg. Above 150 $M_\odot$, there is a dramatic increase. Such a possibility of a 150 $M_\odot$ progenitor—which from general arguments is very unlikely—has been excluded for SN1987A, from the type of progenitor, from the analysis of the light curve, and from the neutrino pulse duration (Woosley, 1987; Burrows, 1987; Mayle and Wilson, 1987).

In conclusion, the total energy release in the ultimate collapse of a star of 8 to 150 $M_\odot$ (!) ranges from 1.5 to 4×10^{53} erg.

2.4 Neutrino emission

This gravitational energy release is considerably larger than the more easily measurable energy released in the form of electromagnetic radiation and as kinetic energy in the expelled layers of matter (10^{50} to 10^{51} erg), and larger than the energy carried away by neutrinos during the initial neutronization phase $p + e^- \rightarrow n + \nu_e$. For a 1.5 $M_\odot$ neutron star, for example, neutronization is expected to take place within the first 100 ms of the collapse, and to release $\sim 10^{52}$ erg in the form of ν_e's of $\sim$ 8 MeV average energy (Burrows, 1987). This is still an order of magnitude smaller than the neutron-star binding energy ΔE.

Most of this energy is expected to be evacuated in few seconds (80% in the first 10 s according to Burrows, 1984) in the form of neutrinos and antineutrinos of all species, maintained in thermal equilibrium (equipartition of energy) through neutral-current interactions $e^+e^- \leftrightarrow \nu_i \bar{\nu}_i$ at temperatures of $\sim$ 3 to 6 MeV (the average energy of neutrinos is $\approx$ 3.15 times the temperature for a Fermi–Dirac gas, and is thus in the 10 to 15 MeV range). These are the surface temperatures for neutrinos escaping from the neutrinosphere, and they are expected to be smaller than the 20–70 MeV

central temperature. The temperatures of ν_μ and ν_τ are expected to be slightly larger than those of $\bar{\nu}_e$ and ν_e, as the latter ones can interact through charged currents in addition to neutral currents, and are thus more efficiently cooled by outer core layers. However, the energy fluxes, which depend on both the temperatures and the radii of the neutrinospheres, are the same for all neutrinos owing to the equipartition principle. All species of neutrinos means here species for which the mass is much smaller than the temperature, i.e. less than of the order of 1 MeV.

2.5 Energy release in the case of SN1987A

The progenitor, which has been finally identified as Sanduleak-69202 (after some hesitation), is a blue star.

The analysis of the light curves (Woosley, 1987) is consistent with the explosion of a star which, on the main sequence, had a mass of $19 \pm 3\ M_\odot$, and which according to Burrows (1987) and Mayle and Wilson (1987) would give birth to a $1.45 \pm 0.1\ M_\odot$ neutron star.

Furthermore, the integrated time distribution of the detected neutrino events shown in Fig. 4 is in excellent agreement with the predictions (Burrows, 1984, 1987) for a $1.4\ M_\odot$ neutron star formation and is in disagreement with black hole formation ($> 1.8\ M_\odot$). The total length of the pulse is $\sim$ 13 s. Black hole formation would lead to much shorter pulses (< 2 s) in Fig. 4, since only the prompt neutrino signal would be seen.

In conclusion, the range for the total gravitational energy release ΔE, consistent with all observations until now, is: $\Delta E = (1.5\text{–}3.5) \times 10^{53}$ erg. This range does not cover all possible published values, but there seems to be a consensus among nuclear astrophysicists that it indeed covers all 'reasonable models' without exotic equations of state (Schaeffer et al., 1987). As explained in the Appendix, we will assume that this range represents a $\pm 2\sigma$ interval, and in the subsequent fit we will take $\Delta E = (2.5 \pm 0.5) \times 10^{53}$ erg.

2.6 Energy carried by $\bar{\nu}_e$'s and the number of neutrino families

2.6.1 Neutrino detection

The Kamiokande and IMB detectors are sensitive to electrons and positrons through Cherenkov light emission. The $e^\pm$ detection threshold is however lower for Kamiokande ($\sim$ 8.5 MeV) than for the IMB experiment ($\sim$ 20 MeV).

In these detectors the rate of $\bar{\nu}_e p \rightarrow n e^+$ events is expected to be at least an order of magnitude larger than the rate of elastic scattering of ν_e ($\bar{\nu}_e$) on electrons. This can be seen from Fig. 5, which shows the cross-sections as a function of the energy for various reactions to which the detectors are sensitive, together with the expected flux of neutrinos and antineutrinos. The temperatures of ν_μ and ν_τ are expected to be slightly larger than those of $\bar{\nu}_e$ and ν_e, as explained above, but their energy fluxes are the same owing to the equipartition principle. As already stated, the neutronization ν_e's give a negligible contribution to the detected signal, whilst for neutrinos emitted at the thermalization stage (the main neutrino pulse), from fig. 5 the total elastic scattering rate on electrons for all species of neutrinos amounts to $\sim$ 10% of the total interaction rate. However, this elastic reaction represents a negligible fraction of the detected events, since in the elastic scattering the recoil electron has an approximately flat energy distribution (from zero to the incident neutrino energy) and thus a much reduced triggering probability, whilst in the inelastic scattering of $\bar{\nu}_e$ on protons, $\bar{\nu}_e p \rightarrow n e^+$, the

One should note that the fit is applied on the high-energy tail of the energy spectrum, especially for the data from the IMB experiment, so that the error might be underestimated. In that sense, the Kamiokande data are more reliable (lower detection threshold), which would favour lower temperatures and higher luminosities.

It is worth mentioning that in all these calculations the triggering efficiency, the threshold effects, and the energy resolution of detectors are taken into account through simple analytical formulas. It would certainly be worth while to include, in the maximum likelihood, a full Monte Carlo simulation of the experiments (apparatus response near detection threshold) in order to deal with these instrumental effects properly and to get the final numerical answer.

It should be said that similar calculations have also been done for the five events detected by the Baksan scintillator detector (Pomanski, 1987). They lead to an even higher luminosity: $L(\bar{\nu}_e) = (17 \pm 8) \times 10^{52}$ erg (Alexeyev et al., 1988).

The Mont Blanc signal (Aglietta et al., 1987) cannot be included in this analysis since it occurred about 4.7 h earlier than the other detected signals, and, if real, would thus correspond to a different physics content (De Rújula, 1987). Furthermore, it would probably cast doubt upon the overall understanding of the mechanism of supernova explosions, and our analysis would then not be justified. It is none the less true that the Kamiokande and IMB bursts agree very well with the standard scenario of stellar collapse adopted by us in this analysis. A discussion of the mutual compatibility of the various observations is given by Schramm (1987b).

2.7 Conclusions on the number of neutrino species from SN1987A

There is a good general agreement between theoretical expectations and observations regarding the neutrino physics of supernova SN1987A. The energy spectrum and the time distribution of events are in excellent agreement with the expectations. We can thus rely on the theory to predict the total number of species of light neutrinos ($m_\nu \lesssim 1$ MeV). The prediction is that the total energy release is equally shared by all species. The number of families is then derived directly from the ratio of the total expected luminosity ΔE to the one observed in $\bar{\nu}_e$: $\Delta E \approx 2N_\nu L(\bar{\nu}_e)$. The factor of 2 takes into account the presence of particles and antiparticles.

Starting from

$$\Delta E = (2.5 \pm 0.5) \times 10^{53} \text{ erg}$$

$$d = 49 \pm 5 \text{ kpc}$$

and

$$L(\bar{\nu}_e) = (6 \pm 1.8) \times 10^{52} \left(\frac{d}{49 \text{ kpc}}\right)^2 ,$$

we obtain

$$N_\nu = 2^{+1.1}_{-0.4}{}^{+1.0}_{-0.8} ,$$

where the second error corresponds to the systematic uncertainty on the total luminosity ($1.5 \times 10^{53} < \Delta E < 3.5 \times 10^{53}$ erg). If we consider this error as Gaussian with a r.m.s. of 0.5×10^{53} erg (so

positron carries the entire energy of the incident antineutrino, diminished by the reaction threshold (1.3 MeV). Thus in a first approximation the contribution from the elastic scattering of neutrinos on electrons can be ignored in the detected signal. Background events (radioactivity, noise, etc.) in the first 13 s amount to 0.2 events in Kamiokande and 0.8 event in IMB, and can also be neglected.

Additional information could, in principle, be gained from the angular distribution of the events. In the elastic scattering of neutrinos on electrons, the recoil electron is strongly correlated with the incident neutrino direction ($\cos\theta > 0.85$), thus giving an indication of the direction of the source. For antineutrino absorption on protons, on the other hand, the positrons are almost isotropically distributed. The data, shown in Fig. 6, exhibit an excess of events in the forward direction which is at the limit of statistics ($\sim$ 5% confidence level) and is mainly present in the IMB data. Two authors (LoSecco, 1989; Van der Velde, 1988) have recently suggested that the effect is real and have attributed it to the combined effect of elastic scattering of all neutrino species on electrons and to some exotic new particles. Their proposals however are not very convincing.

2.6.2 $\bar{\nu}$ luminosity of SN1987A

Assuming, therefore, that the detected events are due to $\bar{\nu}_e$ interactions, the luminosity in $\bar{\nu}_e$ of supernova SN1987A can then be derived from a maximum likelihood adjustment of few parameters on the collected data.

i) The number density of $\bar{\nu}_e$ is assumed to have a Fermi-Dirac form, $n(E)dE = NE^2dE/[(\exp(E/kT) + 1]$, where k is the Boltzmann constant, and T is the emission temperature and is here a free parameter. The relation between the average energy and temperature in a Fermi-Dirac gas is given by $\langle E \rangle = 3.15\ kT$ (kT in MeV).

ii) The temperature T might decrease as a function of time during neutrino emission: $T = T_0 \exp(-t/\tau)$, where τ is a characteristic neutrinosphere cooling time and is a second free parameter.

iii) Finally, the overall normalization N, related to the total number of events, can be adjusted and translated into a third parameter, the most relevant one for this study, i.e. the total $\bar{\nu}_e$ luminosity $L(\bar{\nu}_e)$.

Many such computations have been performed by various authors (Schaeffer et al., 1987; Ellis and Olive, 1987; Krauss, 1987; Schramm, 1987a; Burrows, 1987; Piran et al., 1988; Spergel et al., 1987; Lamb et al., 1987). The results are shown in Table 2. They cluster around $L(\bar{\nu}_e) \approx 6.0 \times 10^{52}$ erg for a source distant (49 $\pm$ 5) kpc. This number has to be

i) increased by $\approx$ 10% for the energy dissipated after the first 13 s and for the energy that is lost in the background of the detectors;

ii) decreased by about 5% for possible background events in the data;

iii) decreased by a further 5% for the elastic scattering contribution.

This leads to

$$L(\bar{\nu}_e) = (6.0 \pm 1.8) \times 10^{52}\ (d/49\ \text{kpc})^2\ \text{erg}\ ,$$

where d is the distance from SN1987A in the LMC to the Earth.

that the above interval corresponds to $\pm 2\sigma$), and using the χ^2 minimization described in the Appendix, the combined fit leads to

$$N_\nu = 2 \, ^{+1.4}_{-0.7} \, ,$$

with $N_\nu < 3.9$ (4.8) at the 90% (95%) confidence level. This central value and limits on N_ν apply only to neutrinos with masses much less than $\sim$ 1 MeV.

2.8 Future prospects for supernova detection

It is worth remembering that SN1987A in the LMC occurred at a distance of $\sim$ 49 kpc and resulted in the observation of $\sim$ 20 events world-wide. A stellar collapse occurring within our galaxy (thus at $<$ 10 kpc) would produce $\sim$ 25 times as many events in detectors having the same sensitivity. With samples of $\sim$ 500 events, the elastic neutrino interactions on electrons should be observable (at the few % level), with their characteristic directionality. Note also that $\sim$ 50% of these directional (elastic) events should be due to ν_μ ($\bar{\nu}_\mu$) and ν_τ ($\bar{\nu}_\tau$), and therefore of higher average energy (fig. 5).

Larger sensitive volume detectors are at present considered. The Super-Kamiokande project, for example, with $\sim$ 32 kilotonnes of water in the active part of the detector (compared with $\sim$ 2.1 kilotonnes in the present one), is expected to yield $\sim$ 4000 detectable neutrino events for a supernova explosion in the region of the galactic centre.

3. NUMBER OF NEUTRINO SPECIES FROM THE PRIMORDIAL NUCLEOSYNTHESIS

3.1 Principle of the method

There is now a wide consensus that our present Universe originated in a Big Bang. The three major facts behind that belief are the following (see, for example, Weinberg, 1972):

i) The observed galaxy recession indicates that the Universe is not static (which agrees with General Relativity), and that it is expanding. This implies that at earlier times it had a higher temperature.

ii) This means that, at earlier times, fusion reactions could have occurred (Gamow, 1946, 1948) and formed ^{4}He, ^{3}He, D, and ^{7}Li. This is usually referred to as the primordial nucleosynthesis. The primordial abundances deduced from present observations are, at least to the first order, in agreement with this model, and in particular there is no way that the amount of ^{4}He that is observed could have been made in stars.

iii) The black-body radiation from this hot epoch is expected to have survived until today (Gamow, 1946, 1948) and is indeed observed as a universal microwave background of temperature 2.7 K (Penzias and Wilson, 1965). For a recent review see, for example, Wilkinson (1987).

The constraints provided by cosmology on the number of light neutrino families are based on the primordial nucleosynthesis in the early Universe. The greater the number of relativistic degrees of freedom at the time of decoupling of proton and neutron weak interactions (at a temperature around 0.75 MeV), the faster the expansion of the Universe, the higher the decoupling temperature, the higher the number of neutrons (that are less depressed by the Boltzmann factor) and thus the larger the primordial abundance of He. The exact amount depends on the ratio η of the number of nucleons to the number of photons in the Universe, which in turn can be determined by the observed amount of D, ^{3}He, and ^{7}Li. This method has been discussed extensively by many authors (Olive et al., 1981a and 1981b; Yang et al., 1984; Boesgaard and Steigman, 1985; Ellis et al., 1986; Steigman, 1987), and our task will be mainly to summarize the observations and update the estimate of the number of neutrino species.

3.2 Summary of the standard cosmology model

Before we go into the detailed predictions, let us summarize the classical results of cosmology (see, for instance, Weinberg, 1972).

3.2.1 Expansion of the Universe

If the Universe is homogeneous and isotropic on a large enough scale—as it appears to be—it can be characterized simply by a scale parameter a(t) [often also written as R(t); this notation has the drawback of leading to the wrong interpretation of R(t) as a 'radius' of the Universe]. The real coordinate x of a galaxy at rest with respect to the expansion is given at time t by

$$x = a(t)\, r \ ,$$

where r is the fixed co-moving coordinate. The rate of expansion is given by the Hubble 'constant'

$$H = \frac{1}{a}\frac{da}{dt} \ .$$

Experimentally, we find that the Universe is expanding and that the light from distant galaxies is red-shifted. If we define the red shift as

$$z = \frac{\Delta\lambda}{\lambda} \ ,$$

it can easily be shown to be given, for an object at rest with respect to the Hubble flow, by the ratio of the scale parameter at the present time ($t = t_0$) to the value at the time of emission ($t = t_1$):

$$1 + z = \frac{a(t_0)}{a(t_1)} \ .$$

At a very large scale, our Universe can be considered as a spatially homogeneous and isotropic space, and its metric is the Robertson-Walker metric,

$$ds^2 = dt^2 - a^2(t)\left(\frac{dr^2}{1 - kr} + r^2\, d\theta^2 + r^2 \sin^2\theta\, d\varphi^2\right) \ ,$$

where k is a constant that can be set to 0 or ± 1 by the proper choice of the units, and is related to the space curvature.

The theory of general relativity then allows us to relate the Hubble constant to the average density ϱ of the Universe by the so-called Friedman equation:

$$H^2 = \frac{8\pi G_N}{3}\varrho - \frac{k}{a^2} + \frac{\Lambda}{3} \ .$$

This equation, which can also be derived (except for the cosmological constant Λ) in Newtonian mechanics, expresses the balance of the kinetic energy given by H^2 and the potential energy (proportional to ϱ). The constant k arises then as an integration constant.

Let us first discuss the case where Λ is zero. It is obvious that if $k = 0$ the density is

$$\varrho_c = \frac{3H^2}{8\pi G_N}$$

the so-called critical density. Since ϱ_c is positive, the expansion rate cannot go through zero and the Universe is always expanding. If we define

$$\Omega = \frac{\varrho}{\varrho_c}$$

in this case $\Omega = 1$, and the Universe is spatially flat (but curved in space-time). On the other hand, if $k > 0$, that is if $\Omega > 1$, the expansion rate can go through zero and the Universe will recollapse. This corresponds to a closed Universe, which is spatially isometric to a 3-sphere. If $k < 0$, which corresponds to $\Omega < 1$, the Universe is open and will expand for ever.

The additional term Λ is called the cosmological constant. It arises naturally in many particle physics models (but with rather large values) and, when it is positive, can be interpreted as the energy density of vacuum (but with negative pressure). The present value of Ω can be determined by weighing galaxies, by measuring their peculiar velocities, or by attempting to measure the spatial curvature directly. The present consensus is that the value of Ω today is $0.1 \leq \Omega_0 \leq 2$. (For references and a recent summary for particle physicists, see Sadoulet, 1988.) The cosmological constant is obtained by measuring simultaneously the Hubble constant, the age of the Universe, and Ω, which are related as shown in Fig. 7. Currently, the data constrain Λ to the interval

$$-1. < \frac{\Lambda}{3H_0^2} < 3. ,$$

where H_0 is the present value of the Hubble 'constant'.

The Friedman equation has to be complemented by two equations expressing the relation between the pressure and the density (equation of state) and the conservation of energy. Let us examine the evolution of the basic parameters for the case of zero cosmological constant.

In the present matter-dominated Universe, the pressure is neglible ($p = 0$). The conservation of energy then states that

$$\frac{d}{dt}[\varrho a^3(t)] = 0 .$$

The Friedman equation can then be solved. For instance, in the absence of a cosmological constant and if $k = 0$,

$$a(t) \propto t^{2/3} .$$

For $t \to 0$, there is an initial singularity. The Friedman equation shows that the Universe cannot be static and that there has been a Big Bang. The present age T_0 of the Universe is of the order of

$$T_0 \approx \frac{1}{H_0} \text{ (e.g. } T_0 = 2/3\, H_0 \text{ for } \Lambda = 0 \text{ and } k = 0) \ .$$

Note also that unless Ω is equal to 1, it evolves very rapidly. For $\Lambda = 0$, it can be shown that during this matter-dominated period

$$1 - \Omega(z)^{-1} = \frac{1 - \Omega_0^{-1}}{1 + z} \ , \tag{3.1}$$

where $\Omega(z)$ is the value of Ω at red shift z, and Ω_0 is the value of Ω today.

During the matter-dominated epoch, the background photon (and neutrino) energies and temperatures evolve as $1/a(t)$ and their energy densities as $a(t)^{-4}$. Therefore at sufficiently early times ($z \gtrsim 3 \times 10^4$), the energy density of the Universe becomes radiation-dominated. It is easy to show that given the above-quoted experimental range for Ω_0 and Λ, the spatial curvature term and the cosmological term are negligible in the radiation-dominated period. For instance, in the case of a null cosmological constant, expression (3.1) shows that even at the end of the radiation-dominated era, Ω is equal to 1 within 3×10^{-4}. For a relativistic fluid

$$p = \frac{\varrho}{3} \ ,$$

the conservation of energy leads to

$$\varrho \propto a(t)^{-4} \ ,$$

and the combination of the Friedman equation and thermal equilibrium gives a temperature

$$T^{-1} \propto a(t) \propto (NDF)^{1/4} t^{1/2}$$

where NDF is the effective number of relativistic degrees of freedom, i.e. the sum of the number of boson states and of 7/8 of the number of fermion states (see, for instance, Weinberg, 1972). The time is related to the temperature by

$$t \approx 2.4\, [NDF]^{-1/2} \left(\frac{1\ MeV}{kT}\right)^2 \text{ seconds} \ .$$

The important point of the above equation is that the evolution speed depends on the number of degrees of freedom: the larger it is, the faster a(t) grows. This is the basis for the constraints on the number of neutrino species provided by primordial nucleosynthesis.

3.2.2 Thermal equilibrium and decoupling

During early times, all interacting species i, j, ℓ, m are in thermodynamic equilibrium through reactions of the type

$$ij \leftrightarrow \ell m \ ,$$

and this goes on as long as the mean collision time is much less than the expansion time 1/H. When the collision time becomes too large, the species involved decouple and their abundance is frozen out. Quantitatively (see, for example, Barrow, 1983), if n_i is the density of particles of a given species i, the evolution of this species is given by

$$\frac{dn_i}{dt} = -3n_i\frac{da/dt}{a(t)} - \langle\sigma_{ij\to\ell m}\,v\rangle\, n_i\, n_j + \langle\sigma_{\ell m\to ij}\,v\rangle\, n_\ell\, n_m \ , \tag{3.2}$$

where the σv terms are the thermally averaged reaction rates in both directions. The first term on the right-hand side accounts for the dilution due to the expansion. The second term accounts for the disappearance of the species i, and the third term for its production. Detailed balance relates the two reaction rates at a temperature T:

$$\frac{\langle\sigma_{ij\to\ell m}\,v\rangle}{\langle\sigma_{\ell m\to ij}\,v\rangle} = \frac{n_i^*\, n_j^*}{n_\ell^*\, n_m^*} \ ,$$

where the n^*'s are the *thermodynamical equilibrium* densities at the temperature (given by the Fermi–Dirac or Bose–Einstein distributions):

$$n_i^* = g_i \int \frac{4\pi q^2\, dq}{h^3}\left[\exp\left(\frac{E-\mu_i}{kT}\right) \pm 1\right]^{-1} ,$$

where μ_i is the chemical potential, E is the energy, g_i is the number of spin states, and the integral is performed over the momenta q. The integral indeed gives the density because of the presence of the chemical potential μ_i, which acts as a normalization constant. The μ_i can be determined through the relation

$$\mu_i + \mu_j = \mu_\ell + \mu_m \ ,$$

which guarantees the equilibrium between the number of particles in the reaction being considered. In particular, if j is the antiparticle $\bar{i}$ of i, we have

$$\mu_i = -\mu_{\bar{i}}$$

since they are in equilibrium with photons (which have $\mu = 0$). If there is no asymmetry between the number of particles and antiparticles,

$$\mu_i = \mu_{\bar{i}} = 0 \ .$$

In the more realistic case where the difference between the number of particles and antiparticles is small compared with the number of photons ($\propto T^3$),

$$\left|\frac{\mu_i}{kT}\right| = \left|\frac{\mu_{\bar{i}}}{kT}\right| \ll 1$$

and the chemical potential can also be neglected. This is often referred to as the non-degeneracy of particle i (see Weinberg, 1972, p. 542).

At temperatures and densities that are high enough for the reaction rates to be much larger than the expansion rate, the last two terms in Eq. (3.2) are essentially equal, and the relative densities of particles are the thermodynamical equilibrium values. At the other extreme, when the last two terms are individually negligible, the particle species i is decoupled from the rest of the system and is just diluted by the expansion: $n_i \propto a^{-3}$. Its density per co-moving volume is frozen out. We can approximate the smooth transition between these two regimes by a brutal transition between thermodynamical equilibrium and free evolution at the 'freeze-out temperature', T_f. Two cases can be singled out:

i) if the freeze-out occurs when the particle i is still relativistic, then its subsequent abundance is proportional to the cube of the decoupling temperature:

$$n_i \propto (a_f/a)^3 T_f^3 \ ;$$

ii) if the freeze-out occurs when the particle i is non-relativistic, and if it is non-degenerate, then its subsequent abundance is determined by the Boltzmann factor at freeze-out:

$$n_i \propto \left(\frac{a_f}{a}\right)^3 \left[\exp\left(-\frac{m_i c^2 - \mu_i}{kT_f}\right)\right]\left(\frac{m_i c^2\, kT_f}{2h^2\pi}\right)^{3/2} g_i \qquad (3.3)$$

(e.g. Weinberg, 1972). Such a case occurs when the cross-sections are large enough for the equilibrium to be maintained until T_f is much smaller than the mass m_i. In particular, if j is the antiparticle of i, and if there is no initial asymmetry ($\mu_i = -\mu_{\bar{i}} = 0$), then most of the $i\bar{i}$ pairs will disappear before freeze-out.

3.3 Primordial nucleosynthesis

Let us now apply the results just discussed to the period of nucleosynthesis. Around a temperature of 10 MeV, the Universe is made up of protons, neutrons, ν's, $\bar{\nu}$'s, $e^{\pm}$, and γ's in thermodynamic equilibrium. Around 2 MeV, light neutrinos decouple because the rate of the weak interaction reactions

$$\nu e \rightarrow \nu e, \qquad e^+ e^- \rightarrow \nu\bar{\nu} \ ,$$

becomes too small. But they are relativistic at that time, and their energy density continues to evolve as a^{-4} and to be important in determining the expansion rate.

At $T_f \approx 0.75$ MeV ($t \sim 1$ s), the protons and neutrons escape equilibrium since the reaction rates

$$n + \nu \leftrightarrow p + e^- \ ,$$

$$n + e^+ \leftrightarrow p + \bar{\nu} \ ,$$

$$n \leftrightarrow p + e^- + \bar{\nu} \ ,$$

become too small. The relative abundance is frozen out at a value which can be computed with the techniques outlined above. While in equilibrium, we have

$$\mu_n + \mu_\nu = \mu_p + \mu_{e^-} \ , \qquad \mu_\nu = -\mu_{\bar{\nu}}, \qquad \mu_{e^+} = -\mu_{e^-} \ .$$

If, as is usually believed, there is no strong initial asymmetry between e^+ and e^- and between ν and $\bar{\nu}$, we have

$$\mu_\nu \approx \mu_{e^-} \approx 0 \qquad \text{and} \qquad \mu_p \approx \mu_n \ .$$

Then, since $m_p \approx m_n$, we have according to Eq. (3.3),

$$\frac{n}{p} = \exp\left(-\frac{\Delta mc^2}{kT_f}\right) , \tag{3.4}$$

where $\Delta m = m_n - m_p$.

The freeze-out temperature is related to the number of relativistic species

$$\text{NDF} = g_\gamma + \frac{7}{8}(g_e + N_\nu g_\nu) = \frac{43}{4} \qquad \text{for} \quad N_\nu = 3 \ ,$$

since there are two states for the photon ($g_\gamma = 2$), two spin states for e^+ and e^- ($g_e = 4$), and one spin state for each ν and $\bar{\nu}$ ($g_\nu = 2$).

The larger the number of species is, the faster is the expansion, the earlier is the weak-interaction freeze-out, and the higher is the decoupling temperature. It can be shown [e.g. Weinberg, 1972, Eqs. (15.7.17) and (15.7.18)] that

$$T_f \sim (\text{NDF})^{+1/6} \ .$$

Finally, according to Eq. (3.4), the higher the decoupling temperature, the higher the n/p ratio.

After this episode, the n/p ratio evolves slowly through the decay of the neutron:

$$n \rightarrow p + e + \bar{\nu} \ .$$

At $T \sim 150$ keV, the electron–positron pairs annihilate reheating the photon bath, but not the already decoupled neutrinos.

In spite of the fact that the binding energy of nuclei such as helium is much greater than this temperature, nuclei cannot yet be formed in significant quantities. At the density in presence, the reactions can only occur through two-body processes:

$$p + n \rightarrow D + \gamma \ ,$$

$$D + D \rightarrow {}^3He + n \ ,$$

$${}^3He + D \rightarrow {}^4He + n \ ,$$

but deuterium is too fragile and is continually destroyed by the ambient photon flux. This mechanism is described in the same formalism as above, with the deuterium-to-nucleon ratio behaving as [see Weinberg, 1972, Eq. (15.7.28)]

$$\frac{D}{N} = \exp\left(-\frac{Q}{kT}\right),$$

where Q is the deuterium binding energy. Between 0.5 and 0.1 MeV, the D concentration, and therefore the reaction rates, are too low for higher elements to reach their thermodynamic equilibrium too. We have to wait until the temperature falls below 100 keV (that is ~ 2 min after the Big Bang) for the deuterium 'bottleneck' to disappear and higher-Z elements to be formed. Rapidly, the elements below ^{7}Be are formed (Fig. 8). Higher-Z elements are not produced in significant numbers because of the Coulomb barriers and the absence of a suitable stable intermediate state, and they will have to wait for fusion in stars to be produced.

All cross-sections are reasonably well known (except for some of the ^{7}Li reactions) in this energy region, and detailed calculations can be performed (Fig. 9, from Yang et al., 1984), giving the primordial abundances as a function of the ratio η of the number of protons to the number of photons (which determines the exact temperature at which deuterium begins to be formed), and the number of species which are relativistic at 0.75 MeV, which, as we have seen, determines the neutron-to-proton ratio at freeze-out. The higher this number is, the higher is the amount of ^{4}He. The minimum expected in the ^{7}Li fraction as a function of η is due to the fact that at low baryon density, the interplay between the two reactions

$$^4\text{He} + {}^3\text{H} \rightarrow {}^7\text{Li}$$

$$^7\text{Li} + \text{p} \rightarrow {}^4\text{He} + {}^4\text{He},$$

leads to a decrease of ^{7}Li with increasing proton concentration, whilst at higher densities

$$^4\text{He} + {}^3\text{He} \rightarrow {}^7\text{Be} \rightarrow {}^7\text{Li}$$

becomes appreciable and rises with proton concentration.

Our task is then to determine η from the measured primordial abundances of D, ^{3}He, and ^{7}Li, which are rapidly varying functions of η but are not sensitive [at the present level of measurement accuracy (see, for example, Matzner, 1986)] to the numbers of neutrinos, and to compare the predicted amount of ^{4}He for the various numbers of neutrinos with the observed value.

3.4 Observed primordial abundances

3.4.1 Experimental difficulties

Unfortunately the measurements of primordial abundances are difficult because, apart from ^{4}He, the abundances are small and the signal is extremely weak, especially in absorption.

It is often somewhat easier to observe the signal in emission through, for instance, recombination in ionized regions (H II regions), but the excitation mechanisms have to be estimated carefully.

Even more fundamental is the fact that it is difficult to ensure that it is indeed the primordial abundance that is measured. The best candidate would be the intergalactic medium, but it is too tenuous to allow any measurement. The best approximation would be the metal-poor gas clouds which are observed in absorption against quasars and which may not have evolved to galaxies.

However, these Lyman-α 'forests' of absorption lines are very difficult to disentangle. Most determinations thus rely on the interstellar medium, which gives more intense signals, but then they have to be corrected for the chemical evolution due to processing by earlier generations of stars. This is usually done by extrapolating to zero metallicity, as 'metals' (everything heavier than He) are produced mainly in stars. For rarer elements, such as ^{7}Li, only the stellar atmospheres allow positive observations and, as discussed below, the question of whether it is really the primordial abundance that is observed is even more crucial. Finally, the determinations based on the solar system, from the composition of the solar wind and the spectra of planetary atmospheres or the analysis of meteorites, are even more uncertain because of the large corrections for astration and fractionation. Table 3 gives a summary of the present determinations.

3.4.2 Deuterium

Deuterium is extremely fragile and is transformed into ^{3}He in stars as soon as the temperature is greater than 6×10^5 K through the reaction $p + D \rightarrow {}^3He + \gamma$. The less uncertain determinations are those based on intergalactic and interstellar gases.

Recently, Carswell et al. (1986) may have observed deuterium in absorption against the quasar 90420-288 at the level of $D/H \approx 4 \times 10^{-5}$. The high red shift ($z_{abs} \approx 3.08571$) and the low metallicity ($\sim 1/5$ solar) of the intervening gas suggests that this value may be close to the primordial value. We may thus infer that

$$4 \times 10^{-5} \leq \left.\frac{D}{H}\right|_p \leq 10^{-4} .$$

Absorption lines generated by intervening gas clouds were observed in the emission spectrum of stars [Vidal-Madjar et al., 1983; Laurent et al., 1979; Ferlet et al., 1980; York, 1983], which may be attributed to deuterium. However, the isotopic shift $\Delta\lambda/\lambda$ from the main hydrogen line is only 80 km/s and could be simulated by velocities in the observed clouds (see, for example, Gry et al., 1983). This may explain why the observed values vary widely from 5×10^{-6} to 10^{-4}. Figure 10 from Boesgaard and Steigman (1985) summarizes the results for the cleaner lines of sight, suggesting that the interstellar D abundance is 0.8 to 2×10^{-5}. These numbers have to be corrected for astration, which may have depleted the amount of deuterium by a factor of 2 to 10 (Audouze and Tinsley, 1976; Clayton, 1985; Delbourgo-Salvador et al., 1985). We are led to believe that

$$10^{-5} \leq \left.\frac{D}{H}\right|_p \leq 2 \times 10^{-4} .$$

Blitz and Heiles (1987) have recently searched for the radio emission of D at 91.6 cm in the direction of the galactic anticentre. Unfortunately, this determination is difficult because of both the weakness of the signal compared with terrestrial interferences and the uncertainties in the excitation mechanism. They may have detected a signal at the level of 5×10^{-5} (compatible with the above estimates). However, this signal is only marginally larger than the noise fluctuations in adjacent channels and therefore needs to be confirmed.

3.4.3 ^3He

Stars can either produce ^{3}He through the pp cycle and the destruction of D, or convert it into ^{4}He (Dearborn et al., 1986). Low-mass stars are net producers, whilst high-mass ones destroy ^{3}He.

Rood and co-workers (Rood et al., 1984; Bania et al., 1987) have been measuring the radioemission line of $^3He^+$ (3.46 cm) in various H II regions. Figure 11 summarizes their results as a function of the distance to the galactic centre. They observe a very large variation, from upper limits at the 10^{-5} level to 1.5×10^{-4}. Even though, on the average (over the mass distribution of stars), ^{3}He is produced, the largest H II regions that they use for their observation may contain gas that has recently been reprocessed through massive stars and may thus have been depleted in ^{3}He. The allowed range is therefore quoted as

$$0.5 \times 10^{-5} \leq \left.\frac{^3He}{H}\right|_p \leq 10^{-4} .$$

3.4.4 $D + {}^3He$

In order to circumvent the difficulty of the destruction of D in stars, Yang et al. (1984) have proposed to study the sum D + ^{3}He. The observed ratio D/H represents only a fraction f of the primordial ratio

$$\frac{D}{H} = f \left.\frac{D}{H}\right|_p ,$$

but the destroyed D has made up ^{3}He. So the observed ^{3}He ratio is

$$\frac{^3He}{H} = (1-f)\, g \left.\frac{D}{H}\right|_p + g \left.\frac{^3He}{H}\right|_p + \frac{^3He_{prod}}{H} ,$$

where g is the fraction of ^{3}He destroyed and $^3He_{prod}$ is the produced ^{3}He. The second equation gives

$$g^{-1} \frac{^3He}{H} > (1-f) \left.\frac{D}{H}\right|_p + \left.\frac{^3He}{H}\right|_p ,$$

or adding the first equation

$$\left.\frac{D + {}^3He}{H}\right|_p < \frac{D}{H} + g^{-1} \frac{^3He}{H}$$

or

$$\left.\frac{D + {}^3He}{H}\right|_p < \frac{D + {}^3He}{H} + (g^{-1} - 1)\, {}^3He/H .$$

It may then be safe to use the presolar observations made with meteorites (carbonaceous chondrites):

$$\left.\frac{D + {}^3He}{H}\right|_p < [4.3 + 1.9\,(g^{-1} - 1)] \times 10^{-5} .$$

Taking $g > 1/4$, which is usually considered as a reasonable estimate (Dearborn et al., 1986), we obtain

$$\left.\frac{D + {}^3He}{H}\right|_p \leq 10^{-4} .$$

3.4.5 ^7Li

The proportion of primordial ^{7}Li is so small that there is no possibility of measuring it in the intergalactic or interstellar medium. Stellar atmospheres have to be used, with all the above-mentioned dangers of destruction or production.

It is, however, the use of this method that has recently led to the most striking advances being made in the field of primordial nucleosynthesis. Spite and Spite (1982) were able to measure ^{7}Li in halo dwarfs, which are very old stars of very low metallicity (i.e. population II). Their results have been confirmed and refined in the last few years by two other groups (Hobbs and Duncan, 1987; Rebolo et al., 1988a). Figures 12a and 12b summarize the results.

i) When plotted against the effective temperature ($T_{eff} \propto$ mass) of the star (Fig. 12a), the ^{7}Li abundance appears to be more or less constant for temperatures above 5500 K. Below this temperature it decreases, and this effect is at least qualitatively understood (D'Antona and Mazzitelli, 1983; Brown and Schramm, 1988) as being due to the increase at low temperature of the convective layer, which drags ^{7}Li to hotter regions of the stars, where it is destroyed.

ii) For stars above 5500 K, the ^{7}Li abundance is independent of the metallicity at low metallicity (Fig. 12b).

iii) An upper limit on ^{9}Be/H of 2.5×10^{-12} for three low-metallicity stars has been obtained by Rebolo et al. (1988b). This means that the ^{7}Li observed in these stars has not been produced by cosmic rays.

These experimental facts suggest that we do observe the primordial abundance at the level

$$\left.\frac{^7Li}{H}\right|_p = (1.4 \pm 0.2) \times 10^{-10} ,$$

(combining the Rebolo et al., and Hobbs and Duncan results at high T_{eff} and low metallicity).

However, some younger stars (population-I stars such as the Hyades) have a higher ^{7}Li concentration (Fig. 12c) (Hobbs and Pilachowski, 1986 and 1988): $^7\text{Li/H} = (1.6 \pm 0.3) \times 10^{-9}$. The ^{7}Li can indeed be formed in a red giant and in novae (Audouze et al., 1983) and supernovae (Dearborn et al., 1989), or be produced as a spallation product of cosmic-ray interactions. So having a higher abundance is not disturbing in itself. But this raises the obvious question: Which of the two concentrations is the primordial one? Is it not possible to imagine that population-II stars, which are 10 times older than the Hyades, have depleted an initial ^{7}Li abundance of 10^{-9} down to 10^{-10}? Several plausibility arguments favour the hypothesis that the population-II value is primordial.

i) As emphasized, the simple behaviour observed for population-II stars as a function of metallicity and temperature is at least qualitatively understood (Kawano et al. 1988; Steigman, 1989), and is suggestive that this is indeed the primary abundance.

However, recently Vauclair (1987, 1988) has suggested that a mixing mechanism proposed by Zahn (1987) for rotating stars could give a depletion rate independent of the effective temperature and therefore generate a plateau such as the one observed in Fig. 12a.

The weakness of this argument is that, for this mechanism to work, all stars must have the same rotation velocities, and no good mechanism has yet been proposed for such a constancy for population-II stars.

ii) Two groups, Baade and Magain (1988) and Sahu et al. (1988), recently set an upper limit on the ^{7}Li abundance in the (low-metallicity) interstellar gas in the Large Magellanic Cloud using SN 1987A as a light source. Their result is compatible with the 1.4×10^{-10} determination from population-II stars, and is incompatible with the higher estimates. The argument would obviously be stronger if there had been a positive observation.

iii) Rebolo et al. (1988a) argue that it is difficult to understand why the depletion in population-II stars at low temperature should be slower than for the Hyades and much faster at temperatures of 6000–6300 K. However, this may be in agreement with the qualitative behaviour expected with metallicity. Lower metallicity naturally leads to a shallower convection zone at a given temperature and therefore, for a given depletion, lower T_{eff} are necessary for population-II stars than for population-I stars. It remains to be seen if this mechanism works quantitatively.

Therefore, although arguments of simplicity favour the population-II abundance value, there is still a theoretical possibility that the population-I value is the primordial one. Answering this question unambiguously would require an understanding of the complex behaviour observed in population-I stars as a function of their age and their temperature (Fig. 12c), including the dip at 6600 K for which several mechanisms have been proposed (Michaud et al., 1984; Vauclair, 1988).

Note, however, that the interpretation of the population-II abundance as primordial requires that ^{7}Li be produced very rapidly at early galactic times in order to explain a high ^{7}Li value for population-I stars of a wide range of ages. This may be compatible with a supernovae origin of ^{7}Li.

Given the above doubts, for our purpose we would then have to use the two values of ^{7}Li.

3.4.6 ^{4}He

Finally, let us turn to the determination of the abundance of ^{4}He. It relies on the emission lines of H II produced by recombination in blue compact galaxies. Shields (1987) has recently reviewed the experimental difficulties and uncertainities in correcting for neutral helium, He^{++} and collisional excitation. It is important to realize, in particular, that the H II regions used are not resolved and that they contain many stars. The assumption of a common temperature is a gross oversimplification. In order to correct for chemical evolution due to stellar nucleosynthesis, the abundance by mass,

$$Y = \frac{3.97\, N_{He}}{N_H + 3.97\, N_{He}} \quad ,$$

is plotted against the abundance of some higher-A element which would be synthesized by stars—oxygen [Kunth and Sargent, 1983 (see also Kunth, 1986) and Peimbert, 1986], nitrogen (Pagel et al., 1986), carbon (Steigman et al., 1986)—and extrapolated to zero (Figs. 13a, b).

These authors obtain for the mass fraction:

0.243 ± 0.003	(Kunth),
0.232 ± 0.013	(Peimbert),
0.236 ± 0.005	(Pagel O/H),
0.238 ± 0.005	(Pagel N/H),
0.235 ± 0.004	(Steigman et al.).

These results, which use partially overlapping data, are compatible, yielding a weighted average of

$$Y_p = 0.236 \pm 0.003 \ ,$$

which may have to be decreased somewhat to take into account the collisional excitation. We propose to take

$$Y_p = 0.235 \pm 0.003 \text{ (stat.)} \pm 0.010 \text{ (syst.)} \ ,$$

where we have followed Shields' estimate of the systematic error.

3.5 Number of neutrinos

In order to treat statistically the observations summarized above, we chose the following central values and errors:

$$\log_e \left.\frac{D}{H}\right|_p = \log_e(4.5 \times 10^{-5}) \pm 0.75 \ ,$$

$$\log_e \left.\frac{^3He}{H}\right|_p = \log_e(2.25 \times 10^{-5}) \pm 0.75 \ ,$$

and for the solar system determination,

$$\log_e \left.\frac{D + {}^3He}{H}\right|_p = \log_e(5 \times 10^{-5}) \pm 0.35 \ ,$$

spanning the ranges 10^{-5} to 2×10^{-4}, 0.5×10^{-5} to 10^{-4}, and 2.5×10^{-5} to 10^{-4} respectively, at the 2σ level. We take for the lithium

$$\log_e \left.\frac{^7Li}{H}\right|_p = \log_e(1.4 \times 10^{-10}) \pm 16\% \text{ (population II) or}$$

$$= \log_e(1.6 \times 10^{-9}) \pm 30\% \text{ (population I).}$$

Because of the uncertainty in the ^{7}Li cross-sections mentioned above, we have added a theoretical uncertainty of 30% (r.m.s. on the logarithm).

For ^{4}He we take

$$Y_p = 0.235 \pm 0.010 \ .$$

The neutron lifetime is taken from the latest issue of the Tables of Particles Properties (1988) as

$$\tau_{1/e} = 896 \pm 10 \, s \ ,$$

leading to

$$\tau_{1/2} = 10.35 \pm 0.12 \, min \ ,$$

a value definitely smaller than the one chosen by Yang et al. We can then construct (as explained in the Appendix) a χ^2 with the theoretical predictions for abundances as a function of η from Yang et al. (1984) [except for the ^{7}Li, which is from Kawano et al. (1988)]. Minimizing this χ^2 yields the following estimates:

i) For population-II ^{7}Li abundance, we get

$$N_\nu = 2.2 \pm 0.7 \pm 0.2 \quad \text{(Solution I)} \ ,$$

where the second error comes from the theoretical uncertainty on ^{7}Li cross-sections. If the theoretical uncertainty is treated as random, we obtain

$$N_\nu = 2.3 \pm 0.8$$

and

$$N_\nu < 3.3 \ (3.6) \text{ at the } 90\% \ (95\%) \text{ CL} \ .$$

The goodness of fit is 93%, indicating excellent consistency between the data and the model. We have also

$$\eta = (4.35^{+0.4}_{-0.6}) \times 10^{-10} \ .$$

Note that η is related to the ratio Ω_b of the baryon density to the critical density:

$$\Omega_b = 0.37 \ \frac{a}{k} m_p \left(\frac{8\pi G_N}{3H^2}\right) T^3 \eta \ ,$$

where a and k are the black-body and the Boltzmann constants, m_p is the mass of the proton, and T is the present temperature of the microwave background. If h is the Hubble constant measured in units of 100 km/s/Mpc, then

$$\Omega_b h^2 = 3.7 \times 10^7 \eta \quad \text{for} \quad T = 2.74\,K$$

$$= (1.61^{+0.16}_{-0.22}) \times 10^{-2}$$

and: $\Omega_b h^2 < 1.85 \times 10^{-2}$ (90% CL) ,

$< 1.92 \times 10^{-2}$ (95% CL) .

ii) If, on the other hand, we take the population-I ^{7}Li abundance, we obtain two solutions:

a) Solution II:

$$N_\nu = 1.8 \pm 0.75$$

and: $N_\nu < 2.6$ (90% CL) ,

< 3.1 (95% CL) ,

corresponding to $\eta = (8.6 \pm 0.6) \times 10^{-10}$ with a goodness of fit of 1.9%. This solution is a poor fit, and presumably should be rejected as being incompatible with the Standard Model, unless our errors are grossly underestimated.

b) Solution III:

$$N_\nu = 3.4 \pm 0.8$$

and: $N_\nu < 4.4$ (90% CL) ,

< 4.7 (95% CL) ,

corresponding to $\eta = (1.6 \pm 0.6) \times 10^{-10}$, but with a very bad goodness of fit of less than 10^{-6} because of the incompatibility with D and D + ^{3}He abundances. The fit is so poor that this solution cannot be retained.

3.6 Discussion

The excellent agreement of the Standard Model with the ^{7}Li abundance of population-II stars is another indication that favours this value as the primordial one. However, it should be noticed that the only solution with population-I ^{7}Li abundance that could be considered (Solution II) leads to more restrictive bounds on the number of neutrinos.

For the population-II solution, it should be noted that our limit

$$N_\nu < 3.6 \quad (95\%\ \text{CL})$$

is strongly dependent on the systematic error that we have chosen to place on the amount of ^{4}He. Had we chosen 0.05 by arguing that it is more representative of the dispersion of values in the three determinations mentioned above, and that the systematic errors that worry Shields would average out over the objects and methods, we would have obtained

$$N_\nu \leq 3.1 \quad (95\%\ \text{CL}) ,$$

a value that we do not, however, recommend because of the possible systematic effect of commonly used assumptions and of the potential bias in the community in favour of the Standard Model, which may cluster the observations more than is warranted.

Let us remind the reader that our limit is a limit on the number of relativistic degrees of freedom at 0.75 MeV, and that, if we exclude the three neutrinos, the electron, and the photon, the number of additional degrees of freedom is bounded by

$$\mathrm{NDF} < 1.2 \quad (95\%\ \mathrm{CL})\ ,$$

where the fermions are computed for 7/8 times their number of spin states. This assumes that the temperature of these particles is the same as that of the neutrinos. However, this will not be the case if they have decoupled much earlier. This could be the case, for instance, for right-handed neutrinos (Olive et al., 1981a; Ellis et al., 1986). The compatibility of our result with the presence of three light right-handed neutrinos would require a decoupling before the quark–hadron transition (Olive et al., 1981a), which can easily be arranged with sufficiently massive additional vector bosons.

Finally, it should be kept in mind that the Standard Model could be wrong. Two unconventional mechanisms are at the moment close to reproducing the primordial abundance data. The quark–hadron transition could lead to a spatial segregation between the neutrinos and the protons (Applegate et al., 1987; Alcock et al., 1987; Fuller et al., 1988). But the model with $\Omega_b = 1$ has considerable difficulty in reproducing in detail the amount of ^{4}He and ^{7}Li [even if the population-I value is chosen (Alcock et al., 1988)]. A late release of energy due, for instance, to the decay of a supersymmetric particle (Dimopoulos et al., 1988a and 1988b, 1989) could also change the standard picture and allow $\Omega_b = 1$. However, much ^{6}Li is also produced, and this may be close to being ruled out (Brown and Schramm 1988; Schramm, private communication, 1989). Unconventional models with $\Omega_b < 1$ are probably viable and will weaken the limit on the number of neutrino families. The motivation for the additional parameters they need becomes, however, unclear.

Other exotic scenarios have recently been reviewed by Matzner (1986). Most of them increase the abundance of ^{4}He, thus making the limit on the number of neutrinos more strict. However, an electron-neutrino degeneracy that would accelerate neutron decay in the early Universe, or a variable gravitational constant, could increase the limit. But here again, there is no justification for the required additional parameters.

3.7 Outlook

Presumably the most important improvement to be made in the next decade in the field of nucleosynthesis would be a reliable measurement of deuterium in the intergalactic medium through the detailed study of Lyman-α systems in the absorption spectra of quasars. Unfortunately, the first generation of spectrometers aboard the Hubble Space Telescope (HST, to be launched in 1989) may have insufficient resolution to unravel their complexity. Radio determination in emission and absorption in the interstellar medium may also be interesting.

More detailed studies of H II regions in young galaxies, made with better angular resolution, will help in refining ionization models and the determination of ^{4}He. The Far Ultraviolet Satellite

Explorer (FUSE), at present in its final stages of study, would help to determine both the ^{3}He and the D abundance in the same objects, and to check for an anticorrelation between ^{3}He and D.

Refinement of stellar models and the collection of more data should allow us to improve our understanding of convection and diffusion, and to clarify the ^{7}Li question. A better knowledge of the nuclear cross-sections for the ^{7}Li abundance calculation is also important.

4. NEUTRINO COUNTING FROM SINGLE-PHOTON PRODUCTION IN e^+e^- ANNIHILATION

4.1 The method

Single-photon production in e^+e^- annihilation as a means of determining the number of neutrino species was first suggested by Dolgov et al. (1972) and by Ma and Okada (1978). The method is based on a radiative correction diagram to Z production, shown in Fig. 14a. Depending on the centre-of-mass energy, the Z can be on-shell or off-shell. The final state is characterized by the production of a single isolated photon, recoiling against a non-interacting system. Within the Standard Model there is, however, another source of single-photon events leading to non-interacting final-state particles, which is due to the diagram shown in Fig. 14b. All neutrino species are produced through the Z in diagram (a), whilst the charged-current diagram (b) gives rise to only $\nu_e\bar{\nu}_e$ pairs.

Clearly, this direct counting method can measure, or put a limit, on the sum $\Sigma\Gamma(Z \to \nu_i\bar{\nu}_i)$, or more generally on the partial width for all Z decay modes into non-interacting particles (ν, $\tilde{\nu}$, $\tilde{\gamma}$, etc.).

If we assume that the only relevant extentions of the Standard Model are additional neutrino families, then for N_ν species of (light) neutrinos, the lowest-order cross-section for $e^+e^- \to \gamma\nu_i\bar{\nu}_i$ is given by (Gaemers et al., 1979)

$$\frac{d^2\sigma}{dE_T^\gamma\, d\cos\theta_\gamma} = \frac{G_F^2\alpha}{6\pi^2}\,\frac{s(1-x_\gamma)}{E_T^\gamma \sin^2\theta_\gamma}\left[(1-\tfrac{1}{2}x_\gamma)^2 + \tfrac{1}{4}x_\gamma^2\cos^2\theta_\gamma\right]$$

$$\times\left\{\frac{m_Z^4\{N_\nu(g_v^2+g_A^2)+2(g_v+g_A)[1-s(1-x_\gamma)/m_Z^2]\}}{[s(1-x_\gamma)-m_Z^2]^2+m_Z^2\Gamma_Z^2} + 2\right\}\,,$$

where E_T^γ is the photon momentum transverse to the beam, and θ_γ the polar angle of emission, $x_\gamma = 2E_\gamma/\sqrt{s}$. The term in the curly bracket proportional to N_ν is due to the s-channel Z propagator, and the last term to the production of electron-neutrinos by W exchange, whilst the second term is the interference between W and Z exchange for electron-neutrinos; m_Z and Γ_Z are the Z mass and total width; and g_V and g_A are the vector and axial-vector $Z \to e^+e^-$ couplings: $g_A = -1/2$ and $g_V = -1/2 + 2\sin^2\theta_w$.

This is a bremsstrahlung process, and the photon distribution is proportional to $(1/E_\gamma)(1/\sin^2\theta_\gamma)$. It is peaked at low energy E_γ and at polar angles θ_γ close to the beam. Because of this, the cross-sections observable in practice are rather small at present (PEP and PETRA) c.m. energies $\sqrt{s}$, which are much smaller than m_Z. An experiment designed to study this process thus needs good photon detection at low E_γ and low θ_γ, and at the same time the veto capability of the detector must extend over as large a solid angle as possible. For example, at $\sqrt{s} = 29$ GeV (PEP) the detectable cross-section for $E_\gamma > 1$ GeV, $\theta_\gamma > 20°$, and $N_\nu = 3$, is 0.04 pb (Hearty et al., 1987). In typical PEP

or PETRA experiments with a sensitivity of $\sim$ 100 events per picobarn, this leads us to expect only a few events. At present, therefore, this method is barely able to determine N_ν, but rather places an upper limit on N_ν. A substantial improvement to the present situation is already expected at TRISTAN energies, where the rate for $\gamma\nu\bar{\nu}$ at $\sqrt{s}$ = 68 GeV should be larger by a factor of $\sim$ 6 for comparable cuts. The situation will change drastically with the Z factories, the SLC and LEP, where the cross-section is enhanced by a factor of $\sim 10^3$. At these machines, N_ν can be determined in several ways: either from a direct measurement of the Z total width with a beam scan across the peak (Altarelli et al., 1986), or operating at the Z peak (Feldman, 1986), or at a c.m. energy slightly above m_Z, if this $\gamma\nu\bar{\nu}$ method is employed (Barbiellini et al., 1981; Simopoulou, 1986).

In the single-photon final state, the photon is the main experimental signature. One must, however, be sure that it is produced in association with no other interacting particles, i.e. it is necessary to be able to detect any other particle that might be produced, down to the smallest possible angle to the beams.

As this is a direct-counting experiment, good control of physical and instrumental backgrounds of same topology is needed. Momentum balance in the transverse plane is the essential background rejection criterion. The main physical background is due to $e^+e^- \rightarrow \gamma e^+e^-$, with the final-state e^+e^- escaping detection, mostly through the beam pipe. This background can be reduced, at the expense of rate, by raising the γ transverse energy threshold E_T^γ, as either the e^+ or the e^- must emerge at a lab. angle:

$$\theta_{lab} > E_T^\gamma/\sqrt{s} = E_T^\gamma/(2\,E_{beam}) \ .$$

Hermetic calorimetry and particle detection down to low angles to the beams is therefore essential in this search, in order to avoid physical backgrounds from $ee \rightarrow \gamma ee$, $\gamma\gamma$, $\gamma\gamma\gamma$ (Hearty et al., 1987; Behrend et al., 1988). Instrumental backgrounds arise from cosmics and beam–gas interactions producing π^0's along the beam lines.

4.2 Results from PEP and PETRA

We discuss in more detail the search performed in the ASP detector at PEP at $\sqrt{s}$ = 29 GeV (Bartha et al., 1986; Hearty et al., 1987). This experiment has the largest sensitivity of all e^+e^- experiments until now (115 events per picobarn), and is best suited to this search. The ASP detector is shown in Fig. 15. It has charged-particle detection and electromagnetic calorimetry over the full solid angle down to 21 mrad from the beam lines. Only radiative Bhabha events $e^+e^- \rightarrow e^+e^-\gamma$, with $E_T^\gamma < 0.6$ GeV, could possibly be mistaken for $e^+e^- \rightarrow \gamma\nu\bar{\nu}$. Photon recognition is achieved in the angular range $20° < \theta_\gamma < 160°$ with lead-glass counters, and single-photon candidates are required to satisfy $E_T^\gamma > 0.8$ GeV and $E_\gamma < 10$ GeV. The requirement $E_\gamma < 10$ GeV is introduced to eliminate background due to $e^+e^- \rightarrow \gamma\gamma$ and $\gamma\gamma\gamma$, with a photon escaping detection in the calorimeter or the beam tube. The ASP Collaboration expected three such events and found four.

For rejection of cosmic-ray interactions, it is required to have an electromagnetic shower shape with a vertex matching for the extrapolated electromagnetic shower direction (expressed in terms of the distance of closest approach to the interaction point). Timing between the calorimeter signal and the beam crossing has also to be consistent with a shower developing outwards from the interaction region.

The efficiency with which photons pass the various selection criteria is determined, as a function of E_T^γ and θ_γ, from the sample of radiative $e^+e^-\gamma$ final states (40,000 kinematically fitted events). A display of an $e^+e^-\gamma$ event in the ASP detector is shown in Fig.16a. The overall efficiency for single photons accompanying $\nu\bar{\nu}$ production is 75% in the ASP fiducial region $20° < \theta_\gamma < 160°$. The requirement that there be no evidence of another particle produced in the event is a crucial one. No significant signal is allowed in any part of the detector, other than that for the γ candidate. The efficiency of this veto is found to be 89%. There are additional signal losses of 6.8%, due to back-scattering from the γ shower, to γ conversions in the beam pipe and tracking chamber, to late γ-conversions, and to triggering efficiency. The overall efficiency for detecting single-photon annihilation processes in the signal region of ASP is 61% (Hearty et al., 1987).

The most probable signal and background contributions from the 24 candidate single-photon events with $E_T^\gamma > 0.8$ GeV (Fig. 17) are estimated by a maximum likelihood method. The expected signal and background probability distributions in the distance of closest approach of the shower to the interaction point (R in Fig. 17) and in E_T^γ are used in the analysis. This procedure yields a signal of 1.6 events for $E_T^\gamma > 0.8$ GeV, $E_\gamma < 10$ GeV, and $20° < \theta_\gamma < 160°$, whilst 2.7 $\gamma\bar{\nu}$ events are expected for $N_\nu = 3$. A schematic display of the clear single-photon event of Fig. 17 with $E_T^\gamma = 3.4$ GeV is shown in Fig. 16b. The probability of observing ≤ 1.6 events is shown in Fig. 18 as a function of the $e^+e^- \to \gamma\nu\bar{\nu}$ cross-section. From this figure we see that $\sigma(ee \to \gamma\nu\bar{\nu}) < 0.069$ pb at 90% CL; this is equivalent to $N_\nu < 7.5$ (90% CL) and $N_\nu < 9.7$ (95% CL). This limit is valid for neutrinos that are light compared with $\sqrt{s}/2$, i.e. for m_ν less than a few GeV.

A similar search has been performed with the MAC detector at PEP, with 1 event observed for 1.1 events expected, yielding $N_\nu < 15.5$ (90% CL) (Fernandez et al., 1985; Ford et al., 1986), and with the CELLO detector at PETRA, yielding $N_\nu < 15$ (90% CL) (Behrend et al., 1986).

More recently, the CELLO Collaboration has analysed data at c.m. energies of 35 and $\sim$ 43 GeV, with experimental sensitivities of 85 and 38 events per picobarn, respectively (Behrend et al., 1988). Within the acceptance of the CELLO experiment, 10 single-photon candidates are observed in the final selection. This event sample contains one clear-cut example of a single-photon event of $E_T^\gamma = 3.6$ GeV, separated out by a requirement of tight pointing to the interaction point. Using again the distance of closest approach to the interaction point for the single-photon candidates, a maximum likelihood method gives 1.3 observed $\gamma\nu\bar{\nu}$ events for 1.9 expected. The remaining events are cosmic-ray background due to the inefficiency of muon chambers. With the 1.3 observed $\gamma\nu\bar{\nu}$ events the CELLO Collaboration gets a central value $N_\nu = 1.3^{+6.7}_{-1.2}$ and a new limit $N_\nu < 8.7$ at 90% CL.

The results for N_ν from these three $e^+e^- \to \gamma\nu\bar{\nu}$ searches have been combined in Behrend et al. (1988) and Johnson (1987). In all experiments combined, the total number of observed $\gamma\nu\bar{\nu}$ events is estimated to be $N_{est} = 3.9$, whilst the total expected number of events is $N_{exp} = 2.8 + 1.1\, N_\nu$.

To arrive at a first approximation, N_{est} can be assumed to be Poisson-distributed around N_{exp}. It can be checked explicitly that for the CELLO and ASP experiments, which dominate the statistical accuracy, this assumption yields confidence limits very close to those obtained more rigorously by Monte Carlo simulations, taking into account fluctuations of the background. Behrend et al. then obtain the central value

$$N_\nu = 1.0^{+2.9}_{-1.0} \quad \text{(all } e^+e^- \text{ experiments combined)} ,$$

and upper limits $N_\nu \leq 4.6$ (90% CL) and $N_\nu \leq 5.8$ (95% CL).

These single-photon e^+e^- annihilation searches have also been used to put upper limits on non-interacting supersymmetric particle final-state production rates, and thus put lower limits on $\tilde{\gamma}$ and $\tilde{\nu}$ masses (Hearty et al., 1987; Behrend et al., 1988).

4.3 Prospects for TRISTAN, the SLC, and LEP

At LEP it is expected that the Z total width Γ^Z_{tot} will be measured with an uncertainty of $\delta\Gamma_{tot} \lesssim \pm 50$ MeV (Altarelli et al., 1986). This is adequate for neutrino counting, as each neutrino species (with $m_\nu \approx 0$) contributes with $\delta\Gamma^Z_{tot} \approx 170$ MeV; thus the uncertainty should be $\delta N_\nu \approx \pm 0.4$. This precision would then allow us to investigate $Z \to \nu_i\bar{\nu}_i$ decays into possibly massive $\geq$ 4th-generation neutrinos with masses up to $m_\nu \approx 30$ GeV.

It is important to reduce the uncertainty $\delta\Gamma_{tot}$ or δN_ν as far as possible, as at the level of $\delta N_\nu < 1.0$ neutrino units, the neutrino counting methods become sensitive to $Z \to \tilde{\nu}\tilde{\nu}$ decays. For a massless sneutrino, the partial rate $\delta\Gamma_Z(Z \to \tilde{\nu}\tilde{\nu}) = 1/2\,\delta\Gamma_Z(Z \to \nu\bar{\nu}) \approx 85$ MeV, and for increasing $m_{\tilde{\nu}}$ it is suppressed by a kinematics factor $(1 - 4m^2_{\tilde{\nu}}/m^2_Z)^{3/2}$. A precision of $\delta N_\nu \approx \pm 0.4$ should make the SLC or LEP sensitive to $m_{\tilde{\nu}} \lesssim 20$ GeV, provided the three sneutrinos are mass-degenerate and that there are only three massless neutrinos. Otherwise, there is a possible trade-off between a possible $\geq$ 4th-generation massive neutrino and massive sneutrinos.

The direct counting method, i.e. by measuring the cross-section of $e^+e^- \to \gamma\nu\bar{\nu}$, is probably more adequate if such a good precision $\delta\Gamma^Z_{tot}$ cannot be achieved directly, as may be the case with the SLC. The rate of $\gamma\nu\bar{\nu}$ events should be measured a few GeV above the Z peak. Figure 19a shows the expected cross-section for $e^+e^- \to \gamma\nu\bar{\nu}$ versus $\sqrt{s}$, for single photons in the (20–160)° polar-angle range, with $E_\gamma \geq 20\%\ E_{beam}$ (Burke, 1987). Figure 19b shows the photon energy spectra in 2 GeV steps from $\sqrt{s} = 94$ to 104 GeV ($m_Z = 92$ GeV is assumed) (Simopoulou, 1986). As shown in Fig.19a, the cross-sections at the SLC and LEP will be $\sim 10^3$ times larger than at present PEP and PETRA energies, yielding $\sim 10^3$ single-photon events for similar acceptances and for a sensitivity of 100 pb^{-1}. Note that the gain over the present situation is already substantial at TRISTAN, up to a factor of ≈ 6 for $\sqrt{s} = 68$ GeV. In the $\sqrt{s}\,(e^+e^-) = 100$ GeV region, the interesting photon energy range is ~ 2 to ~ 14 GeV (Fig. 19b). The bremsstrahlung spectrum does not fall off as sharply as it does below the Z peak; in fact it has a bump due to the recoil on-shell Z. This makes the counting rate rather insensitive to the threshold cut and to the absolute energy-scale uncertainties. For this method to work, as already discussed, a hermetic detector is, however, needed in order to guarantee the production of a single photon accompanied by only non-interacting particles ($\nu\bar{\nu}$, $\tilde{\nu}\tilde{\nu}$, $\tilde{\gamma}\tilde{\gamma}$, etc.). This is not needed for N_ν determination from Γ^Z_{tot} obtained by an event-rate measurement in an energy scan across the Z peak.

5. LIMIT ON THE NUMBER OF NEUTRINO TYPES FROM $p\bar{p} \to Z\,(\to \nu_i\bar{\nu}_i)$ + JET

5.1 The method

This method, first suggested by Denegri (1984) and by Chaichian and Hayashi (1984), is based on $p\bar{p} \to Z$ + jet production followed by $Z \to \nu\bar{\nu}$, which is the QCD analogue of the QED process

$e^+e^- \to Z + \gamma$. The simplest Z + jet QCD gluon-bremsstrahlung production mechanism is represented by diagram (a) in Fig. 20. A high transverse momentum Z is produced recoiling against a (gluon) jet, with the Z decaying (invisibly) into neutrino pairs. Topologically this is a large missing-transverse-energy (E_T^{miss}) monojet event. The analogous W + jet production mechanism is represented by diagram (b) in Fig. 20.

The average Z transverse momentum $p_T^Z \approx E_T^{jet}$, balancing the recoil jet transverse energy generated by QCD radiative effects, is ≈ 8.5 GeV/c at $\sqrt{s} = 630$ GeV (Stubenrauch, 1987; Albajar et al., 1988a; Ansari et al., 1987b). High-p_T Z production is needed in this method in order to have an adequate experimental signature and a good background rejection. A $Z \to \nu\bar{\nu}$ decay with a low p_T^Z cannot be detected in a $p\bar{p}$ collision, since a longitudinal missing energy cannot be measured in hadron colliders because numerous beam fragments always escape detection in the beam pipes. Missing transverse energy can, however, be detected. It shows up as an energy/momentum imbalance in the transverse plane. For a significant missing transverse energy, a cut is however required, which depends on the specific features of the apparatus. For example, $E_T^{miss} \geqslant 15$ GeV in the UA1 experiment (CERN), and $\geqslant 25$ GeV in experiments UA2 (CERN) (before upgrading) and CDF (Fermilab). The large-E_T recoil jet thus provides a selective hardware trigger—which is essential in view of the large $p\bar{p}$ event rates—and a topological event signature.

The neutrino counting Z mode of diagram (a) in Fig. 20 is connected directly to the observable $Z \to e^+e^-$ decay mode as follows:

$$\frac{d\sigma}{dE_T^{jet}}\left[p\bar{p} \to Z\left(\to \sum_1^{N_\nu} \nu\bar{\nu}\right) + \text{jet} + X\right] = \frac{N_\nu\,\Gamma(Z \to \nu\bar{\nu})}{\Gamma(Z \to e^+e^-)}\,\frac{d\sigma}{dE_T^{jet}}\,[p\bar{p} \to Z(\to e^+e^-) + \text{jet} + X]$$

$$= N_\nu\,\frac{1}{1 - 4\sin^2\theta_w + 8\sin^4\theta_w}\,\frac{d\sigma}{dE_T^{jet}}\,.$$

The ratio of $Z \to \nu\bar{\nu}$ (for one neutrino flavour) to $Z \to e^+e^-$ partial rates is very close to 2; for $\sin^2\theta_w = 0.230$ it is equal to 1.99.

The above relation shows explicitly the dependence on N_ν and allows us, in principle, to normalize the expected monojet signal to observed $Z \to e^+e^-$ decays. In practice, however, as the cross-section for $Z \to e^+e^-$ is smaller by a factor of ~ 6 than the neutrino signal [$BR(Z \to e^+e^-) \approx 3\%$, whilst $BR(Z \to \Sigma\,\nu\bar{\nu}) \approx 18\%$ for $N_\nu = 3$], the expected signal is estimated using the observed $W(\to e\nu)$ + jet [diagram (b) in Fig. 20] differential cross-section shape $(1/\sigma_W)\,(d\sigma_W/dp_T^W)$ shown in Fig. 21 (Stubenrauch, 1987; DiLella, 1987). The rate of $W(\to e\nu)$ + jet is comparable to the expected neutrino signal, as the W and Z total production cross-sections are in the ratio $\sigma_W/\sigma_Z \sim 3.5$ (Altarelli et al., 1984), which is partially compensated by the branching ratios $BR(W \to e\nu) \approx 9\%$ and $BR(Z \to \Sigma\nu\bar{\nu}) \approx 18\%$ for $N_\nu = 3$. The predicted $E_T^{jet} \approx p_T^{W,Z}$ shapes are very similar, with $\langle p_T^Z \rangle$ being about 15% larger than $\langle p_T^W \rangle$ (Altarelli et al., 1984).

As in the case of $e^+e^- \to \gamma\nu\bar{\nu}$, it is necessary not only to detect the jet but also to control the non-interacting system against which it is recoiling. This is more complicated in $p\bar{p}$ interactions than in $e^+e^- \to \gamma\nu\bar{\nu}$, as numerous low-$p_T$ hadronic beam-fragments are now present. They partly escape

detection at low angles to the beams and through the beam pipes, and thus can generate an imbalance in the transverse plane.

The most dangerous instrumental background is, however, provided by hard parton–parton scattering, where one of the jets either escapes detection or is not recognized as a jet. This occurs if a jet points towards a crack or a dead region in the apparatus, or if it is produced at small forward angles. Hermetic calorimetry extending to small angles to the beams is essential for this search. The threshold of $E_T^{jet} \approx E_T^{miss}$ detection/selection is, in fact, set by these two-jet fluctuations. In conclusion, to control the instrumental backgrounds a high $E_T^{jet} \approx E_T^{miss}$ cut-off is needed, i.e. the jet E_T (or event E_T^{miss}) is also the main background rejection criterion.

This method also requires muon detection and momentum measurement. A $W(\rightarrow \mu\nu)$ + jet event [diagram (b), Fig. 20], with the muon escaping detection, easily fakes a $Z(\rightarrow \nu\bar{\nu})$ + jet event owing to the confusion caused by the always-present beam fragments. The cross-sections for both processes are comparable at the same E_T^{jet}, as previously explained, whilst the W and Z (and therefore the recoil jet) transverse momentum distributions are almost the same.

Hermetic photon detection is also needed in order to keep the γ + (gluon) jet final states under control. The direct-photon jet production rate is somewhat larger than the Z + jet signal at large $E_T^{\gamma} \approx p_T^Z \approx E_T^Z \approx E_T^{jet} \geqslant 20$ GeV (Albajar et al., 1988a).

Other physics backgrounds more closely related to specific features of the apparatus are discussed in the following.

5.2 Results from UA1

Monojet events with a significant E_T^{miss} have been detected and analysed by the UA1 experiment at the CERN $p\bar{p}$ Collider (Albajar et al., 1987b). This analysis gives a limit on additional neutrino species of $\Delta N_\nu < 7$. We now discuss this result and the limitations of the method.

A typical monojet event observed by UA1 is shown in Fig. 22. The jet, with a large transverse energy, $E_T \approx 43$ GeV, is clearly visible in both the central tracking detector and in the calorimeters. All soft-particle tracks or calorimetric cells with p_T or $E_T \leq 1$ GeV produced with the hard collision are suppressed in this display in order to exhibit the monojet topology of the event more clearly.

The upper limit on N_ν is obtained by comparing the observed event numbers and jet E_T spectra with theoretical expectations, once the known instrumental and physics backgrounds have been subtracted. The main instrumental backgrounds are cosmics, beam-halo interactions, and fluctuations in the calorimeter response to large-E_T dijet events. In UA1, the calorimetric coverage extends down to 0.2° from the beam lines. Dijet fluctuations are estimated from detailed Monte Carlo studies of the apparatus and of the experimental E_T^{miss} distribution. The E_T cut-off is in the $E_T^{jet} \approx E_T^{miss}$ 10 to 15 GeV range. Cosmics and halo events are rejected through appropriate technical cuts and by careful studies of events on interactive graphics displays (for example, Giraud-Héraud, 1988).

The expected Standard Model sources of genuine events of large E_T^{miss} are $W \rightarrow \tau\nu$ decays, W + jet events [diagram (b) of Fig. 20] where the $W \rightarrow e, \mu, \tau + \nu$ decay products overlap the jet, and heavy-flavour production $c\bar{c}$, $b\bar{b}$, or possibly $t\bar{t}$, followed by a semileptonic decay. The $W \rightarrow e\nu$ decays are easily recognized and removed. These various physics backgrounds have been Monte Carlo generated, and the UA1 apparatus response has been fully simulated.

UA1 observes a total of 56 events containing one (or more) high-E_T jets ($E_T > 12$ GeV), with an (isolated) E_T^{miss} measured at a $\geq 4\sigma$ significance level (Albajar et al., 1987a,b). Most of these events are monojets (53 out of 56 events). The majority are due to $W \to \tau\nu$ production followed by a $\tau \to$ hadrons + ν decay. A τ-likelihood (L_τ) is assigned to each event on the basis of jet collimation and jet charged-particle multiplicity (Albajar et al., 1987a). The scatter plot of L_τ versus the jet E_T is shown in Fig. 23. Most of the τ decays are removed by an $L_\tau < 0$ cut, which leaves a sample of 22 relatively broad monojets and 2 dijet events. These events are then interpreted in terms of: residual $W \to \tau\nu$ decays; fluctuations of detector response to dijet production; possible heavy-flavour ($c\bar{c}$, $b\bar{b}$ contributions; and high-p_T W and Z production, this last being the signal searched for.

Including the effect of the $\geq 4\sigma$ significance selection cut on E_T^{miss}, the net acceptance of UA1 to detect a E_T^{miss} event from $Z \to \nu\bar{\nu}$ is 1.8 %. This gives approximately 2.0 expected events from $Z \to \nu\bar{\nu}$ for each neutrino species. Apart from the $W \to \tau\nu$ events, this is the largest source of high-E_T monojets in the UA1 signal region. All the known Standard Model sources, including $Z \to \nu\bar{\nu}$ with $N_\nu = 3$, account for 21 ± 5 events, to be compared with the 24 events observed. The error on the expected number of events includes all absolute normalization and Monte Carlo simulation uncertainties. The E_T^{jet} and E_T^{miss} distributions for this sample are shown in Figs. 24a,b. The solid curve is the sum of expected contributions. The agreement between data and Monte Carlo expectations is satisfactory.

Because of the limited statistics, UA1 does not yet determine N_ν by this method, but rather gives an upper limit. From the number of events observed at $E_T^{jet} < 40$ GeV compared with the predicted one, the limit on the number of neutrino species is (Albajar et al., 1987b)

$$N_\nu < 10 \text{ at a } 90\% \text{ CL} .$$

In Fig. 25 the expected contribution for seven extra neutrino species is compared with the data. The upper limit on N_ν determined by this method is comparable with the one from individual e^+e^- experiments.

5.3 Discussion and future prospects

The main limitations of this method are the following.

1) The production of a high-p_T Z represents only a small fraction of the total Z production cross-section ($\sigma_Z \approx 1.6$ nb at $\sqrt{s} = 630$ GeV). A QCD calculation by Altarelli et al. (1984) predicts $(4 \pm 1.5)\%$ of Z's produced with $p_T^Z > 30$ GeV/c at $\sqrt{s} = 630$ GeV. The observed p_T^W distribution (shown in Fig. 21) confirms the validity of this QCD expectation (Stubenrauch, 1987; Ansari et al., 1987b; Albajar et al., 1988a). There is an additional suppression factor of ~ 5 for the $Z \to \nu_i\bar{\nu}_i$ decay branching ratio of $\approx 18\%$ for $N_\nu = 3$. Each additional neutrino type increases this branching ratio by $\leq 6\%$. With present experimental sensitivities ($\lesssim 1$ event per picobarn), only a few events are thus expected, and the main limitation is statistical.

This is, however, a direct counting method, and a significant part of the error is due to the uncertainty in the expected signal, i.e. in the absolute production rate of high-p_T Z's, as is visible in Fig. 21. The theoretical uncertainty in the total Z production cross-section and in the fraction of events at large p_T (> 30 GeV/c) is approximately 30%. This is due to the various possible choices of structure functions, of the value of α_s (or Λ_{QCD}), and of the Q^2 scale that is appropriate to high-p_T W

and Z production (Altarelli et al., 1984, 1985). Normalizing the expected theoretical p_T^Z distribution to the observed rates of $Z \to e^+e^-$, $\mu^+\mu^-$ + jet events, or of $W \to e\nu,\mu\nu,\tau\nu$ + jet events, certainly helps. None of these cross-sections is, however, larger than the $Z(\to \nu\bar{\nu})$ + jet signal, as already mentioned. Ultimately, it is the systematics in this absolute normalization that limits the accuracy on N_ν in this method.

2) The other limitation is the uncertainty in the expected number of known physics background events. The uncertainty is either in the absolute cross-section or in the kinematical confusion region between the various processes.

The production of a $W \to \tau\nu$ followed by $\tau \to \nu_\tau$ + hadrons can be normalized to the observed $W \to e\nu$ cross-section. It can be discriminated against by selecting monojets of charge multiplicity greater than 4 or 5. With a good apparatus-simulation Monte Carlo, this contribution to the topological confusion region can be estimated reliably.

A more difficult background is the high-p_T W production, where the W decay products e, μ, or τ overlap the recoil jet. Because of the W decay neutrino, this fakes a monojet event with large E_T^{miss}. The amount of overlap depends on the granularity of the apparatus and on the muon-recognition capability. The estimate of this background depends on the realism of apparatus-simulation Monte Carlos, and on having sufficient statistics of high-p_T W events to tune experimental spectra. In the signal region of UA1, for example, this type of background is estimated at approximately 2.0 events, which is comparable with the contribution of one neutrino species (Albajar et al., 1987b).

3) Another source of systematic error in the accepted signal cross-section and in the known physics backgrounds is the uncertainty in the energy calibration of the detector for hadronic jets. Fortunately, most of the signal is concentrated in the 20 GeV $< E_T^{jet} <$ 40 GeV range (Figs. 21 and 23), where good control of the jet response is provided by τ-jets from $W \to \tau\nu$, with $\tau \to$ hadrons + ν. These τ decays are constrained to reproduce the known $W(\to e\nu)$ mass.

Beyond the simplest extension of the Standard Model with additional neutrino families, another possible source of monojet events is the production of a fourth-generation heavy lepton from $W \to L\nu$ (Albajar et al., 1988a), or of supersymmetric particles. If present, these contributions would only tend to reduce the limit on N_ν, as they compete for the same number of observed events. The absence of excess E_T^{miss} events has been used by UA1 to put lower bounds on the masses of the scalar lepton, the $\tilde{q}$, and the $\tilde{g}$ (Albajar et al., 1987b,c).

6. LIMITS ON THE NUMBER OF LIGHT NEUTRINOS FROM THE MEASUREMENT OF $R = \sigma(W \to \ell\bar{\nu})/\sigma(Z \to \ell\bar{\ell})$

6.1 The method

The number of $W \to \ell\bar{\nu}$ and $Z \to \ell\bar{\ell}$ events observed in experiments UA1, UA2, or CDF is sensitive, through the W and Z leptonic branching ratios, to additional open channels such as $W \to t\bar{b}$ and $Z \to \nu_i\bar{\nu}_i$. The absolute production rates themselves, $\sigma(W \to \ell\bar{\nu})$ and $\sigma(Z \to \ell\bar{\ell})$, are, however, not suitable for deducing N_ν directly, as the uncertainties are too large. This is due, on the one hand, to the $\sim$ 30% spread in the theoretical predictions on W and Z production rates (Altarelli et al., 1984, 1985), and on the other hand to the systematic uncertainty in the experimental luminosity, which is, for example, $\approx$ 8% for UA2 and $\approx$ 10% for UA1. What is considered instead—as was initially suggested by Cabibbo (1983)—is the ratio

$$R = \sigma(W \to \ell\bar{\nu})/\sigma(Z \to \ell\bar{\ell}) = (\sigma_W/\sigma_Z)BR(W \to \ell\bar{\nu})/BR(Z \to \ell\bar{\ell}) \ ,$$

as in this ratio most of the experimental and theoretical uncertainties cancel. The number N_ν of neutrino species clearly affects the $Z \to \ell\bar{\ell}$ branching ratio directly. The ratio R, however, also depends significantly on the t-quark mass if $45 < m_t < 75$ GeV, as for $m_t < 45$ GeV both the $Z \to t\bar{t}$ and the $W \to t\bar{b}$ channels are open, whilst for $45 < m_t < 75$ GeV, only $W \to t\bar{b}$ remains (Denegri, 1986; Halzen, 1986).

The (t-quark mass-dependent) central value and upper limit on N_ν is obtained from the comparison of the directly measured value of R with its theoretical expectation at the corresponding c.m. energy. The latter can be expressed in terms of the total and partial widths of the W and Z as follows:

$$R_{th} = \left[\frac{\sigma_W}{\sigma_Z}\right] \left[\frac{\Gamma^W_{e\nu}\,\Gamma^Z_{tot}}{\Gamma^Z_{ee}\,\Gamma^W_{tot}}\right] \equiv R_\sigma \cdot R_\Gamma\,(m_t, \Delta N_\nu) \ . \qquad (6.1)$$

The ratio of total production cross-sections R_σ can be reliably calculated in QCD and is a slowly varying function of $\sqrt{s}$, whilst the second term R_Γ, which is predicted by the electroweak Standard Model, contains all the dependence on the number of neutrino families and on the t-quark mass through the ratio $\Gamma^Z_{tot}/\Gamma^W_{tot}$.

In conclusion, this method consists in measuring R, assuming that all terms on the right-hand side of Eq. (6.1) are known (in particular Γ^W_{tot}), except for Γ^Z_{tot}. This then allows us to determine Γ^Z_{tot} indirectly, and therefore N_ν. In the following, we briefly discuss each of these points.

6.2 Experimental measurements of R

The collider experiments UA1 and UA2 have measured the ratio R at $\sqrt{s} = 630$ GeV (Albajar et al., 1987d; Ansari et al., 1987a), and have evaluated the uncertainties originating from the relative W and Z selection and detection efficiencies, from the background subtraction, and from the statistical error in the number of observed events. The results of the two experiments have been combined (Albajar et al., 1987d) using a maximum likelihood method, leading to

$$R = 8.4^{+\,1.2}_{-\,0.9}$$

and

$$R < 10.1 \ (90\%\ \text{CL}) \ ,$$

$$R < 10.5 \ (95\%\ \text{CL}) \ .$$

The uncertainties in these measurements are predominantly of statistical origin, owing to the limited number of Z events. As discussed in the following, it is this experimental error $\delta R/R \approx 14\%$ that is at present the main limitation in determining N_ν. With the advent of ACOL at the CERN Collider, these errors should be substantially reduced, and independent measurements at $\sqrt{s} = 1.8$ TeV should soon be expected from the Fermilab Collider.

6.3 Standard Model predictions for R

6.3.1 Determination of $R_\Gamma = \Gamma^W_{e\nu}\Gamma^Z_{tot}/\Gamma^Z_{ee}\Gamma^W_{tot}$

The possible additional neutrinos are assumed to be light with respect to the Z, which is here produced on-shell. This allows us to neglect any phase-space suppression in $Z \to \nu\bar{\nu}$ (for $m_\nu < 10$ GeV the suppression does not exceed 4%). It is also assumed that the charged-lepton partners (L_i) of these additional neutrinos, and the quarks of the same generations (Q_i), are heavy enough for their contribution to the W and Z total widths to be neglected, i.e. $W \to L_i\bar{\nu}_i$ or $Z \to Q_i\bar{Q}_i$ decays are kinematically forbidden. In subsection 6.5 we will discuss what happens if this requirement is relaxed. The ratio R_Γ depends on the various partial decay-widths of the W and Z. These can all be expressed in terms of the two partial widths:

$$\Gamma^W_{e\nu} = \frac{G_F}{6\pi\sqrt{2}} m_W^3 , \qquad \Gamma^Z_{\nu\nu} = \frac{G_F}{12\pi\sqrt{2}} m_Z^3 . \tag{6.2}$$

More specifically, if we neglect the masses of all fermions except the t-quark, the various partial rates are:

$$\Gamma^W_{\mu\nu} = \Gamma^W_{\tau\nu} = \Gamma^W_{e\nu} \qquad \Gamma^Z_{ee} = \Gamma^Z_{\mu\mu} = \Gamma^Z_{\tau\tau} = C_\ell\Gamma^Z_{\nu\nu}$$

$$\Gamma^W_{ud} = \Gamma^W_{cs} = 3\cos^2\theta_C K\Gamma^W_{e\nu} \qquad \Gamma^Z_{dd} = \Gamma^Z_{ss} = \Gamma^Z_{bb} = 3 C_d K\Gamma^Z_{\nu\nu}$$

$$\Gamma^W_{us} = \Gamma^W_{cd} = 3\sin^2\theta_C K\Gamma^W_{e\nu} \qquad \Gamma^Z_{uu} = \Gamma^Z_{cc} = 3 C_u K\Gamma^Z_{\nu\nu}$$

$$\Gamma^W_{tb} = 3 PS_W(m_t) K_W(m_t)\Gamma^W_{e\nu} \qquad \Gamma^Z_{tt} = 3 C_u PS_Z(m_t) K_Z(m_t)\Gamma^Z_{\nu\nu} .$$

Here θ_C is the Cabbibo angle, and C_ℓ, C_u, and C_d are twice the axial and vector $(c_A^2 + c_V^2)$ $Z \to f\bar{f}$ couplings for charged-leptons, and for u-type and d-type quarks, respectively; they are given in Table 4 (Albert et al., 1980); K is the final-state QCD radiative correction factor $(1 + \alpha_s/\pi)$; $K_W(m_t)$ and $K_W(m_t)$ are the t-quark mass dependent QCD radiative corrections to the processes $W \to t\bar{b}$ and $Z \to t\bar{t}$ respectively (Alvarez et al., 1987; Kühn et al., 1986). The phase-space factors PS_W and PS_Z include also a V–A contribution (Albert et al., 1980).

To evaluate the widths, the Standard Model prediction of the W and Z masses (Marciano, 1987) is needed:

$$m_W = 38.68 \pm 0.03 \text{ GeV}/\sin\theta_w \qquad m_Z = m_W/\cos\theta_w .$$

With $\sin^2\theta_w = 0.230 \pm 0.005$, which is the present world average (Amaldi et al., 1986; Costa et al., 1988), these relations give

$$m_W = 80.7 \text{ GeV} , \qquad m_Z = 91.9 \text{ GeV} ,$$

which is in excellent agreement with values measured in UA1 and UA2 (Ansari et al., 1987a; Perrault, 1987; Locci, 1987; Albajar et al., 1988a).

Figure 26a shows the total widths Γ^W_{tot} and Γ^Z_{tot} as a function of m_t, for three neutrino flavours. Each additional massless neutrino adds $\approx$ 170 MeV to Γ^Z_{tot}. The total variation of Γ^W_{tot} as a function of m_t is almost 700 MeV. From relations (6.2), a variation of m_W and m_Z by $\pm 1\%$ implies a $\pm 3\%$

variation of partial and total widths. However, R_Γ is independent of the mass scale, if expressed in terms of m_t/m_W, and depends very slightly on $\sin^2\theta_w$, varying by $< 0.5\%$ over the allowed range of $\sin^2\theta_w$. The variation of R_Γ with m_t is shown in Fig. 26b for $N_\nu = 3$, 4, and 5; the step-like behaviour is due to the ratio of the total widths shown in Fig. 26a. For t-quark masses of 50 and 100 GeV, the values of R_Γ (for $N_\nu = 3$) are 2.74 and 3.23, respectively.

6.3.2 Evaluation of R_σ

The second theoretical input in this method is the ratio R_σ of the total cross-sections, which can be quite reliably calculated in QCD. None the less, R_σ is not known with a precision comparable to that of R_Γ. It suffers from uncertainties in $\sin^2\theta_w$ and, more importantly, in the structure functions relating the partonic and hadronic cross-sections (Altarelli et al., 1984, 1985; Colas et al., 1988; Diemoz et al. 1988). Simplifying, R_σ can be written as:

$$R_\sigma = \frac{\sigma_W}{\sigma_Z} \approx \frac{2\, f_{u\bar{d}}\,(m_W^2/s)\,|V_{ud}|^2}{C_u\, f_{u\bar{u}}\,(m_Z^2/s) + C_d\, f_{d\bar{d}}\,(m_Z^2/s)} \quad , \tag{6.3}$$

where $f_{q\bar{q}}(\tau) = \tau(dL^{q\bar{q}}/d\tau)$ are the appropriate partonic luminosities, i.e. constrained products of quark densities, and $\sqrt{s}$ is the $p\bar{p}$ c.m. energy. This expression shows explicitly the dependence of R_σ on the structure functions in $\tau(dL^{q\bar{q}}/d\tau)$, and on $\sin^2\theta_w$, through $m_Z - m_W$ and the coefficients C_u and C_d (Table 4).

The quark densities, for valence and sea u- and d-quarks, evaluated at $Q^2 = m_W^2$ according to the parametrization of GHR (Glück et al., 1982), DO (Dukes and Owens, 1984), EHLQ (Eichten et al., 1984) and DFLM (Diemoz et al., 1988), are shown in Fig. 27. Figure 28 shows the variation of R_σ at $\sqrt{s} = 630$ GeV as a function of $\sin^2\theta_w$, for these different sets of structure functions evaluated at $Q^2 = m_{W,Z}^2$ (Colas et al., 1988). Theoretical expectations for R_σ at $\sqrt{s} = 630$ GeV vary from about 2.95 to 3.5.

As first suggested by Halzen (1986), it is, however, possible to reduce the uncertainty in R_σ using available experimental data on deep-inelastic μ–N scattering at large Q^2. As can be seen from the relation (6.3), R_σ is determined essentially by the ratio d(x)/(u(x) of quark densities in the region around $x_W \approx m_W/\sqrt{s} = 0.13$ and $x_Z \approx m_Z/\sqrt{s} = 0.15$ at $\sqrt{s} = 630$ GeV (and at $x \approx 0.05$ for $\sqrt{s} = 1.8$ TeV). This ratio d(x)/u(x) is in turn given by the measured ratio of the F_2 deep-inelastic structure functions $F_2^n(x)/F_2^p(x)$.

The data on F_2^n/F_2^p of the two most recent μ-deuterium and μ-hydrogen deep-inelastic experiments, EMC (Aubert et al., 1987) and BCDMS (Milsztajn, 1989; Voss, 1987), are shown in Fig. 29 (Stubenrauch, 1987; Colas et al., 1988). They are compared with theoretical expectations for various sets of structure functions. In the region of interest ($0.05 \lesssim x \lesssim 0.4$ for UA1/2), both sets of data are between the EHLQ1 and DO1 curves and close to the GHR or DFLM expectations. According to Fig. 28, this means a value of R_σ between 3.1 and 3.4. The analysis of Colas et al. (1988) yields for R_σ,

$$R_\sigma \text{ (muon data)} = 3.25 \pm 0.10 \ ,$$

while a comprehensive analysis of neutrino deep-inelastic scattering data, from which the new set of structure functions (DFLM) is extracted (Diemoz et al., 1988), gives similarly

$$R_\sigma \text{ (neutrino data)} = 3.28 \pm 0.15 \ ,$$

As a central value appropriate for W and Z data at $\sqrt{s} = 630$ GeV, we take $R_\sigma = 3.25$, and as a reasonable lower limit, $R_\sigma = 3.15$. At this stage, we will treat the theoretical uncertainty in R_σ as a possible systematic shift. All the ingredients needed to obtain N_ν are now at hand.

6.4 Limit on N_ν as a function of m_t

The expected variation of $R = R_\sigma R_\Gamma$ as a function of m_t for $N_\nu = 3$ and 5 is shown in Fig. 30 for the central value $R_\sigma = 3.25$, with the hatched band showing the effect of the theoretical uncertainty $\delta R_\sigma = \pm 0.1$. A lower value of R_σ is clearly less constraining for N_ν. These theoretical predictions are compared with the combined UA1 and UA2 experimental central value and upper limits (90% and 95% CL) of R in the same figure. Figure 30 shows clearly that N_ν is limited to < 6, and for large t-quark masses the constraint is even stronger.

From the relation (6.1), the (indirect) upper limit on the Z total width is given by

$$\Gamma^Z_{tot} < \Gamma^Z_{tot,up}(m_t) = \left(\frac{R_{up}}{R_\sigma}\right) \left(\frac{\Gamma^Z_{ee}}{\Gamma^W_{e\nu}}\right) \Gamma^W_{tot}(m_t) \ .$$

where R_{up} is the experimental upper limit on R. If the measured central value R is used instead in this expression, it yields an indirect measure of Γ^Z_{tot} itself. The dependence of Γ^W_{tot} on m_t for three fermion generations is given in Fig. 26a. With this upper limit on the Z width, and if we assume that the excess over what is expected for three generations ($\Gamma^Z_{tot,3G}$, Fig. 26a) can only be due to new neutrino flavours, the upper limit on $\Delta N_\nu = N_\nu - 3$ as a function of m_t is given by

$$\Delta N_\nu < [\Gamma^Z_{tot,up}(m_t) - \Gamma^Z_{tot,3G}(m_t)]/\Gamma^Z_{\nu\nu} \ .$$

This limit is independent of the precise value of the Z mass.

Figure 31 shows the central value and the upper limit on N_ν as a function of m_t. The central value of N_ν is obtained from the measured central value of R and using the theoretical central value $R_\sigma = 3.25$. The upper limit on N_ν is obtained by taking the lower value $R_\sigma = 3.15$ from the possible systematic uncertainty range in R_σ, and combining it with the experimental 90% CL upper limit on R.

The conclusions are the following. Independently of the t-quark mass, the limits on the number of neutrinos are: $N_\nu < 5.5 \pm 0.5$ (90% CL) and $N_\nu < 6.3 \pm 0.5$ (95% CL) (Ansari et al., 1987a; Albajar et al., 1987d; Colas et al., 1988). The uncertainty in the upper limit reflects the theoretical uncertainty in R_σ, which is treated here as a systematic error. If the t-quark mass is higher than about 75 GeV, then according to this method, a fourth-generation light neutrino is rather unlikely, as is shown in Figs. 30 and 31. We will come back to this point in Section 7, when combining all the results, and discuss it quantitatively in the Appendix.

The central value N_ν itself is given by the central theoretical expectation $R_\sigma = 3.25$. As present UA1 results imply that $m_t > 45$ GeV (Albajar et al., 1988b), Fig. 31 then gives

$$N_\nu = 2.2^{+2.0}_{-1.4}{}^{+0.5}_{-0.4} \quad (\text{for } m_t = 50 \text{ GeV}) ,$$

$$N_\nu = 0.0^{+1.7}_{-1.3}{}^{+0.4}_{-0.3} \quad (\text{for } m_t = 100 \text{ GeV}) ,$$

where the first error comes from the experimental measurement of R and the second one from the theoretical uncertainty on R_σ.

Combining the two errors (as explained in the Appendix), we get:
for $m_t = 50$ GeV

$$N_\nu = 2.2^{+2.2}_{-1.5}$$

$$\text{and } N_\nu < 5.1 \quad (90\% \text{ CL})$$
$$< 5.8 \quad (95\% \text{ CL})$$

and for $m_t = 100$ GeV (or, more generally, for $m_t \geq m_W$)

$$N_\nu = 0^{+2.0}_{-1.3}$$

$$\text{and } N_\nu < 2.5 \quad (90\% \text{ CL})$$
$$< 3.1 \quad (95\% \text{ CL}) .$$

Incidentally, it may be worth noting here that, according to Fig. 30, if $m_t > 75$ GeV, the observed residual excess of $\Delta N_\nu < 0.4$ (at 95% CL) would exclude sneutrinos of mass $m_{\tilde{\nu}} < 20$ GeV, provided there are only three neutrino flavours and that the three sneutrinos are mass-degenerate.

6.5 Effects of a possible fourth-generation charged lepton or quark

How would the presence of fourth-generation fermions—a heavy lepton L or a b′ quark, modify these conclusions?

For a heavy lepton with the minimal mass $m_L = 41$ GeV allowed by UA1 (Albajar et al., 1987b), the total width Γ^W_{tot} in the denominator of Eq. (6.1) gets an additional contribution, $\delta\Gamma^W_{tot} = \Gamma(W \to L\nu_4) \approx 139$ MeV, while Γ^Z_{tot} in the numerator gets, in addition, $\delta\Gamma^Z_{tot} = \Gamma(Z \to \nu_4\nu_4) \approx 170$ MeV, as in this case $N_\nu \geq 4$ necessarily (we assume that $m_{\nu_4} \sim 0$). If there is no other fermion lighter than the W, the new upper limit on N_ν is given by the dashed curve in Fig. 32. One more neutrino flavour is allowed for any t-quark mass, i.e. the upper limit in Fig. 31 (shown as a shaded band in Fig. 32) moves up by about one neutrino unit. As m_L tends towards m_W, however, this limit on N_ν gradually falls back onto the one shown in Fig. 31.

The presence of a fourth-generation b′-quark, on the other hand, with $m_{b'} < m_Z/2$, contributes to Γ^Z_{tot} with a $Z \to b'\bar{b}'$ decay mode. This reinforces the limit on N_ν, as, within the measured excess Γ^Z_{tot} width, allowance must now be made for $Z \to b'\bar{b}'$. For $m_{b'} = 32$ GeV, the minimal mass allowed by UA1 (Albajar et al., 1988b), Γ^Z_{tot} gets $\delta\Gamma^Z_{tot} = \Gamma(Z \to b'\bar{b}') \approx 196$ MeV in addition to the ≈ 170 MeV from the $Z \to \nu_4\nu_4$ mode. If also $m_L > m_W$, the new limit is given by the dotted curve in Fig. 32. It drops by about 1.1 neutrino units for all m_t, and the t-quark mass would be severely

limited from above in this case. As $m_{b'}$ tends towards $m_Z/2$, this limit moves up towards the one shown in Fig. 31.

Finally, for $m_{b'} = 32$ GeV and $m_L = 41$ GeV (dash-dotted curve in Fig. 32), the limit accidentally almost coincides with the one for no L, no b′.

6.6 Conclusions on neutrino counting from $\sigma(W \to \ell\bar{\nu})/\sigma(Z \to \ell\bar{\ell})$ and future prospects

In conclusion, the measurement of R allows us to estimate the number of neutrino generations. The result depends on the t-quark mass. The upper bound that can be placed is no worse than $N_\nu < 6.0$ at 90% CL. A fourth-generation heavy lepton below the W mass would degrade this limit by at most one unit. A fourth-generation b′-quark could only strengthen the limit.

This method depends on the ratio of $W \to \ell\bar{\nu}$ and $Z \to \ell\bar{\ell}$ events observed. It is therefore much less affected by absolute normalization uncertainties, both experimental and theoretical, than are the direct counting methods. The present experimental error of $\delta R/R \approx 14\%$ is largely due to limited Z statistics. It corresponds to an uncertainty in N_ν of $\delta N_\nu^{exp} \approx \pm 1.8$ units. It can be reduced to about $\delta N_\nu \approx \pm 0.5$ units with a factor of ≥ 12 increase in statistics, when systematics takes over (in the experimental conditions of UA1). The theoretical uncertainty $\delta R_\sigma \approx \pm 0.10$, corresponding to a contribution of $\delta N_\nu^{th} \approx \pm 0.5$ units, is difficult to reduce without new data or new constraints on the structure functions.

It is none the less worth noticing that when going to Fermilab energies the dispersion of theoretical predictions for the ratio R_σ diminishes, as can be seen from Fig. 33. (The energy dependence of R_σ has been obtained with the EUROJET Monte Carlo; sea contributions are included.) This can be understood from Fig. 29, as at $\sqrt{s} = 1.8$ TeV the W and Z productions sample the structure functions at $x \approx 0.05$, and the ratios $F_2^n/F_2^p \sim \sigma_W/\sigma_Z$ come together with diminishing values of x. However, the uncertainty δR_σ cannot be significantly reduced until there are no more-constraining measurements of F_2^n/F_2^p at high Q^2 and low values of x (Fig. 29), and the heavy quark sea contributions are not better known, or until other ways are found to reduce the ambiguity due to structure functions, as discussed, for example, by Berger et al. (1988) or by Stubenrauch (1987) for the related experimental problems. The ultimate accuracy of this method for neutrino counting is therefore about $\delta N_\nu \approx \pm 0.7$ to ± 0.4 neutrino units, depending on the t-quark mass and the $p\bar{p}$ collision energy.

7. SUMMARY AND CONCLUSIONS

We have described four approaches for estimating the number of neutrino generations, the monojet method providing only an upper limit. Figures 34 and 35, and Table 5, summarize the results obtained.

The method based on the energy released in the SN1987A yields

$$N_\nu = 2^{+1.4}_{-0.7} .$$

The uncertainty in the total energy release from the collapse of the iron core contributes about 0.5 neutrino units.

The current measurements of the primordial abundances lead to

$$N_\nu = 2.4 \pm 0.8$$

if we assume that the ^{7}Li primordial abundance is given by the population-II stars. None of the fits with ^{7}Li abundance from population-I stars is good. The only acceptable one gives lower N_ν values.

The combined result from single-photon searches in all e^+e^- experiments gives a central value

$$N_\nu = 1.0^{+2.9}_{-1.0} \ .$$

For the combined result of UA1 and UA2, the central value of N_ν is

$$N_\nu = 2.2^{+2.2}_{-1.5} \quad (\text{for } m_t = 50 \text{ GeV}) \ ,$$

and

$$N_\nu = 0^{+2.0}_{-1.3} \quad (\text{for } m_t = 100 \text{ GeV}) \ .$$

The theoretical uncertainty in R_σ accounts for an error of half a unit.

The upper limits from laboratory experiments having a 95% CL are at the $N_\nu < 3$ to 5.8 level, depending on the mass of the t-quark. It is quite remarkable that these four different methods give estimates of the same order of magnitude, although in principle they are sensitive in a different way to particles other than light neutrinos.

The supernova luminosity is sensitive to any energy loss through the emission of other light particles such as axions (Mayle and Wilson, 1987; Raffelt and Seckel, 1988; Burrows et al., 1989).

The primordial nucleosynthesis depends on the number of relativistic degrees of freedom at ~ 0.75 MeV.

The e^+e^- and $p\bar{p}$ experiments limit the number of particles coupling to the Z, including, for instance, supersymmetric particles such as $\tilde{\nu}$ and $\tilde{h}$ of masses that are less than half the Z mass.

The agreement obtained indicates that these additional phenomena are not important and that the Standard Model is a good approximation of reality. Inside its framework, we could combine all our estimates. In order to do so, we minimize a global χ^2 constructed as explained in the Appendix. Our procedure of treating systematic errors of random Gaussian variables is justified by the number of different methods and assumptions used. Choosing the ^{7}Li abundance from population-II stars, this global minimization procedure leads to

$$N_\nu = 2.1^{+0.6}_{-0.4} \quad \text{for } m_t = 50 \text{ GeV}$$

and

$$N_\nu = 2.0^{+0.6}_{-0.4} \quad \text{for } m_t = 100 \text{ GeV}$$
$$\text{or, more generally, if } m_t \geq m_W,$$

with the 90% and 95% confidence limit of

$$N_\nu < 2.9 \text{ or } 2.7 \text{ (90\% CL) for } m_t = 50 \text{ GeV or } 100 \text{ GeV} ,$$
$$N_\nu < 3.2 \text{ or } 2.9 \text{ (95\% CL) for } m_t = 50 \text{ GeV or } 100 \text{ GeV}$$

respectively.

Taken at face value, these numbers would lead us to exclude, as being unlikely, the presence of a fourth generation and would suggest a relatively light t-quark mass. However, the χ^2 values obtained by four families (Table 6) are still acceptable and, as argued in the Appendix, this may be a more conservative approach. We therefore conclude that *in the framework of the Standard Model, at most four generations are allowed.*

It should be noted, however, that significant biases may exist. They are of various types. The Standard Model acts, to a certain extent, as an implicit constraint on the published experimental values, in particular in the case of primordial abundances. Moreover, direct counting experiments based on the rejection of events, such as the e^+e^- experiments, may be biased by an implicit intent to get rid of the 'background', which will yield a low value of the number of neutrinos.

Incidentally, with the ^{7}Li abundance from population-II stars, this global fit gives for the baryon cosmological density

$$\Omega_b h^2 = (1.61^{+0.16}_{-0.22}) \times 10^{-2}$$

with upper limits of

$$< 1.85 \times 10^{-2} \quad (90\% \text{ CL})$$
$$< 1.92 \times 10^{-2} \quad (95\% \text{ CL})$$

These four determinations of the number of neutrino species are subject to considerably different types of theoretical uncertainties. The supernova estimates suppose a knowledge of the binding energy of the collapsing star. The nucleosynthesis values rely mainly on the assumption that primordial ^{7}Li abundance is given by population-II stars. In addition to being less attractive, the other choice of using population-I for this purpose leads to a much poorer fit in the Standard Model. The final error also depends heavily on the assumed uncertainties in the modelling of H II regions when determining ^{4}He abundances. The e^+e^- result is rather direct, but relies on the assumption of a universal coupling between the neutrinos and the Z. The estimates are made for neutrinos whose masses are negligible as compared with the e^+e^- centre-of-mass energy (29 to 43 GeV). The present calculations do not yet take into account higher-order corrections (Berends et al., 1986), but the effect is expected to be small. The $p\bar{p}$ value also relies on universality and assumes that the neutrino masses are smaller than $\approx$ 10 GeV. It is based on the ratio R_σ of W to Z production, which is well understood in the framework of the parton model, and is rather well constrained by μ and ν deep inelastic scattering, in spite of current disagreement between the experiments. The $p\bar{p}$ value assumes that there are no significant contributions to Γ^W_{tot} and Γ^Z_{tot} beyond those expected from the Standard Model. The effect of a heavy lepton or a b′-quark modifies the limit by $\approx \pm 1$ unit.

In the near future, the major improvement may come from accelerators. While current accelerator values of N_ν are all based on indirect measurements of the Z total width (the present direct measurement of Γ^Z_{tot} by UA1/2 would provide a much looser limit, $N_\nu < 30$), the direct measurement of this width at the SLC or LEP with an expected accuracy of $\delta\Gamma^Z_{tot} \leqslant 50$ MeV should definitely settle the question of the number of neutrino species (for m_ν up to $\sim$ 30 GeV), and thereby

probably the number of fermion generations. Simultaneously, the discovery, or the absence, of a t-quark in the W mass region will clarify the picture for the determination of N_ν in $p\bar{p}$ collisions. In the meantime, a substantial improvement can be expected from the higher-statistics measurements of W and Z production being performed at the CERN and Fermilab $p\bar{p}$ colliders. The supernova estimate will probably not improve noticeably before we have the chance of detecting the neutrinos from a supernova in our galaxy. The primordial abundance determination may improve through a better understanding of the depletion of ^{7}Li, through more precise determinations of the nuclear cross-sections involved in its production, and through better measurements of the ^{4}He and D abundances. The Hubble Space Telescope to be launched in 1989 and the currently studied Far Ultraviolet Satellite Explorer (FUSE) will probably have a great impact on this subject during the coming decade.

Acknowledgements

For the astrophysical determination, we are grateful for discussions with S. Woosley, R. Schaeffer and S. Bludman.

The input on nucleosynthesis from J. Audouze, D. Schramm, J. Silk, G. Steigman, M. Turner, S. Vauclair and J.P. Zahn was greatly appreciated.

This work has been supported in part by the US Department of Energy under Contract No. DE-AC03-76SF00098.

REFERENCES

Aglietta, M., et al., 1987, Europhys. Lett. **3**, 1315 and 1321.

Albajar, C., et al., 1987a (UA1 Collab.), Phys. Lett. B **185**, 233.

Albajar, C., et al., 1987b (UA1 Collab.), Phys. Lett. B **185**, 241.

Albajar, C., et al., 1987c, (UA1 Collab.), Phys. Lett. B **198**, 261.

Albajar, C., et al., 1987d, (UA1 Collab.), Phys. Lett. B **198**, 271.

Albajar, C., et al., 1988a, (UA1 Collab.), 'Studies of the Intermediate Vector Boson Production and Decay in UA1 at the CERN Super Proton Synchrotron Collider', CERN-EP/88-168 (1988), to be published in Z. Phys. C.

Albajar, C., et al., 1988b, (UA1 Collab.), Z. Phys. C **37**, 489.

Albert, D., et al., 1980, Nucl. Phys. B **166**, 460.

Alcock, C., G. Fuller and G. Mathews, 1987, Astrophys. J. **320**, 439.

Alcock, C., G. Fuller, B. Myer and G. Mathews, 1988, Lawrence Livermore Lab. preprint

Alexeyev, E.N., et al., 1988, Phys. Lett. B **205**, 209.

Altarelli, G., R.K. Ellis, M. Greco and G. Martinelli, 1984, Nucl. Phys. B **246**, 12.

Altarelli, G., R.K. Ellis and G. Martinelli, 1985, Z. Phys. C **17**, 617.

Altarelli, G., et al., 1986, in *Physics at LEP*, eds. J. Ellis and R. Peccei (CERN 86-02, Geneva), Vol. 1, p. 3.

Alvarez, T., et al., 1987, Nucl. Phys. B **301**, 1.

Amaldi, U., et al., 1986, Phys. Rev. D **26**, 1385.

Ansari, R., et al., 1987a (UA2 Collab.), Phys. Lett. B **186**, 440.

Ansari, R., et al., 1987b (UA2 Collab.), Phys. Lett. B **194**, 158.

Applegate, J.H., C.J. Hogan and R.J. Scherrer, 1987, Phys. Rev. D **35**, 1151.

Arnison, G., et al., 1983a (UA1 Collab.), Phys. Lett. B **122**, 103.

Arnison, G., et al., 1983b (UA1 Collab.), Phys. Lett. B **126**, 398.

Arnison, G., et al., 1983c (UA1 Collab.), Phys. Lett. B **129**, 273.

Arnison, G., et al., 1983d (UA1 Collab.), Phys. Lett. B **134**, 469.

Aubert, J.-J., et al., 1987, Nucl. Phys. B **293**, 740.

Audouze, J. and B. Tinsley, 1976, Annu. Rev. Astron. and Astrophys. **14**, 43.

Audouze J., O. Boulade, G. Malinie and Y. Poilane, 1983, Astron. and Astrophys. **127**, 164.

Baade, D. and P. Magain, 1988, Astron. and Astrophys. **194**, 237.

Bagnaia, P., et al., 1983 (UA2 Collab.), Phys. Lett. B **129**, 130.

Bania, T.M., R.T. Rood, and T.L. Wilson, 1987, Astrophys. J. **323**, 30.

Banner, M., et al., 1983 (UA2 Collab.), Phys. Lett. B **122**, 476.

Barbiellini, G., B. Richter and J.L. Siegrist, 1981, Phys. Lett. B **106**, 414.

Barrow, J.D., 1983, Fundam. Cosmic Phys. **8**, 83-200.

Bartha, G., et al., 1986 (ASP Collab.), Phys. Rev. Lett. **56**, 685.

Behrend, H.J., et al., 1986 (CELLO Collab.), Phys. Lett. B **176**, 247.

Behrend, H.J., et al., 1988 (CELLO Collab.), Phys. Lett. B **215**, 186.

Berends, F.A., G.J.H. Burgers and W.L. Van Neerven, 1986, Phys. Lett. B **177**, 191.

Berger, E.L., F. Halzen, C.S. Kim and S. Willenbrock, 1988, Univ. Wisconsin report MAD/PH/400, ANL-HEP-PR-88-12.

Bionta, R.M., et al., 1987, Phys. Rev. Lett. **58**, 1494.

Blitz, L. and C. Heiles, 1987, Astrophys. J. Lett. **313**, L95.

Boesgaard, A.M. and G. Steigman, 1985, Annu. Rev. Astron. and Astrophys. **23**, 319.

Braunschweig, W., et al., 1988 (TASSO Collab.), Z. Phys. C. **38**, 331.

Brown, L. and D.N. Schramm, 1988, Astrophys. J. Lett. **329**, L103.
Burke, D.L., 1987, SLAC-PUB 4284, 1987.
Burrows, A., 1984, Astrophys. J. **283**, 848.
Burrows, A., 1987, Arizona State Univ., theory preprint 87-34; and Proc. Telemark 1987, eds. V. Barger et al. (World Scientific, Singapore), p. 28.
Burrows, A., M.S. Turner and R.P. Brinkmann, 1989, Phys. Rev. D **39**, 1020.
Cabibbo, N., 1983, in *Proc. 3rd Topical Workshop on Proton-Antiproton Collisions,* Rome, 1983, eds. C. Bacci and G. Salvini (CERN 83-04, Geneva), p. 567.
Carswell, R. et al.,1986. Preprint.
Chaichian , M. and M. Hayashi, 1984, Phys. Rev. **D30**, 243.
Clayton, D.D., 1985, Astrophys. J. **290**, 428.
Cline, D., D.N. Schramm and G. Steigman, 1987, Comments Nucl. Part. Phys. **17**, No. 3, 145.
Colas, P., D. Denegri and C. Stubenrauch, 1988, Z. Phys. C **40**, 527, and references therein.
Costa, G., et al., 1988, Nucl. Phys. B **297**, 244.
D'Antona, F. and I. Mazzitelli, 1983, Astron. and Astrophys. **138**, 431.
Dearborn, D.S.P., D.N. Schramm, and G. Steigman, 1986, Astrophys. J. **302**, 35.
Dearborn, D., D. Schramm, G. Steigman and T. Truran, 1989, 'The Shocking Development of Lithium (and Boron) in Supernovae', submitted to Astrophys. J.
Delbourgo-Salvador, P., C. Gry, G. Malinie and J. Audouze, 1985, Astron. and Astrophys. **150**, 53.
Denegri, D., 1984, CERN UA1 TN 84/03. (See also Denegri, D., 1985, CERN UA1 TN 85/28.)
Denegri, D., 1986, in *Proc. 6th Topical Workshop on Proton-Antiproton Collider Physics,* Aachen, 1986, eds. K. Eggert, H. Faissner and E. Radermacher (World Scientific, Singapore, 1987), p. 32.
De Rújula, A., 1987, Phys. Lett. **193**, 525.
Diemoz, M., F. Ferroni, E. Longo and G. Martinelli, 1988, Z. Phys. C **39**, 31.
DiLella, L., 1987, in *Proc. the Cargèse Summer Institute on Particle Physics,* 1987 (Plenum Press, Inc., New York), p. 556.
Dimopoulos, S., R. Esmailzadeh, H. Hall and G. Starkman, 1988a, Astrophys. J. **330**, 545.
Dimopoulos, S., R. Esmailzadeh, H. Hall and G. Starkman, 1988b, Phys. Rev. Lett. **60**, 7.
Dimopoulos, S., R. Esmailzadeh, H. Hall and G. Starkman, 1989, Nucl. Phys. B **311**, 699.
Dolgov, A.D., L.B. Okun' and V.I.Z. Zacharov, 1972, Nucl. Phys. B **41**, 197.
Dukes, D.W., and J.F. Owens, 1984, Phys. Rev. D **30**, 49.
Eadie, W.T., D. Drijard, F.E. James, M. Roos and B. Sadoulet, 1971, *Statistical Methods in Experimental Physics* (North Holland Publ. Co., Amsterdam-London).
Eichten, E., I. Hinchliffe, K. Lane and C. Quigg, 1984, Rev. Mod. Phys. **56**, 579.
Ellis, J., K. Enqvist, D.V. Nanopoulos and S. Sarkar, 1986, Phys. Lett. B **167**, 457.
Ellis, J., and K.A. Olive, 1987, Phys. Lett. B **193**, 525.
Feldman, G., 1986, MARK II/SLC Physics Working Group Note 02, Asilomar.
Ferlet, R., et al., 1980, Astrophys. J. **242**, 576.
Fernandez, E., et al., 1985 (MAC Collab.), Phys. Rev. Lett. **54**, 1118.
Ford, W.T., et al., 1986 (MAC Collab.), Phys. Rev. D **33**, 3472.
Fujimoto, M.I., et al., 1986, Astrophys. J. **305**, 246.
Fuller, G.M., C.R. Mathews and C.R. Alcock, 1988, Phys. Rev. D **37**, 1380.
Gaemers, K.J.F., R. Gastmans and F.M. Renard, 1979, Phys. Rev. D **19**, 1605.
Gamow, G., 1946, Phys. Rev. **70**, 572.
Gamow, G., 1948, Phys. Rev. **74**, 505.
Giraud-Héraud, Y., 1988, Thèse de doctorat d'État, Univ. de Paris-Sud (Orsay), Collège de France report, 88-01.

Glück, M., E. Hoffmann and E. Reya, 1982, Z. Phys. C **13**, 119.
Gry, C., C. Laurent and A. Vidal-Madjar, 1983, Astron. and Astrophys. **124**, 99.
Haines, T.J., 1987, Proc. Telemark IV: Neutrino Masses and Neutrino Astrophysics, Ashland, 1987 (World Scientific, Singapore, 1987), p. 63.
Halzen, F., 1986, Phys. Lett. B **182**, 388.
Hearty, C., et al., 1987 (ASP Collab.), Phys. Rev. Lett. **58**, 1711.
Hillebrandt, W., 1987, in *High-Energy Phenomena around Collapsed Stars*, ed. F. Pacini (Reidel Publ. Co., Dordrecht), p. 73.
Hirata, K., et al., 1987, Phys. Rev. Lett. **58**, 1490.
Hitlin, D., 1987, in *Proc. Int. Symp. on Lepton and Photon Interactions at High Energies*, Hamburg, 1987 (North-Holland Publ. Co., Amsterdam, 1988), p. 179.
Hobbs, L.M. and D.K. Duncan, 1987, Astrophys. J. **317**, 796.
Hobbs, L.M. and C. Pilachowski, 1986, Astrophys. J. Lett. **311**, L37–L40.
Hobbs, L.M. and C. Pilachowski, 1988, to be published in Astrophys. J.
Johnson, A.S., 1987, in *Proc. 22nd Rencontres de Moriond,* Les Arcs, 1987, eds. T. Monmerle and J. Tran Thanh Van (Editions Frontières, Gif-sur-Yvette), Vol. 1, p. 119.
Kawano, L., D. Schramm and G. Steigman, 1988 Astrophys. J. **327**, 750.
Krauss, L.M., 1987, Nature **329**, 689.
Kühn, J.H., A. Reiter and P.M. Zerwas, 1986, Nucl. Phys. B **272**, 560.
Kunth, D. and W.L.W. Sargent, 1983, Astrophys. J. **273**, 81.
Kunth, D., 1986, in Publ. of the Astronomical Society of the Pacific **98**, 984.
Lamb, D.Q., et al., 1987, to appear in *Supernova 1987A in the Large Magellanic Cloud, Proc. George Mason Workshop,* ed. M. Kafatos (Cambridge Univ. Press, New York).
Laurent, C., A. Vidal-Madjar and D.G. York, 1979, Astrophys. J. **229**, 923.
Locci, E., 1987, Proc. Int. Eur. Conf. on High-Energy Physics, Uppsala, 1987 (Univ. Uppsala, Sweden, 1987).
LoSecco, J.M., 1989, Phys. Rev. D **39**, 1013.
Ma, E. and J. Okada, 1978, Phys. Rev. Lett. **41**, 287.
Malone, R.C., M.B. Johnson and H.A. Bethe, 1975, Astrophys. J. **199**, 741.
Marciano, W., 1987, BNL report 40379, 'Weak Currents and Future Z-Mass Measurements', talk given at the 1987 SLAC Summer Institute Topical Conference.
Matzner, R.A., 1986, in Publ. of the Astronomical Society of the Pacific **98**, 1049.
Mayle, R. and J. Wilson, 1987, Lawrence Livermore Lab. preprint.
Michaud, G., G. Fontaine and G. Beaudet, 1984, Astrophys. J. **282**, 206.
Milsztajn, A., 1989, private communication; Thèse de doctorat d'État, Univ. de Paris-Sud (Orsay).
Olive, K.A., et al., 1981a, Astrophys. J. **246**, 557.
Olive, K.A., D.N. Schramm and G. Steigman, 1981b, Nucl. Phys. B **180**, 497.
Pagel, B.E.J., et al., 1986, in Publ. of the Astronomical Society of the Pacific **98**, 1005.
Pandharipande, V.R., 1971, Nucl. Phys., A **178**, 123.
Peimbert, M., 1986, in Publ. of the Astronomical Society of the Pacific **98**, 1057.
Penzias, A. A. and R.W. Wilson, 1965, Astrophys. J. **142**, 419.
Perrault, C., 1987, Thèse de doctorat, LAPP (Annecy); see also Tables of Particle Properties, 1988, Phys. Lett. B. 204.
Piran, T., et al., 1988, *Proc. Moriond Conf. on Dark Matter,* eds. J. Audouze and J. Tran Thanh Van (Éditions Frontières, Gif-sur-Yvette), p. 453.
Pomanski, A., 1987, communication at the 22nd Rencontres de Moriond, Les Arcs, unpublished.
Raffelt, G. and D. Seckel, 1988, Phys. Rev. Lett. **60**, 1793.

Rebolo, R., P. Molaro and J.E. Beckman, 1988a, Astron. **192**, 192.
Rebolo, R. et al., 1988b, Astron. and Astrophys. **193**, 193.
Rood, R.T., T.M. Bania and T.L. Wilson, 1984, Astrophys. J. **280**, 629.
Sadoulet, B., 1988, in *Proc. 15th SLAC Summer Institute on Particle Physics,* ed. E.C. Brenan, (Stanford University, Calif.), p. 277.
Sahu, K.C., M. Sahu and R. Pottasch, 1988, Astron. and Astrophys. Lett. **207** L1.
Schaeffer, R., 1984, in *École d'été de Physique des particules,* Gif-sur-Yvette (Éditions CNRS, Paris), p. 19.
Schaeffer, R., Y. Declais and S. Jullian, 1987, Nature **330**, 142.
Schramm, D.N., 1987a, Comments Nucl. Part. Phys. **17**, 239.
Schramm, D.N., 1987b, in *Proc. Int. Symp. on Lepton and Photon Interactions at High Energies,* Hamburg, 1987 (North-Holland Publ. Co., Amsterdam, 1988), p. 471.
Shields, G.A., 1987, in *Proc. 13th Texas Symp. on Relativistic Astrophysics,* Chicago, 1986, ed. M.L. Ulmer (World Scientific, Singapore), p. 192.
Simopoulou, E., 1986, in *Physics at LEP,* eds. J. Ellis and R. Peccei (CERN 86–02, Geneva), Vol. 1, p. 197.
Spergel, D.N., et al., 1987, Science **237**, 1471.
Spite, F. and M. Spite, 1982, Nature **297**, 483.
Steigman, G., K.A. Olive, D.N. Schramm and M.S. Turner, 1986, Phys. Lett. B **176**, 33.
Steigman, G., 1987, in *Proc. 13th Texas Symp. on Relativistic Astrophysics,* Chicago, 1986, ed. M.P. Ulmer (World Scientific, Singapore), p. 173.
Steigman, G., G. Gallagher and D.N. Schramm, 1989, to be published in Comments on Astron. and Astrophys.
Stubenrauch, C., 1987, 'Étude de la production des bosons W et Z dans l'expérience UA1', Thèse de doctorat d'État, Univ. de Paris-Sud (Orsay), published as Note CEA–N–2532.
Trimble, V., 1987, in *High-Energy Phenomena around Collapsed Stars,* ed. F. Pacini (Reidel Publ. Co., Dordrecht), p. 105.
Van Der Velde, J.C., 1988, *Proc. Moriond Conf. on Dark Matter,* eds. J. Audouze and J. Tran Thanh Van (Éditions Frontières, Gif-sur-Yvette), p. 429.
Vauclair, S., 1987, Observatoire Midi-Pyrénées preprint No. 64, submitted to Astrophys. J.
Vauclair, S., 1988, *Proc. Moriond Conf. on Dark Matter,* eds. J. Audouze and J. Tran Thanh Van (Éditions Frontières, Gif-sur-Yvette), p. 269.
Vidal-Madjar, A., et al., 1983, Astron. and Astrophys. **120**, 58.
Voss, R., 1987, in *Proc. Int. Symp. on Lepton and Photon Interactions at High Energies,* Hamburg, 1987 (North-Holland Publ. Co., Amsterdam, 1988), p. 581.
Wagoner, 1973, Astrophys. J. **179**, 343.
Weaver, T.A. and Woosley, S.E., 1980, *in Supernova Spectra,* ed. R. Meyerott and G.H. Gillespie, (AIP, New York), 1973.
Weinberg, S., 1972, *Gravitation and Cosmology,* (John Wiley & Sons, Inc., New York).
Wilkinson, D., 1987, in *Proc. 13th Texas Symp. on Relativistic Astrophysics,* ed. M.L. Ulmer, (World Scientific, Singapore), p. 209.
Woosley, S.E., 1987, preprint UCRL–98001, December 1987.
Woosley, S.E. et al., 1986, Astrophys. J. **302**, 19.
Yang, J., et al., 1984, Astrophys. J. **281**, 493.
York, D.G., 1983, Astrophys. J. **264**, 172.
Zahn, J.P., 1987, in *The Internal Solar Angular Velocity,* eds. B.R. Durney and S. Sofia (Reidel Publ. Co., Dordrecht), p. 201.

Table 1a

Measured properties of the 12 electron events detected in the neutrino burst (from Hirata et al., 1987). The electron angle is relative to the direction of SN 1987A.

Event No.	Event time (s)	No. of PMTs (N_{hits})	Electron energy (MeV)	Electron angle (°)
1	0	58	20.0 ± 2.9	18 ± 18
2	0.107	36	13.5 ± 3.2	15 ± 27
3	0.303	25	7.5 ± 2.0	108 ± 32
4	0.324	26	9.2 ± 2.7	70 ± 30
5	0.507	39	12.8 ± 2.9	135 ± 23
6	0.686	16	6.3 ± 1.7	68 ± 77
7	1.541	83	35.4 ± 8.0	32 ± 16
8	1.728	54	21.0 ± 4.2	30 ± 18
9	1.915	51	19.8 ± 3.2	38 ± 22
10	9.219	21	8.6 ± 2.7	122 ± 30
11	10.433	37	13.0 ± 2.6	49 ± 26
12	12.439	24	8.9 ± 1.9	91 ± 39

Table 1b

Characteristics of the contained neutrino events recorded on 23 February 1987 by the IMB Collaboration (from Bionta et al. 1987)

Event No.	Time (Universal Time)	No. of PMTs (N_{hits})	Energy (MeV)	Angular distribution (°)
33162	7:35:41.37	47	38	74
33164	7:35:41.79	61	37	52
33167	7:35:42.02	49	40	56
33168	7:35:42.52	60	35	63
33170	7:35:42.94	52	29	40
33173	7:35:44.06	61	37	52
33179	7:35:46.38	44	20	39
33184	7:35:46.96	45	24	102

Table 2

Compilation of neutrino luminosities $L(\bar{\nu}_e)$ for SN1987A obtained by various authors, in units of 10^{52} erg

Krauss (1987)	5 within a factor of 2
Schaeffer et al. (1987)	8 ± 2.5
Ellis and Olive (1987)	6.6 within a factor of 2
Schramm (1987a)	4.5 ± 1.5
Lamb et al. (1987)	6.6 within a factor of 3
Burrows (1987)	4 within a factor of 1.3
Piran et al. (1988)	5.9 ± 1.8
Spergel et al. (1987)	6.1 ± 1.8

Table 3
Primordial abundances

Elements	'Intergalactic'	Interstellar optical	Interstellar radio	Stellar atmosphere	Solar system	Results by number
Deuterium	Low metallicity, Lyman-α forest; but not first-generation of HST	COPERNICUS H II region, UV Lyman, $\Delta\lambda/\lambda \cong 80$ km/s. **Difficulties:** High-velocity clouds; reprocessing correction.	DI line (91.6 cm) in the direction of the galactic anticentre. **Difficulties:** Long excitation temperature	Unreliable	Meteorites, solar wind, spectrum of planet. **Difficulties:** Evolution fractionation	$D/H = 10^{-5} - 2 \times 10^{-4}$
^{3}He		**Future:** FUSE: Blue wing of ^{4}He Lyman (60 nm), $\Delta\lambda/\lambda \cong 17$ km/s.	H II regions $^3He^+$ 3.46 cm	Unreliable	Solar wind, meteorites	$^3He/H = 0.5 \times 10^{-5} - 10^{-4}$
^{3}He + D					Meteorites	$(^3He + D)/H = 2.5 \times 10^{-5} - 10^{-4}$
^{4}He	Low metallicity, Lyman-α forest; but not first-generation of HST	H II regions in compact blue galactic (young/ low metallic). **Difficulties:** Ionization correction factor; correction for evolution		Fit to HR plot in - population-II stars - B stars		By mass $Y_p = 0.235 \pm 0.010$. By number: $^4He/H = 0.077 \pm 0.003$.
^{7}Li				Population-II stars $\lambda = 671$ nm. **Difficulties:** convection; population-I stars	Solar wind, meteorites (not primordial)	$^7Li/H = 1.4 \pm 0.2 \times 10^{-10}$ (Population I = $1.6 \pm 0.3 \times 10^{-9}$)

Table 4

Values of the lepton, up-like quark, and down-like quark neutral-current coupling strengths, for three values of $\sin^2\theta_w$: the present world average, and $\pm 2\sigma$

$x = \sin^2\theta_w$	0.220	0.230	0.240
$C_\ell = 1 - 4x + 8x^2$	0.5050	0.5032	0.5018
$C_u = 1 - \frac{8}{3}x + \frac{32}{9}x^2$	0.5800	0.5748	0.5697
$C_d = 1 - \frac{4}{3}x + \frac{8}{9}x^2$	0.7450	0.7404	0.7358

Table 5

Results from the fits (with systematic errors combined)

Method	Central value	$\pm 1\sigma$	90% CL upper limit	95% CL upper limit	Goodness of fit
Supernova	2	$^{+1.4}_{-0.7}$	3.9	4.8	99%
Nucleosynthesis:					
Population-II ^{7}Li					
$\eta = (4.3 \pm 0.6) \times 10^{-10}$	2.3	± 0.8	3.3	3.6	93%
Population-I ^{7}Li					
Solution 2: $\eta = (8.6 \pm 0.6) \times 10^{-10}$	1.6	± 0.75	2.6	3.1	1.9%
Population-I ^{7}Li					
Solution 3: $\eta = (1.6 \pm 0.6) \times 10^{-10}$	3.4	± 0.8	4.4	4.7	$< 10^{-6}$
e^+e^-	1	+2.9	4.6	5.8	
W and Z production					
$m_t = 50$ GeV	2.2	$^{+2.2}_{-1.5}$	5.1	5.8	
$m_t = 100$ GeV	0	+2	2.5	3.1	
Global fit*)					
$m_t = 50$ GeV	2.1	$^{+0.6}_{-0.4}$	2.9	3.2	99%
$m_t = 100$ GeV	2	$^{+0.6}_{-0.4}$	2.7	2.9	97%

*) Using population-II ^{7}Li abundance

Table 6

Goodness of fit (in %) for global fit*)

m_t	No. of neutrinos		
(GeV)	3	4	5
50	95	36	1.7
100	77	11	0.1

*) Using population-II ^{7}Li abundance

APPENDIX

STATISTICAL METHOD

Although a Bayesian approach, which considers unknown parameters as random variables, would have been equally legitimate, we have followed the more general practice of considering the true values of the parameters as fixed, and their estimates as random variables. This attitude leads to the choice of prescriptions, such as confidence intervals, that will give wrong results in only a small proportion of the experiments. Note that it is inconsistent to mix Bayesian 'confidence intervals' with the usual ones, since their definition and interpretation are quite different.

In order to be able to write down a χ^2, we have treated theoretical and observational uncertainties on a similar footing, assuming, for simplicity, that the preferred theoretical values were distributed in a normal (Gaussian) way. In the case where only a range of acceptable values was known, we have assumed that it represented a $\pm 2\sigma$ interval of a normal variable. Therefore our definition of acceptability is that only in $\sim$ 5% of the cases such an estimated range would not include the true value of the parameter considered. Although this procedure is arbitrary for a small number of theoretical assumptions involved in a particular result, it becomes legitimate when a larger number of such assumptions are made as shown by the central limit theorem [see, for example, Eadie et al. (1971)].

We have constructed χ^2 functions and minimized them with respect to N_ν and the other free parameters. For instance, for the case of the primordial nucleosynthesis, we considered

$$\chi^2 = \left[\frac{Y_p - \theta_1(\eta, \tau_{1/2}, N_\nu)}{\sigma_{Y_p}}\right]^2 + \left[\frac{\log(D/H) - \theta_2(\eta)}{\sigma[\log(D/H)]}\right]^2$$

$$+ \left[\frac{\log(^3He/H) - \theta_3(\eta)}{\sigma[\log(^3He/H)]}\right]^2 + \left[\frac{\log[(D + {}^3He)/H] - \theta_4(\eta)}{\sigma[\log(D + {}^3He)/H]}\right]^2$$

$$+ \left[\frac{^7Li/H - \theta_5(\eta)}{\sigma(^7Li/H)}\right]^2 + \left[\frac{10.35 - \tau_{1/2}}{0.12}\right]^2,$$

where the θ_i are the relevant theoretical functions taken from Yang et al. (1984) [except for the ^{7}Li, which is taken from Kawano et al. (1988)], and the last term takes into account the uncertainty in the neutron lifetime, and for which the σ's are the corresponding experimental errors.

For variables that are not Gaussian, we made an appropriate change of variables so that the new variable is Gaussian. For instance, in the case of the $p\bar{p}$ determination, we made a change of variable $u = g(R)$, so that the $\pm 1\sigma$, and 90% and 95% upper-confidence-level values of R given in subsection 6.2 corresponded to $u = \pm 1$, 1.28, and 1.64, respectively. The g(R) is then distributed normally with zero mean and unity variance. The χ^2 can then be written

$$\chi^2 = [g(R)]^2 + \left\{\frac{[R/R_T(N_\nu)] - R_\sigma}{\sigma_{R_\sigma}}\right\}^2$$

and minimized with respect to R and N_ν.

The $\pm 1\sigma$ interval (containing in 68% of the cases the true value of the parameter), and the 90% and 95% upper confidence intervals have been defined by the value of N_ν for which the χ^2, minimized

with respect to all other parameters, is increased with respect to the minimum value by 1, $(1.28)^2$, and $(1.64)^2$, respectively.

It may be useful to recall the distinction between confidence level and goodness of fit: they correspond to two different questions. A confidence level on N_ν is placed by asking what is the probability, for a given N_ν, of getting an estimate $\hat{N}_\nu$ that is further from N_ν than the current estimate. The method relies on the fact that if N_ν is the true value asymptotically, then

$$\frac{(\hat{N}_\nu - N_\nu)^2}{\sigma^2_{\hat{N}_\nu}}$$

(where $\sigma^2_{\hat{N}_\nu}$ is the variance of the $\hat{N}_\nu$) should behave as a χ^2 of one degree of freedom. The value of N_ν at the 'α% upper confidence level' is the value of N_ν *above* the best estimate, for which this probability is α%. The 'goodness of fit' for a given value of N_ν is the probability to have a χ^2 larger than that obtained for this *given* value.

One may choose to reject a value of N_ν if it is bigger than the value at the α% upper confidence level or, alternatively, if the goodness of fit is worse than a chosen value of $(1-\alpha)$. Both procedures are acceptable in the sense that the experimenter systematically choosing either prescription will, in the long run, be wrong in only $(1 - \alpha)$% of his experiments. However, the confidence level is more powerful, i.e. more discriminating, against a wrong hypothesis regarding the number of neutrinos [see, for example, Eadie et al. (1971)].

This discussion presupposes that the errors are properly estimated and that no bias has been introduced. In our case, where the best fit is unusually good, there is a significant difference between the two methods, the confidence-level prescription rejecting four families whilst the goodness of fit for four families is still acceptable. Two attitudes may be taken:

i) It could be argued that the too good value of the best fit χ^2 could be traced back to an overly conservative estimate of the errors. If this were true, the confidence-level method would be preferable because it is less sensitive to a wrong evaluation of the errors. This is the line of argument behind the usual choice of the confidence level in experimental physics, since in the most common case, where errors are underestimated, this method is more conservative.

ii) It could be also argued that the extremely good fit could be attributed to an unconscious bias towards the Standard Model. In that case, the goodness of fit is more reliable. In our case, it is also more conservative, and we chose *not* to reject the possibility of four families.

Figure captions

Fig. 1 The neutrino burst from SN1987A observed in the Kamiokande detector on 23 February, 1987. The vertical axis is a measure of recoil electron energy in terms of the number of photomultipliers hit ($E_{el} \approx 10$ MeV corresponds to $N_{hit} \approx 25$) (Hirata et al., 1987).

Fig. 2 a) Comparison of the energy versus time-of-arrival correlation between IMB and Kamiokande neutrino events (Haines, 1987).

Fig. 2 b) Energy spectrum of Kamiokande and IMB neutrino events after efficiency corrections (Haines, 1987).

Fig. 3 Masses for the few neutron stars where it has been measured (Trimble, 1987).

Fig. 4 Integrated time distribution of the detected neutrino events of Kamiokande and IMB. The model calculations (Burrows, 1987) are normalized to the Kamiokande data. Curves A and B are for a core of mass 1.4 $M_\odot$.

Figs 5 Cross-sections for ν ($\bar{\nu}$) induced reactions in (a), and expected ν ($\bar{\nu}$) fluxes in (b), as a function of energy.

Fig. 6 Angular distribution of observed neutrino events, as measured by the electron angle, the forward direction being away from the LMC.

Fig. 7 Relation between the cosmological constant Λ, the Hubble constant H, and the age of the Universe T_0, for various values of the average density Ω_0. The regions of positive and negative curvatures are indicated.

Fig. 8 Evolution with time and temperature of the primordial abundances and of the baryon density ϱ_B, as calculated by Wagoner (1973).

Fig. 9 Predicted abundances of ^{4}He (by mass), D, ^{3}He, and ^{7}Li (by relative number to H) as a function of η for $\tau_{1/2} = 10.6$ min, as calculated by Yang et al. (1984). For ^{4}He, the predictions for $N_\nu = 2, 3, 4$ are shown and the size of the error bar shows the range of Y_p, which corresponds to $10.4 < \tau_{1/2} < 10.8$ min. Note the changes in the abundance scales.

Fig. 10 Observed D/H ratios inferred for the insterstellar medium toward hot stars. The distances on the x-axis are uncertain, but they serve to spread out the data points (Boesgaard and Steigman, 1985).

Fig. 11 Observed ^{3}He/H abundance (by number), in units of 10^{-5}, as a function of the Galactic radius for each detected H II region.

Fig. 12 Observed ^{7}Li abundances for population II, as a function of effective temperature (a) and metallicity (b) (Rebolo et al., 1988a and b; Hobbs and Duncan, 1987), and for population I (c) (Hobbs and Pilachowski, 1988).

Fig. 13 Observed ^{4}He abundances in metal-poor dwarf galaxies and other objects as a function of O/H (a) and (N/H) (b). After Pagel et al. (1986).

Fig. 14 Diagrams leading to single-photon production accompanied by neutrinos in e^+e^- annihilation, in (a) through a Z exchange, and in (b) through a W exchange.

Figs. 15 Transverse (a) and longitudinal (b) views of the ASP detector at PEP. For a detailed description of the apparatus, see Bartha et al. (1986) and Hearty et al. (1987).

Fig. 16 a) A typical radiative $e^+e^- \to \gamma e^+e^-$ Bhabha event seen in the ASP detector (Burke, 1987).

Fig. 16 b) The single-photon event with $E_T^\gamma = 3.4$ GeV seen in the ASP detector (Burke, 1987).

Fig. 17 Scatter plot of the distance of closest approach to the interaction point R versus the photon transverse momentum p_T^γ for the single-photon candidates of the ASP Collaboration (Hearty et al., 1987).

Fig. 18 Probability of observing ≤ 1.6 $\gamma\nu\bar{\nu}$ events as a function of the $e^+e^- \to \gamma\nu\bar{\nu}$ cross-section (Hearty et al., 1987).

Fig. 19 a) Energy dependence of the cross-section for $e^+e^- \to \gamma\nu\bar{\nu}$ (for $N_\nu = 3$), for photons at polar angles $> 20°$ from the beams and with $E_\gamma > 0.2\, E_{beam}$ (Burke, 1987).

Fig. 19 b) Photon energy spectra from $e^+e^- \to \gamma\nu\bar{\nu}$ at c.m. energies of a few GeV above the Z peak ($m_Z = 92$ GeV is assumed); the photon cross-section is integrated over the angular range $20° < \theta_\gamma < 160°$ (Simopoulou, 1986).

Fig. 20 Gluon bremsstrahlung diagrams leading to large-p_T production of a Z in diagram (a) and of a W in diagram (b).

Fig. 21 Shape of the W transverse momentum distribution observed by the UA1 and UA2 Collaborations at $\sqrt{s} = 630$ GeV [Stubenrauch (1987) for UA1 and DiLella (1987) for UA2]. The solid line is the QCD calculation of Altarelli et al. (1984) for DO1. The shaded area is the perturbative QCD calculation with its theoretical uncertainty, in the range of interest for the neutrino counting monojet search; this calculation has been extended to higher p_T^W values as indicated (dashed lines) with the EUROJET Monte Carlo.

Fig. 22 A typical monojet event seen in the UA1 detector. Only tracks with $p_T > 1$ GeV/c and calorimeter cells with $E_T > 1$ GeV are shown (Albajar et al., 1987b).

Fig. 23 Scatter plot of the τ-likelihood L_τ versus the transverse energy of the highest-E_T jet in the sample of 56 large and isolated missing transverse energy events of UA1. The different symbols indicate the charged multiplicity of the jet (Albajar et al., 1987b).

Fig. 24 Missing transverse energy (a) and jet transverse energy (b) for UA1 events passing the cut $L_\tau < 0$ (24 events), compared with the sum of all expected contributions, including $N_\nu = 3$ (Albajar et al., 1987b).

Fig. 25 Jet transverse energy distribution for background-subtracted data (including the contribution for $N_\nu = 3$) passing the cut $L_\tau < 0$ (points with error bars), compared with the expected contribution for seven extra massless neutrino species (solid line) (Albajar et al., 1987b).

Fig. 26a Total widths of the W and Z as a function of the t-quark mass, assuming three generations, for $\sin^2\theta_w = 0.230$, $m_W = 80.7$ GeV, $m_Z = 91.9$ GeV.

Fig. 26b The ratio R_Γ of $W \to \ell\nu$ to $Z \to \ell\ell$ branching ratios as a function of m_t, for $N_\nu = 3$, 4, and 5.

Fig. 27 Valence and sea u- and d-quark momentum distributions for various sets of structure function parametrizations, evaluated at $Q^2 = m_W^2$.

Fig. 28 Dependence of $R_\sigma = \sigma_W/\sigma_Z$, the ratio of W to Z total production cross-sections, on $\sin^2\theta_w$ for various choices of structure functions: DO 1, 2; GHR; EHLQ 1, 2; DFLM, calculated with EUROJET at $\sqrt{s} = 630$ GeV. For comparison, the values from Altarelli et al. (1984) at $\sin^2\theta_w = 0.217$ are also shown.

Fig. 29 Comparison of the EMC and BCDMS deep-inelastic muon-scattering data on the ratio of structure functions F_2^n/F_2^p with predictions from various sets of structure functions calculated at the appropriate Q^2, from Stubenrauch (1987) and Colas et al. (1988).

Fig. 30 Comparison between the theoretical predictions for the ratio R as a function of m_t, with the theoretical input $R_\sigma = 3.25 \pm 0.1$, and the experimental results of UA1/2. The continuous horizontal line represents the UA1 and UA2 combined measurement of R, and the hatched lines are the 90% and 95% CL upper limits implied by this measurement (Albajar et al., 1987d). The theoretical expectations are shown for three and five massless neutrinos. The shaded band corresponds to the theoretical uncertainty $\delta R_\sigma = \pm 0.1$.

Fig. 31 Total number of light neutrino species N_ν (solid line) as extracted from the combined UA1 and UA2 measurement of R, and the 90% CL upper limit on this number, as a function of m_t. The theoretical input for the central value N_ν is $R_\sigma = 3.25$, and for the upper limit on N_ν the value $R_\sigma = 3.15$ is used (see text for details). The lower limit of three is indicated by the dashed line. The present TRISTAN and UA1 lower limits on m_t are shown.

Fig. 32 Upper limits on the number of neutrino species, from the combined UA1/2 measurement of R, as a function of m_t, for the various heavy lepton or/and heavy b′-quark fourth-generation scenarios indicated (see text for details).

Fig. 33 Variation of the ratio of total production rates $R_\sigma = \sigma_W/\sigma_Z$ with $\sqrt{s}$ from CERN to Fermilab $p\bar{p}$ Collider energies, according to the various sets of structure functions indicated (EUROJET calculation).

Fig. 34 Compilation of central values and 90% CL upper limits on the number of neutrino flavours N_ν, from cosmology, astrophysics, and particle physics. The central value of N_ν from UA1 and UA2 is for the central theoretical expectation $R_\sigma = 3.25$ and for $m_t = 50$ GeV. The upper limit is for the 'worst case': $R_\sigma = 3.15$ and $m_t = 50$ GeV. The abbreviations used for the cosmological and astrophysical limits are: EENS ≡ Ellis et al., 1986; SOST ≡ Steigman et al., 1986; K ≡ Krauss 1987; EO ≡ Ellis et Olive, 1987; SDJ ≡ Shaeffer et al., 1987; DSS ≡ this paper.

Fig. 35 The χ^2 as a function of the number of neutrino families for the various methods and the global fits. The theoretical uncertainties have been treated as random, as explained in the Appendix. The number of degrees of freedom of the fits is given in parenthesis.

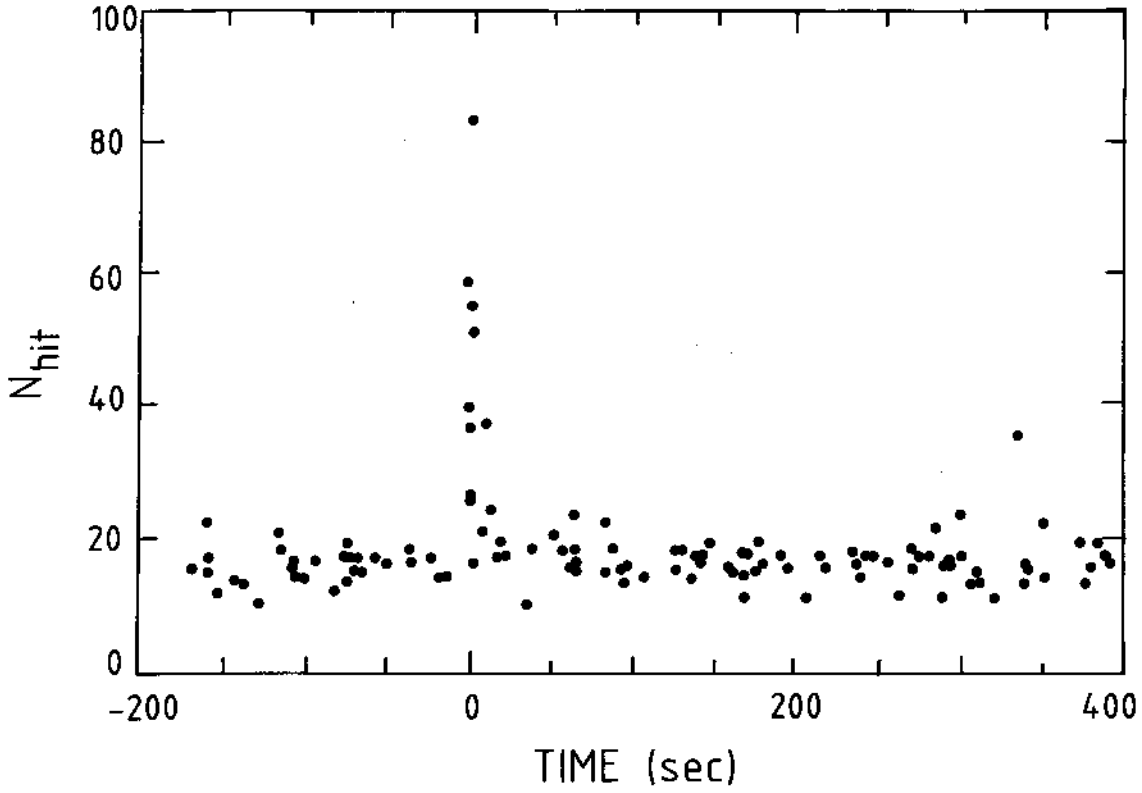
100
80
60
40
20
0
N_{hit}
-200
0
200
400
TIME (sec)

Fig. 1

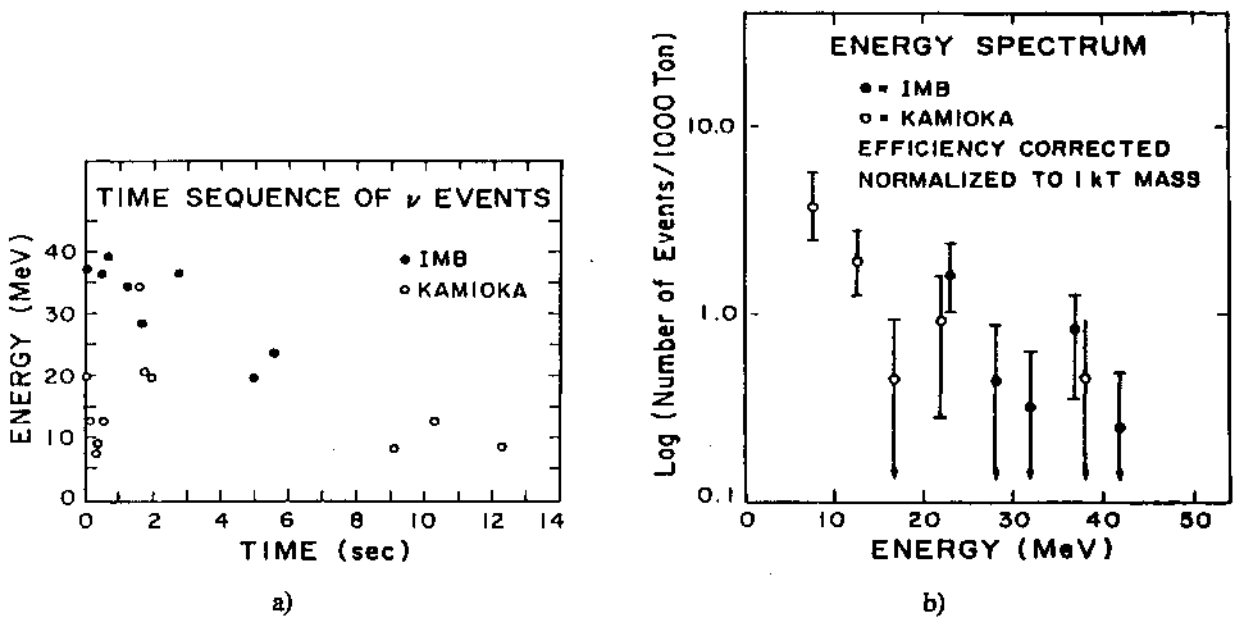
TIME SEQUENCE OF ν EVENTS
• IMB
○ KAMIOKA
ENERGY (MeV)
TIME (sec)
ENERGY SPECTRUM
• IMB
○ KAMIOKA
EFFICIENCY CORRECTED
NORMALIZED TO 1 kT MASS
Log (Number of Events/1000 Ton)
ENERGY (MeV)

a) b)

Fig. 2

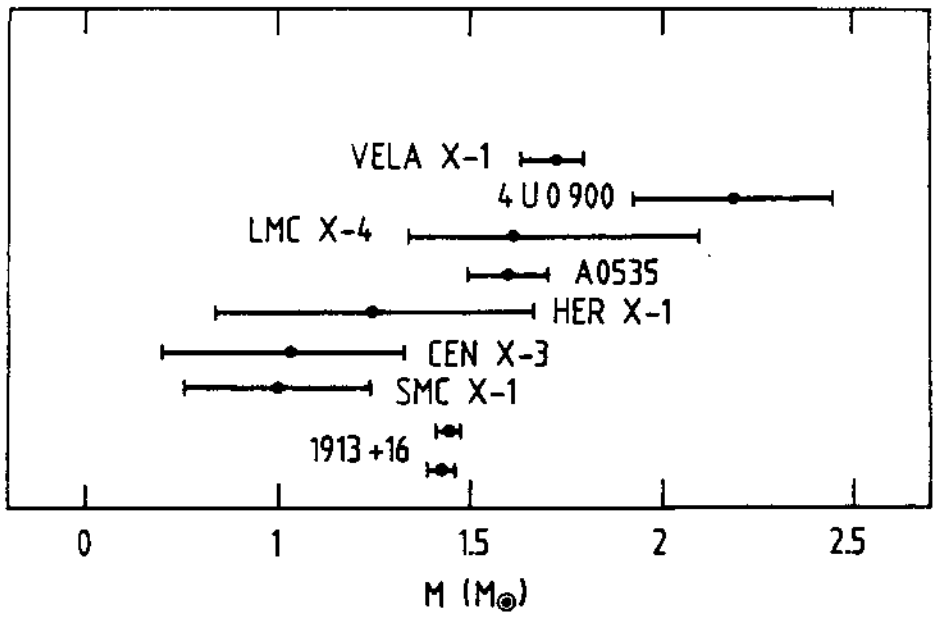
VELA X-1
4 U 0 900
LMC X-4
A0535
HER X-1
CEN X-3
SMC X-1
1913 +16
0
1
1.5
2
2.5
M (M⊙)

Fig. 3

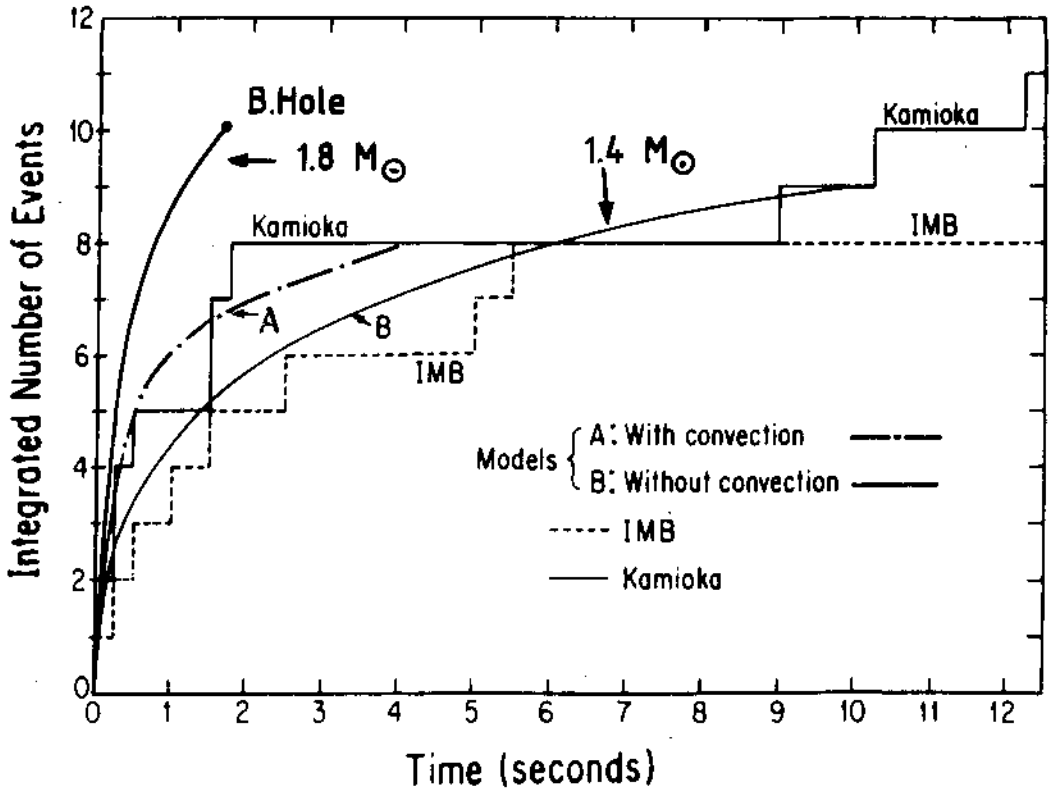
B.Hole
1.8 M⊙
1.4 M⊙
Kamioka
Kamioka
IMB
IMB
A
B
Models { A: With convection
B: Without convection
IMB
Kamioka
Integrated Number of Events
Time (seconds)
0
2
4
6
8
10
12
0
1
2
3
4
5
6
7
8
9
10
11
12

Fig. 4

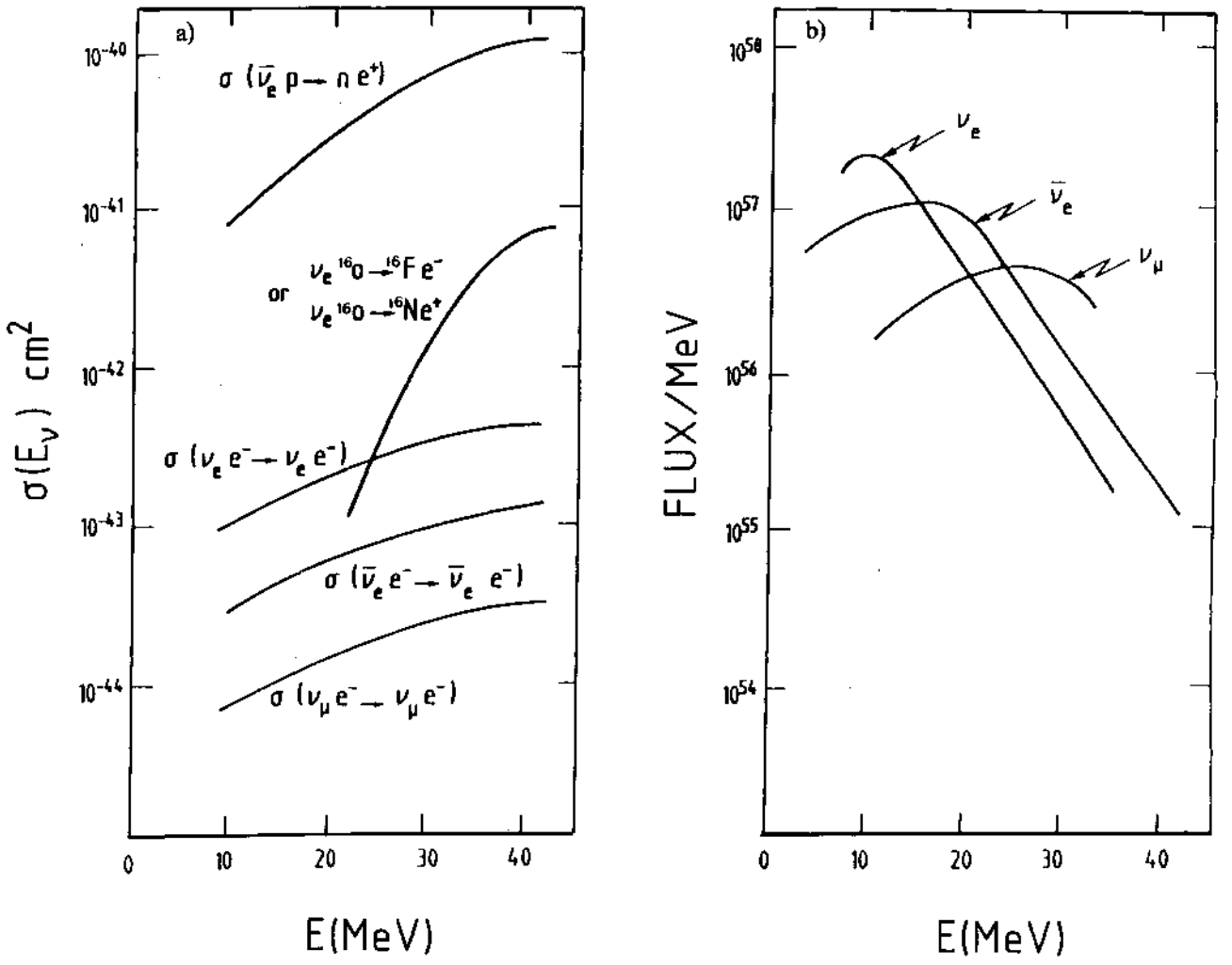
a)
10^{-40}
10^{-41}
10^{-42}
10^{-43}
10^{-44}
$\sigma(E_\nu)$ cm^2
$\sigma(\bar{\nu}_e p \rightarrow n e^+)$
$\nu_e {}^{16}O \rightarrow {}^{16}F e^-$
or
$\nu_e {}^{16}O \rightarrow {}^{16}Ne^+$
$\sigma(\nu_e e^- \rightarrow \nu_e e^-)$
$\sigma(\bar{\nu}_e e^- \rightarrow \bar{\nu}_e e^-)$
$\sigma(\nu_\mu e^- \rightarrow \nu_\mu e^-)$
0
10
20
30
40
E(MeV)
b)
10^{58}
10^{57}
10^{56}
10^{55}
10^{54}
FLUX/MeV
ν_e
$\bar{\nu}_e$
ν_μ
0
10
20
30
40
E(MeV)

Fig. 5

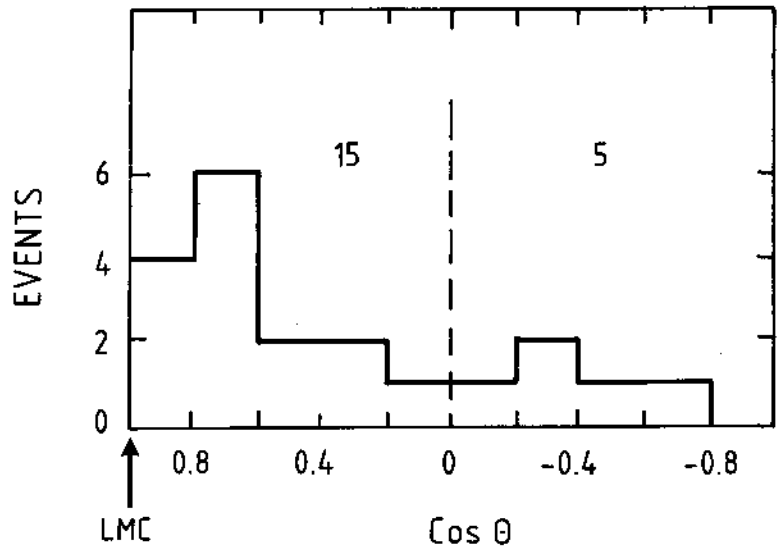
EVENTS
6
4
2
0
15
5
0.8
0.4
0
-0.4
-0.8
LMC
Cos Θ

Fig. 6

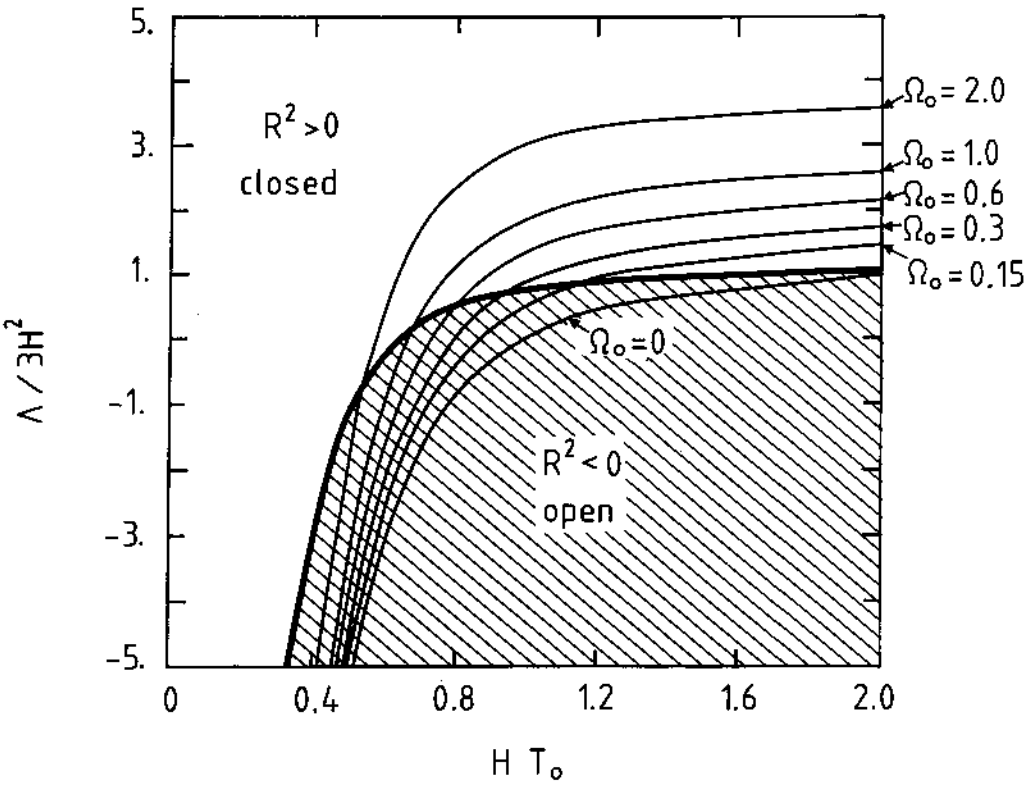
5.
3.
1.
-1.
-3.
-5.
0
0.4
0.8
1.2
1.6
2.0
Λ / 3H²
H T₀
R² > 0
closed
R² < 0
open
Ω₀ = 2.0
Ω₀ = 1.0
Ω₀ = 0.6
Ω₀ = 0.3
Ω₀ = 0.15
Ω₀ = 0

Fig. 7

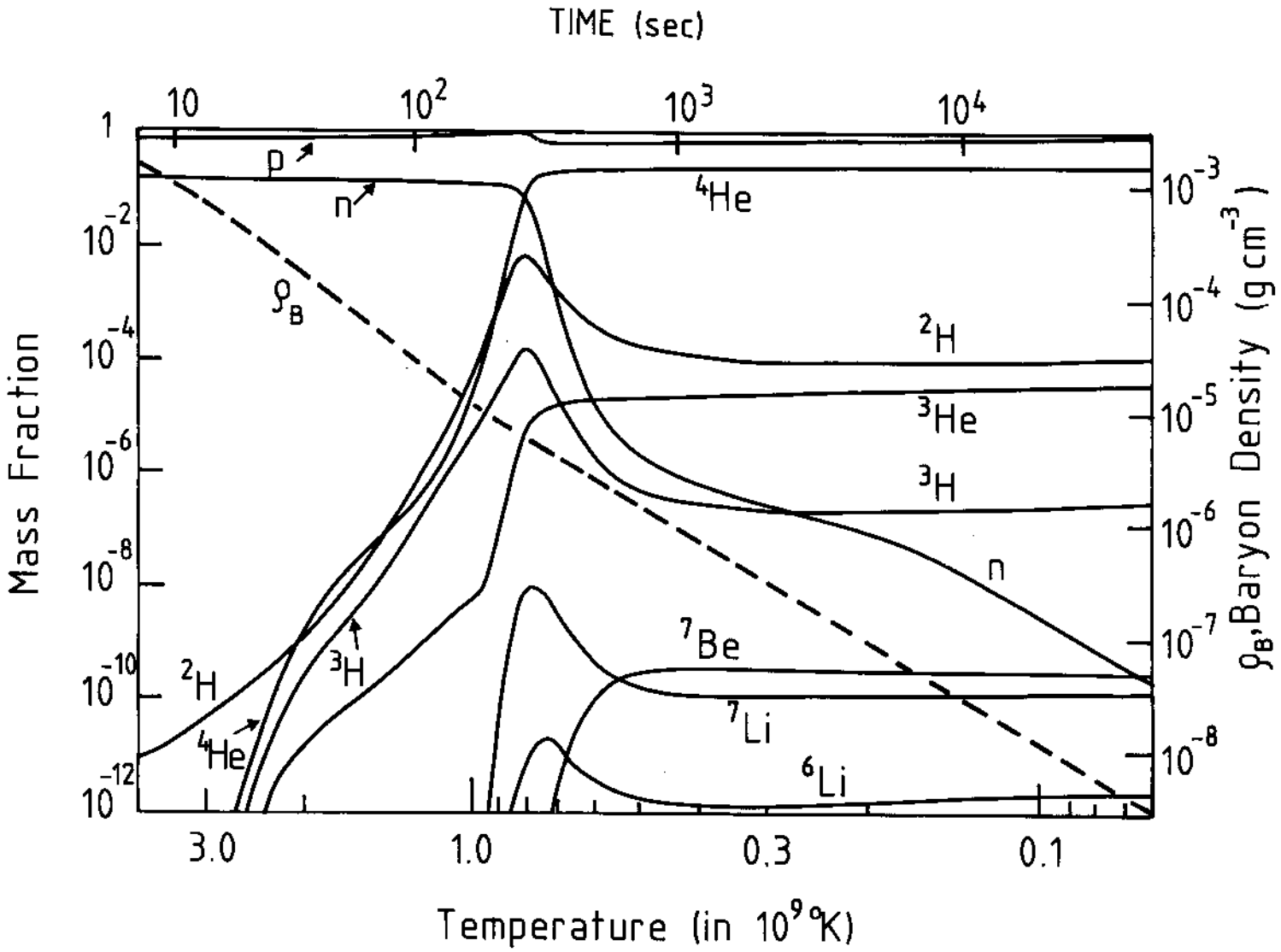
TIME (sec)
10
10^2
10^3
10^4
1
10^{-2}
10^{-4}
10^{-6}
10^{-8}
10^{-10}
10^{-12}
Mass Fraction
p
n
^{4}He
ϱ_B
^{2}H
^{3}He
^{3}H
n
^{7}Be
^{7}Li
^{6}Li
^{2}H
^{3}H
^{4}He
10^{-3}
10^{-4}
10^{-5}
10^{-6}
10^{-7}
10^{-8}
ϱ_B, Baryon Density (g cm^{-3})
3.0
1.0
0.3
0.1
Temperature (in 10^9 °K)

Fig. 8

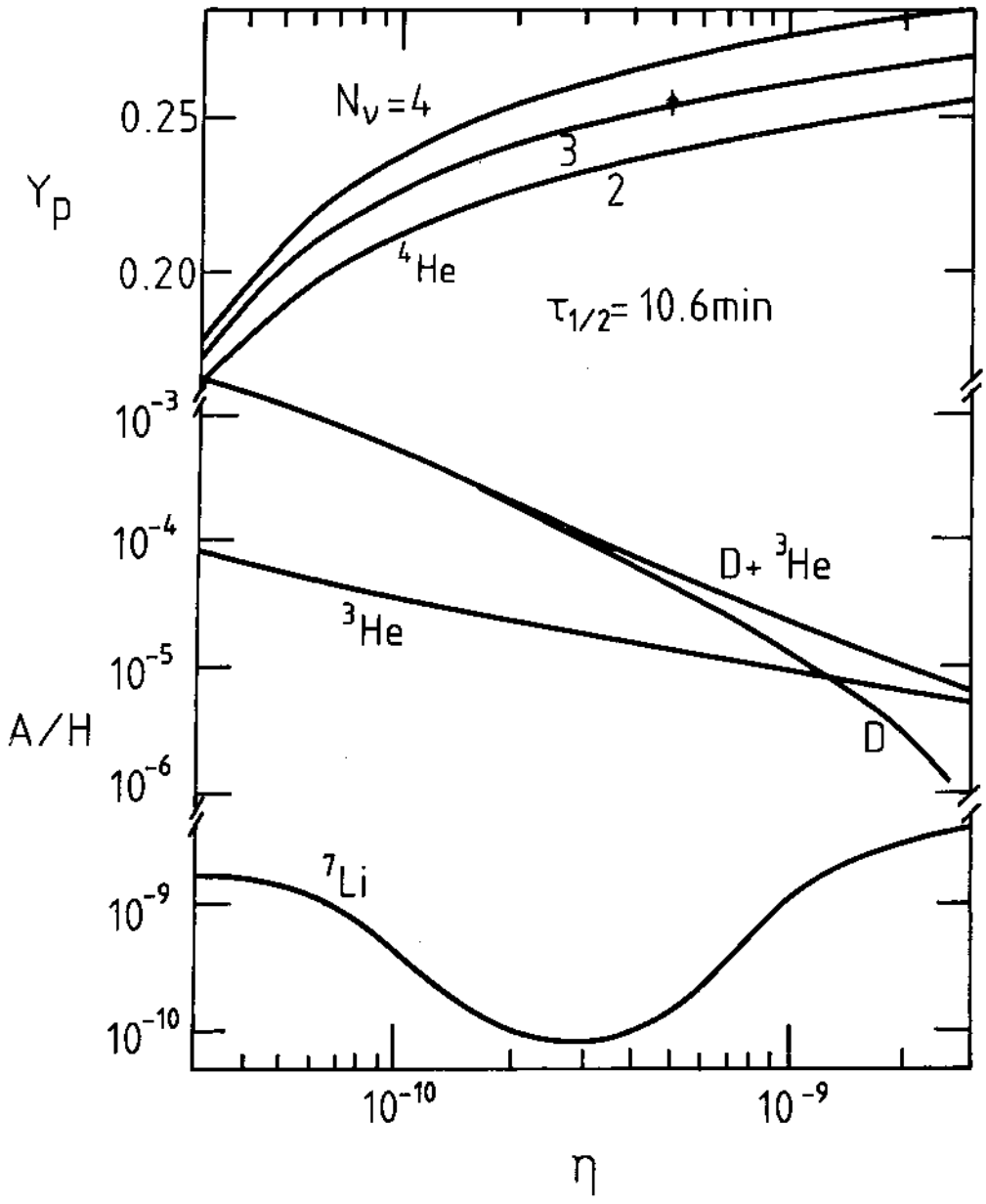
0.25
0.20
Y_p
$N_\nu = 4$
3
2
^{4}He
$\tau_{1/2}$= 10.6min
10^{-3}
10^{-4}
10^{-5}
10^{-6}
A/H
D+ ^{3}He
^{3}He
D
^{7}Li
10^{-9}
10^{-10}
10^{-10}
10^{-9}
η

Fig. 9

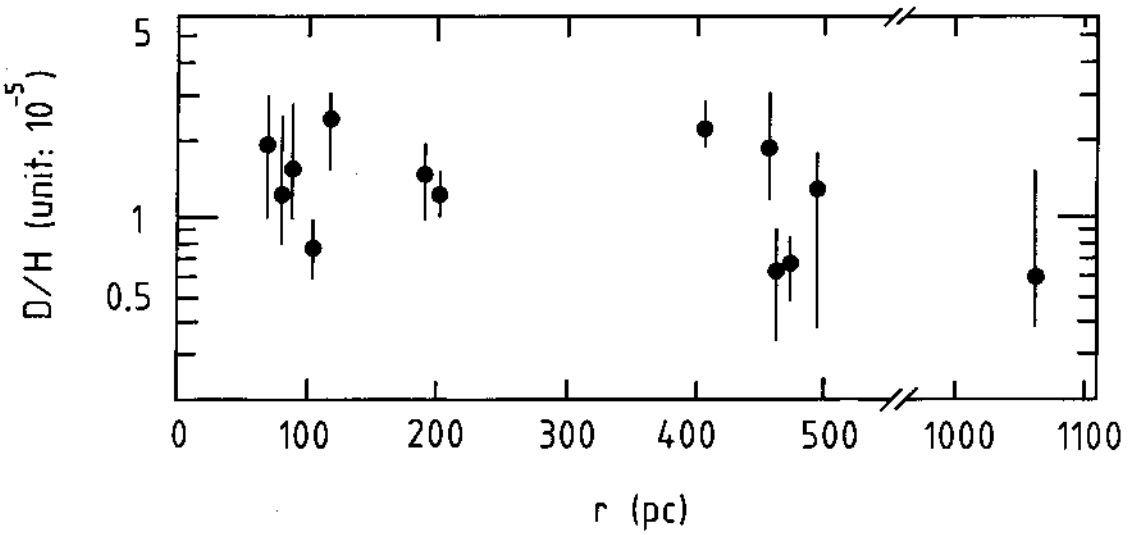
D/H (unit: 10^{-5})
5
1
0.5
0
100
200
300
400
500
1000
1100
r (pc)

Fig. 10

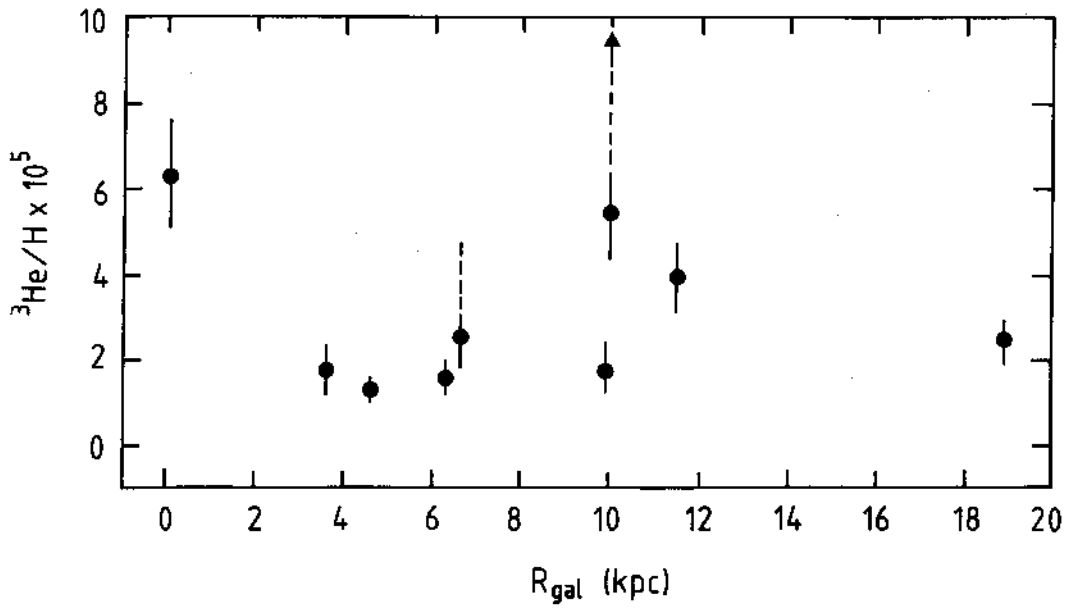
^{3}He/H x 10^5
10
8
6
4
2
0
0
2
4
6
8
10
12
14
16
18
20
R_{gal} (kpc)

Fig. 11

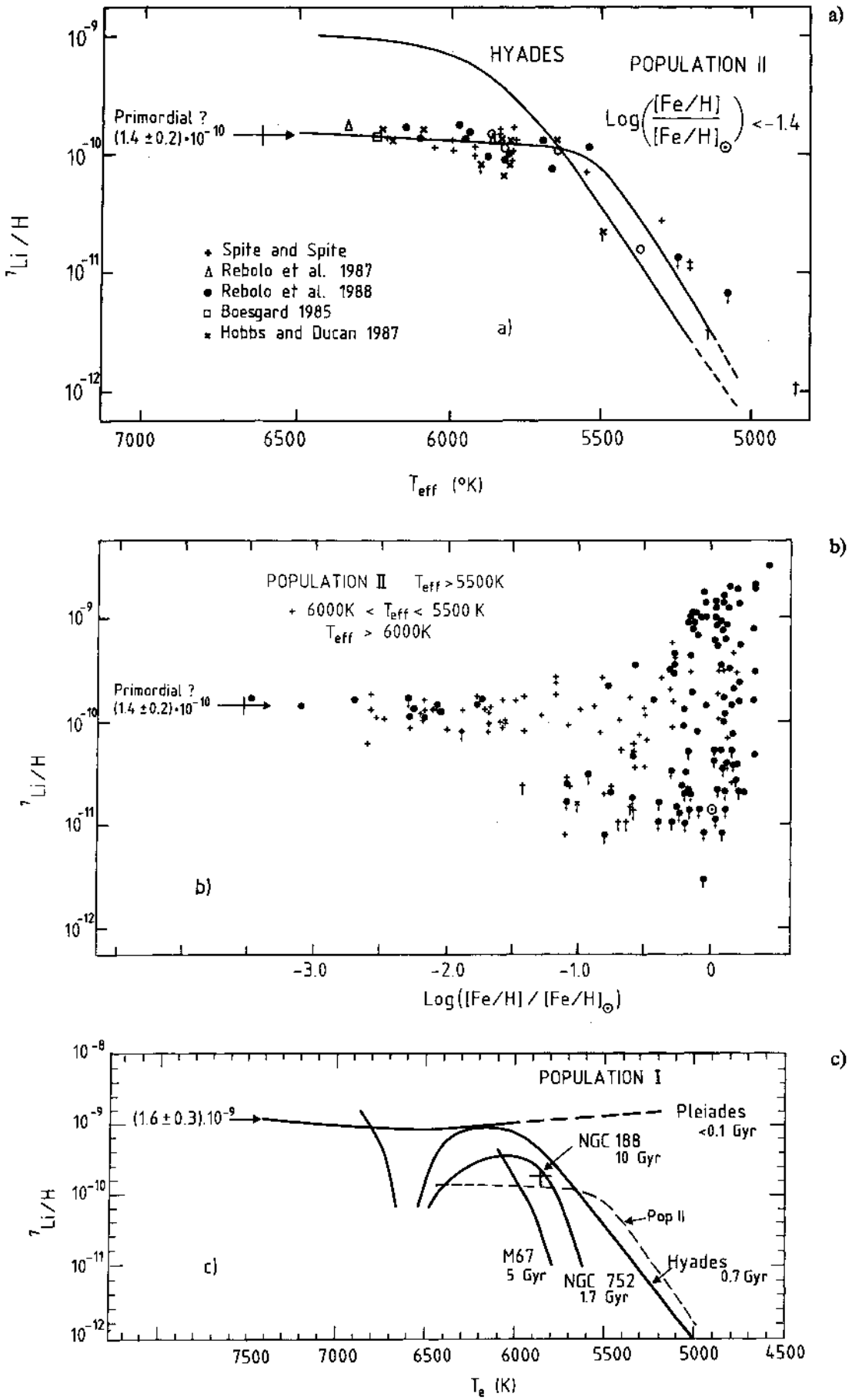
a)
HYADES
POPULATION II
Log([Fe/H]/[Fe/H]⊙) <-1.4
Primordial ?
(1.4 ±0.2)·10⁻¹⁰
Spite and Spite
Rebolo et al. 1987
Rebolo et al. 1988
Boesgard 1985
Hobbs and Ducan 1987
a)
⁷Li / H
T_eff (°K)
b)
POPULATION II T_eff > 5500K
+ 6000K < T_eff < 5500 K
T_eff > 6000K
Primordial ?
(1.4 ±0.2)·10⁻¹⁰
b)
Log([Fe/H] / [Fe/H]⊙)
c)
POPULATION I
(1.6 ± 0.3).10⁻⁹
Pleiades
<0.1 Gyr
NGC 188
10 Gyr
Pop II
M67
5 Gyr
NGC 752
1.7 Gyr
Hyades
0.7 Gyr
c)
T_e (K)

Fig. 12

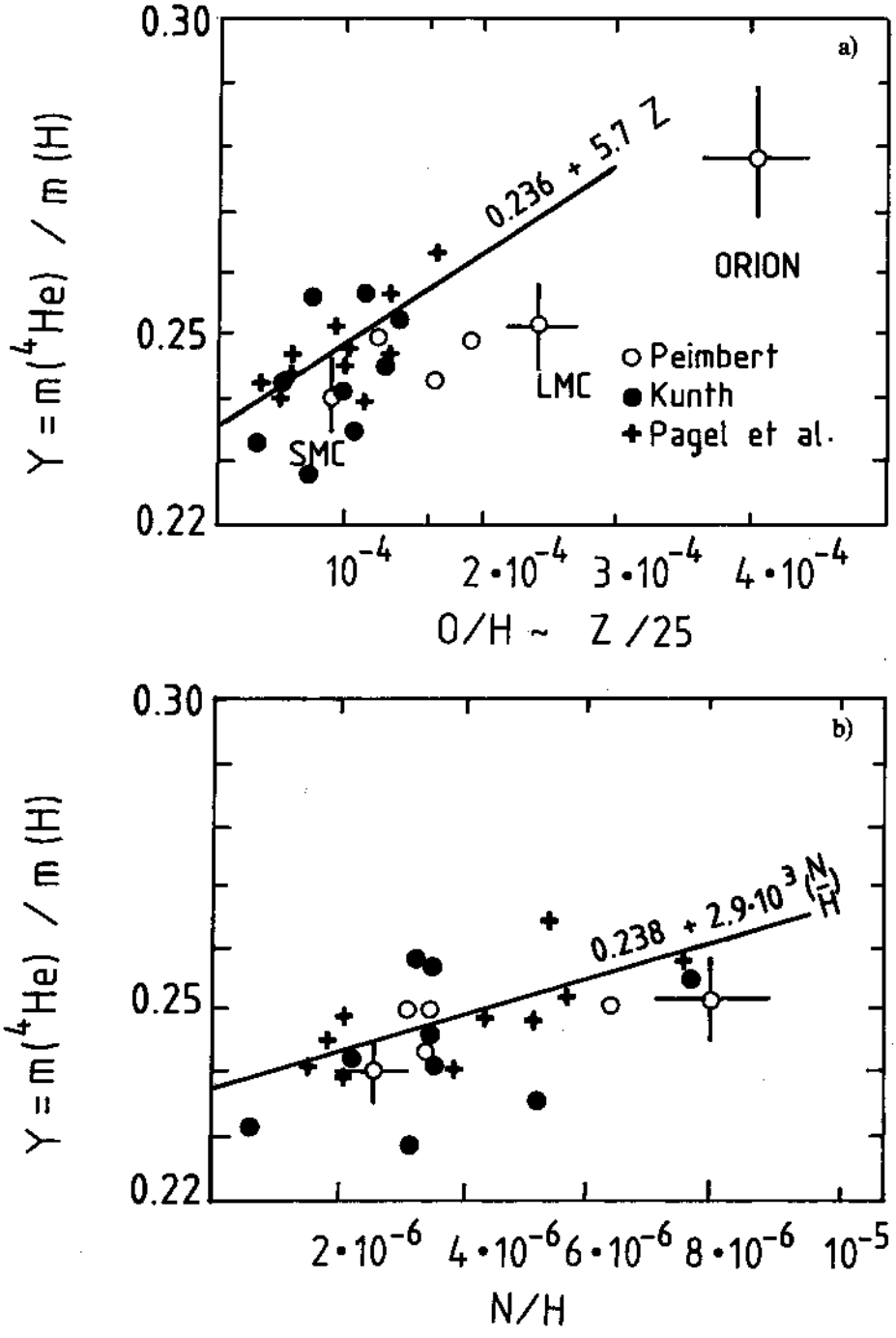
a)
0.30
0.25
0.22
Y = m(⁴He) / m (H)
0.236 + 5.7 Z
ORION
LMC
SMC
Peimbert
Kunth
Pagel et al.
10⁻⁴
2·10⁻⁴
3·10⁻⁴
4·10⁻⁴
O/H ~ Z/25
b)
0.30
0.25
0.22
Y = m(⁴He) / m (H)
0.238 + 2.9·10³ (N/H)
2·10⁻⁶
4·10⁻⁶
6·10⁻⁶
8·10⁻⁶
10⁻⁵
N/H

Fig. 13

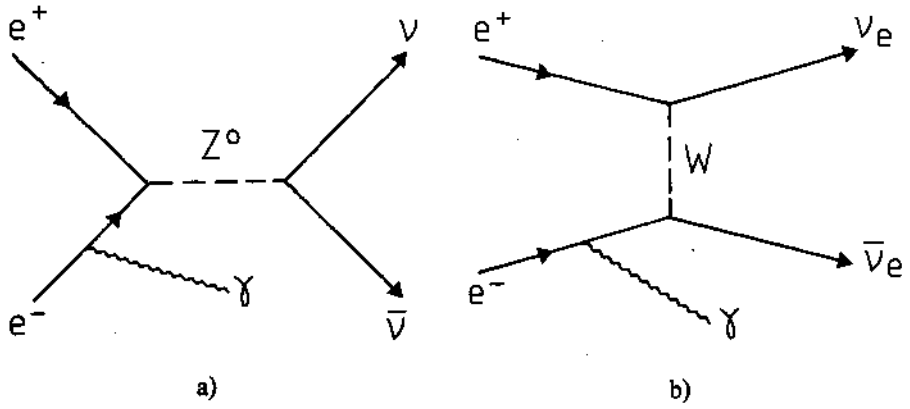
e+
e−
Z°
ν
ν̄
γ
a)
e+
e−
W
νe
ν̄e
γ
b)

Fig. 14

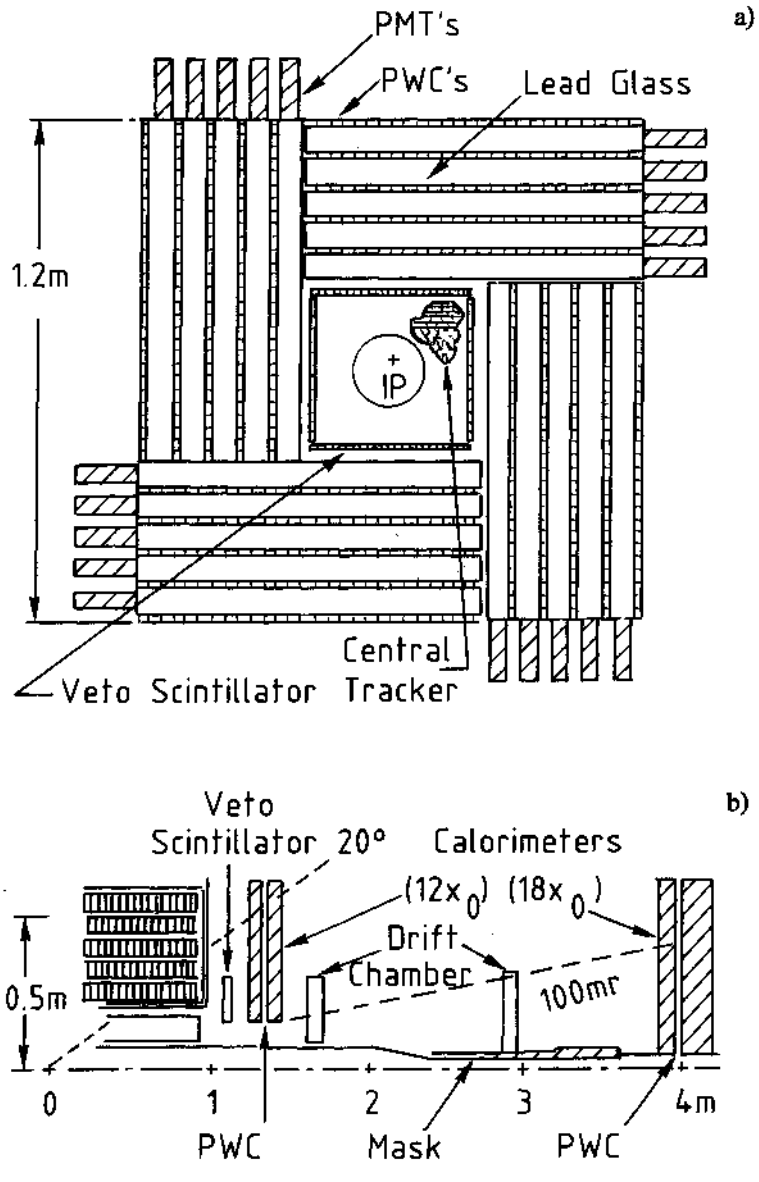
a)
PMT's
PWC's
Lead Glass
1.2m
IP
Central
Veto Scintillator Tracker
b)
Veto
Scintillator
20°
Calorimeters
(12x0)
(18x0)
Drift
Chamber
100mr
0.5m
0
1
2
3
4m
PWC
Mask
PWC

Fig. 15

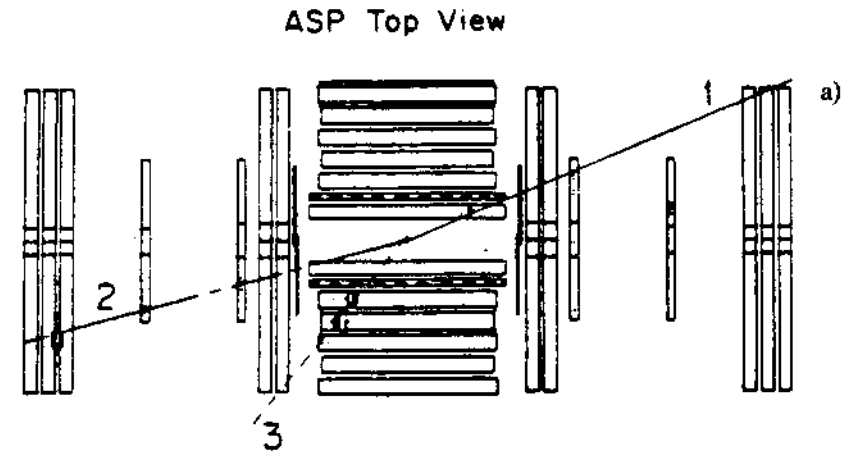

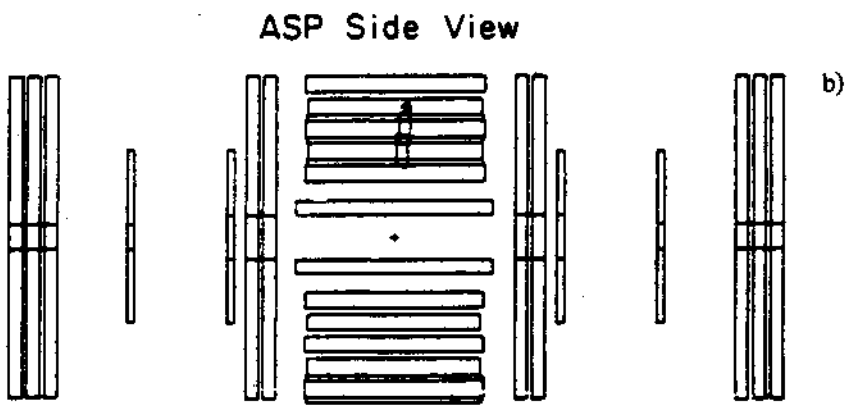

Fig. 16

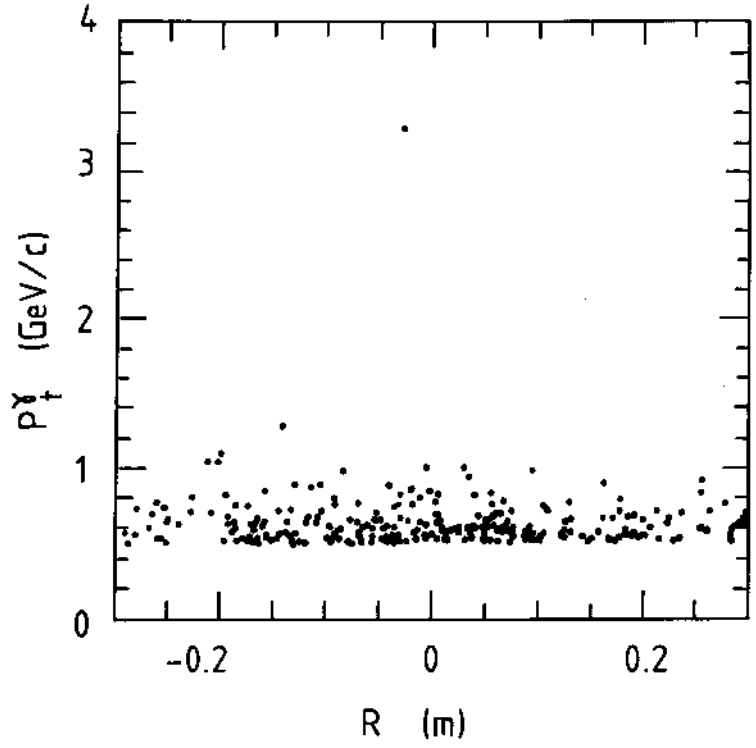
4
3
2
1
0
p_t^γ (GeV/c)
-0.2
0
0.2
R (m)

Fig. 17

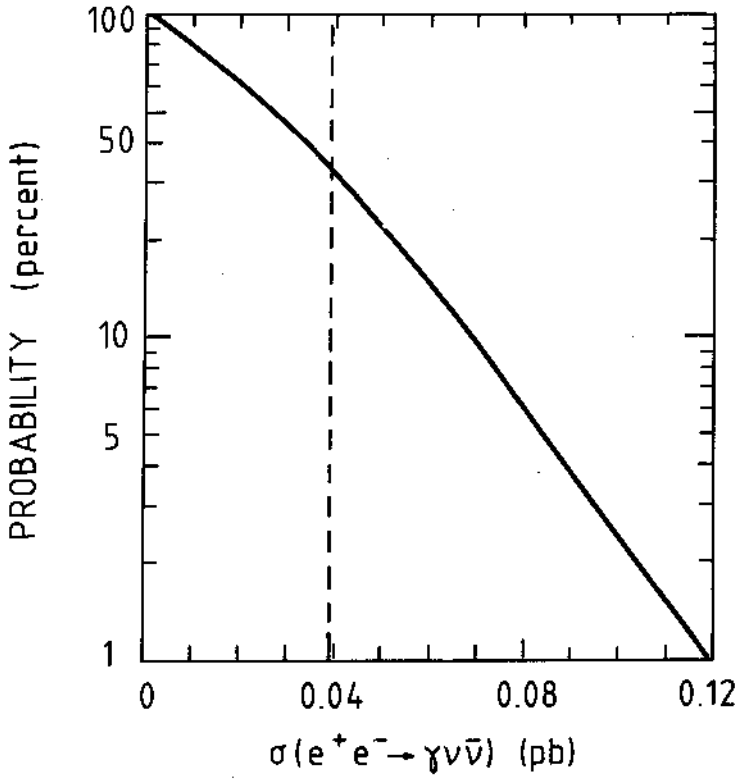
100
50
10
5
1
PROBABILITY (percent)
0
0.04
0.08
0.12
$\sigma(e^+e^- \to \gamma\nu\bar{\nu})$ (pb)

Fig. 18

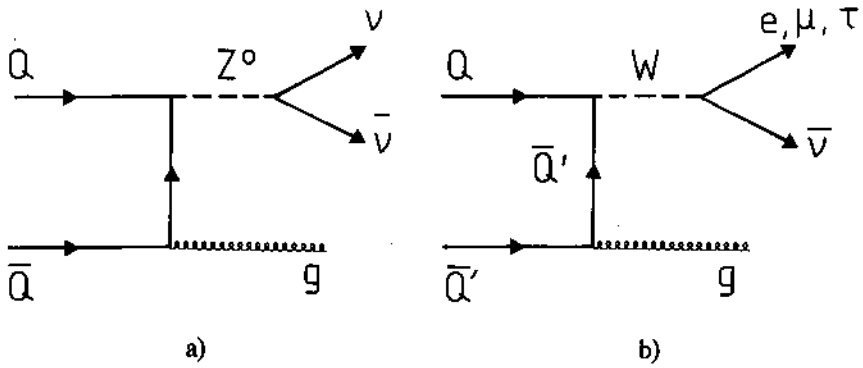
Q
Z°
ν
ν̄
Q̄
g
a)
Q
W
e, μ, τ
ν̄
Q̄′
Q̄′
g
b)

Fig. 20

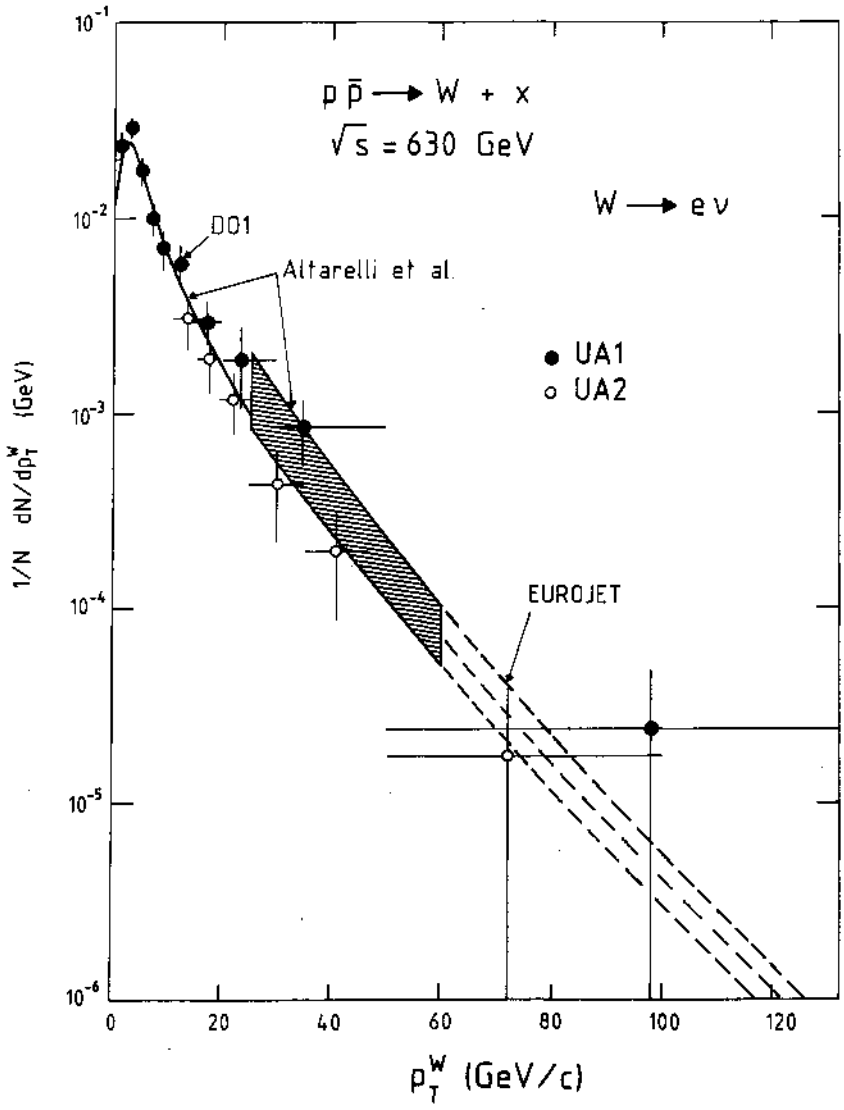
p p̄ → W + x
√s = 630 GeV
W → e ν
DO1
Altarelli et al.
UA1
UA2
EUROJET
1/N dN/dp_T^W (GeV)
p_T^W (GeV/c)
10^-1
10^-2
10^-3
10^-4
10^-5
10^-6
0
20
40
60
80
100
120

Fig. 21

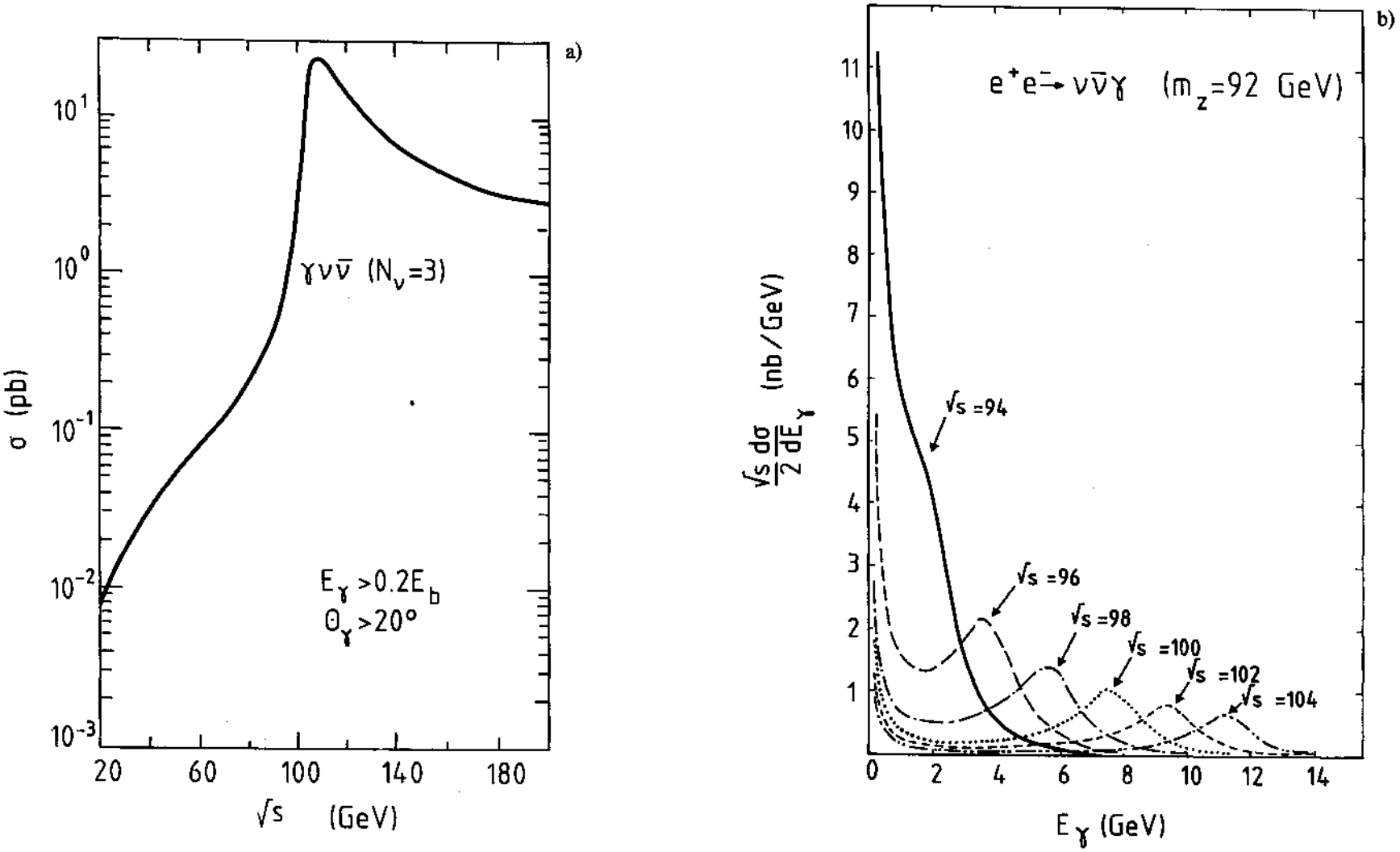
a)
σ (pb)
10^1
10^0
10^{-1}
10^{-2}
10^{-3}
$\gamma\nu\bar{\nu}$ (N_ν=3)
$E_\gamma > 0.2E_b$
$\Theta_\gamma > 20°$
20
60
100
140
180
$\sqrt{s}$ (GeV)
b)
$e^+e^- \to \nu\bar{\nu}\gamma$ (m_z=92 GeV)
$\frac{\sqrt{s}}{2}\frac{d\sigma}{dE_\gamma}$ (nb/GeV)
$\sqrt{s}$ =94
$\sqrt{s}$ =96
$\sqrt{s}$ =98
$\sqrt{s}$ =100
$\sqrt{s}$ =102
$\sqrt{s}$ =104
0
2
4
6
8
10
12
14
E_γ (GeV)

Fig. 19

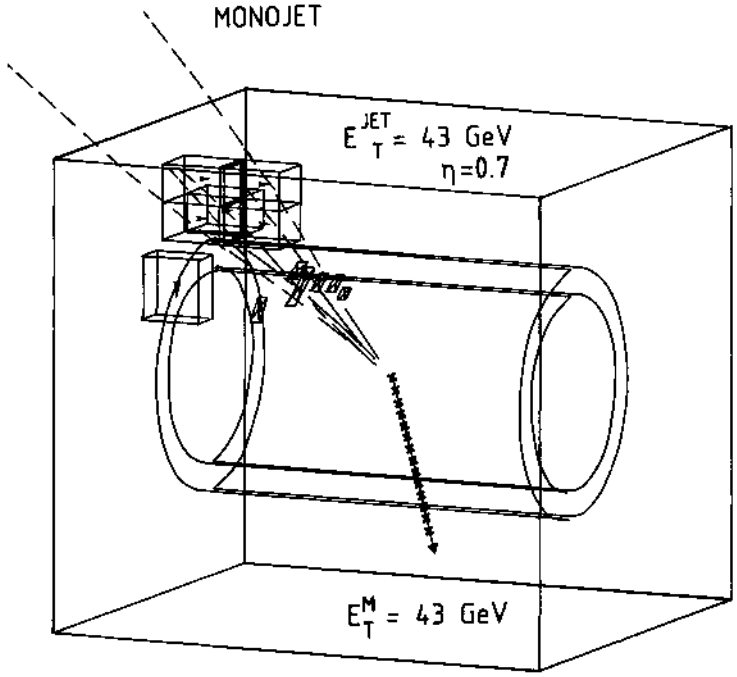
MONOJET
E_T^{JET} = 43 GeV
η=0.7
E_T^M = 43 GeV

Fig. 22

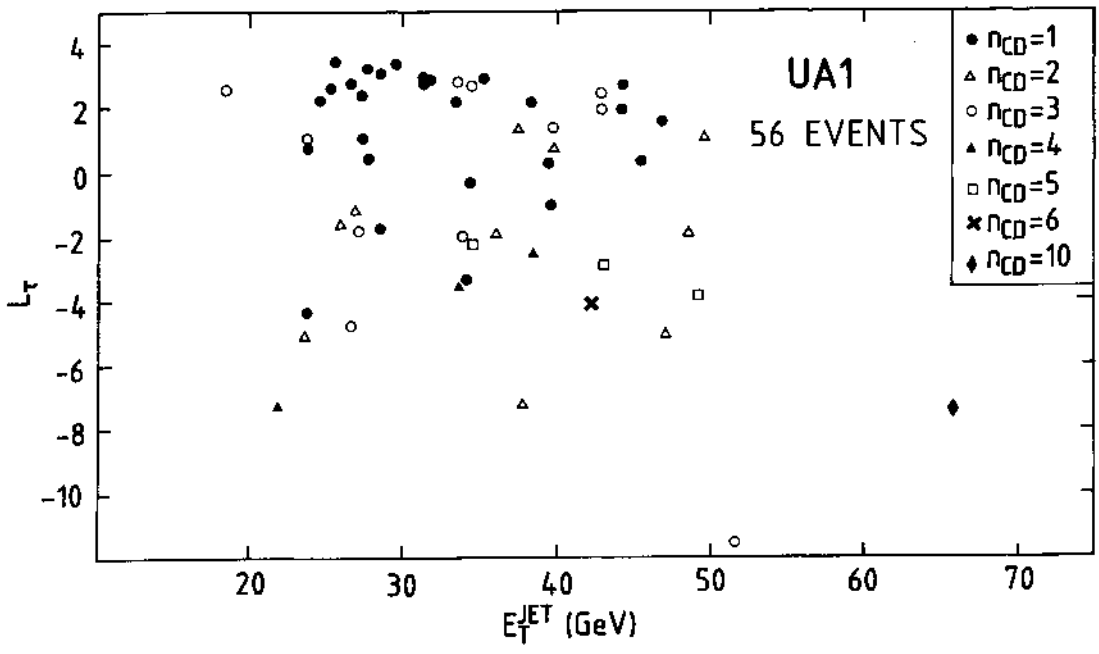
UA1
56 EVENTS
n_{CD}=1
n_{CD}=2
n_{CD}=3
n_{CD}=4
n_{CD}=5
n_{CD}=6
n_{CD}=10
L_T
E_T^{JET} (GeV)

Fig. 23

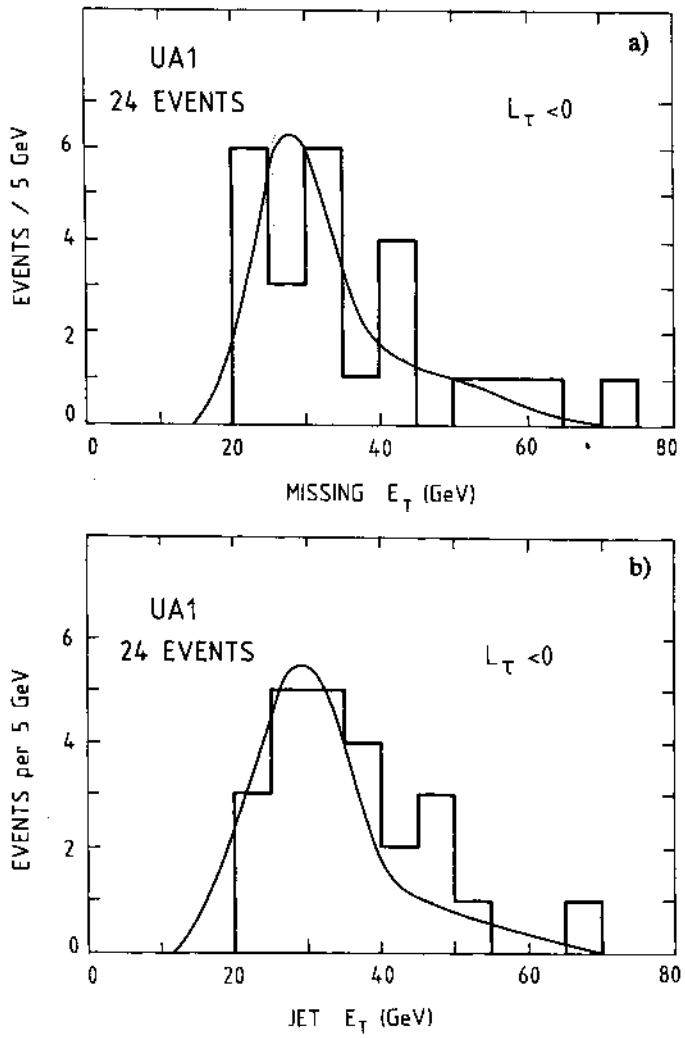
a)
UA1
24 EVENTS
L_τ <0
EVENTS / 5 GeV
MISSING E_T (GeV)
b)
UA1
24 EVENTS
L_τ <0
EVENTS per 5 GeV
JET E_T (GeV)

Fig. 24

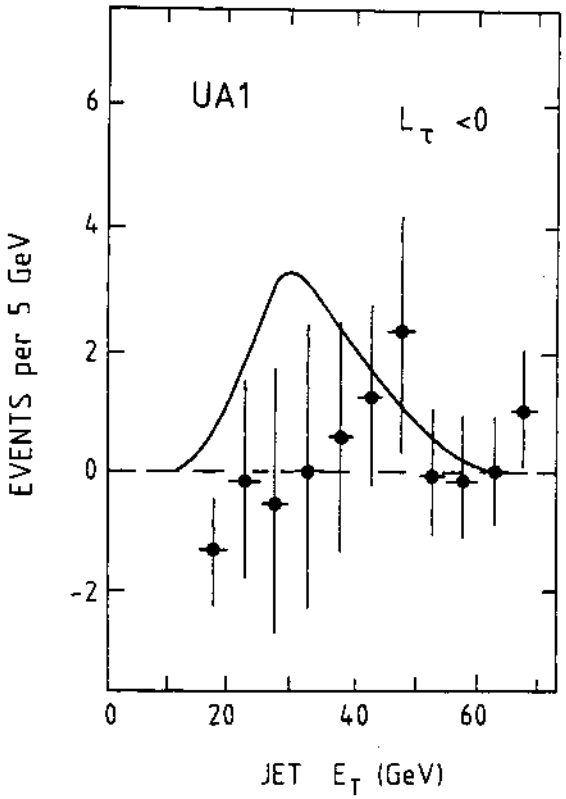
UA1
L_τ <0
EVENTS per 5 GeV
JET E_T (GeV)

Fig. 25

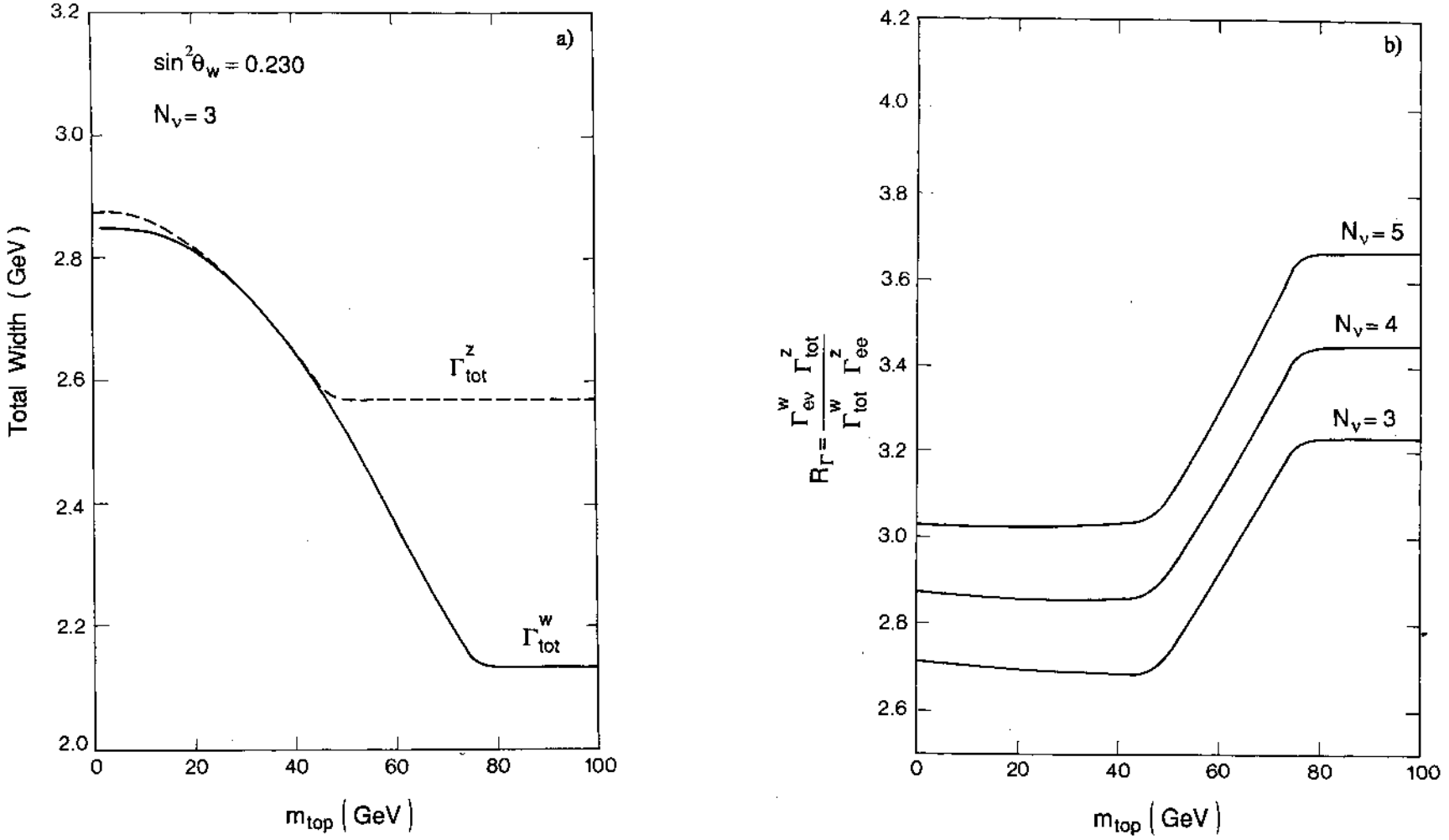
a)
$\sin^2\theta_W = 0.230$
$N_\nu = 3$
Γ^z_{tot}
Γ^w_{tot}
Total Width (GeV)
m_{top} (GeV)
3.2
3.0
2.8
2.6
2.4
2.2
2.0
0
20
40
60
80
100
b)
$N_\nu = 5$
$N_\nu = 4$
$N_\nu = 3$
$R_\Gamma = \frac{\Gamma^w_{e\nu}}{\Gamma^w_{tot}} \frac{\Gamma^z_{tot}}{\Gamma^z_{ee}}$
4.2
4.0
3.8
3.6
3.4
3.2
3.0
2.8
2.6
0
20
40
60
80
100
m_{top} (GeV)

Fig. 26

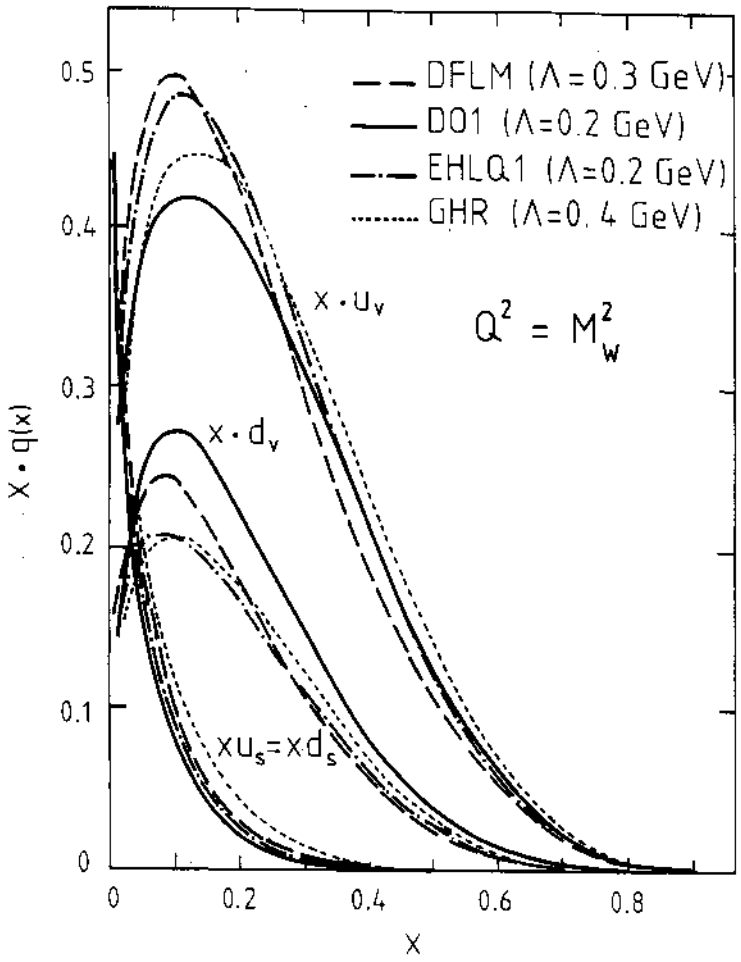
DFLM (Λ = 0.3 GeV)
D01 (Λ=0.2 GeV)
EHLQ1 (Λ=0.2 GeV)
GHR (Λ=0.4 GeV)
x · u_v
x · d_v
xu_s=xd_s
Q² = M_W²
x · q(x)
x
0
0.1
0.2
0.3
0.4
0.5
0.2
0.4
0.6
0.8

Fig. 27

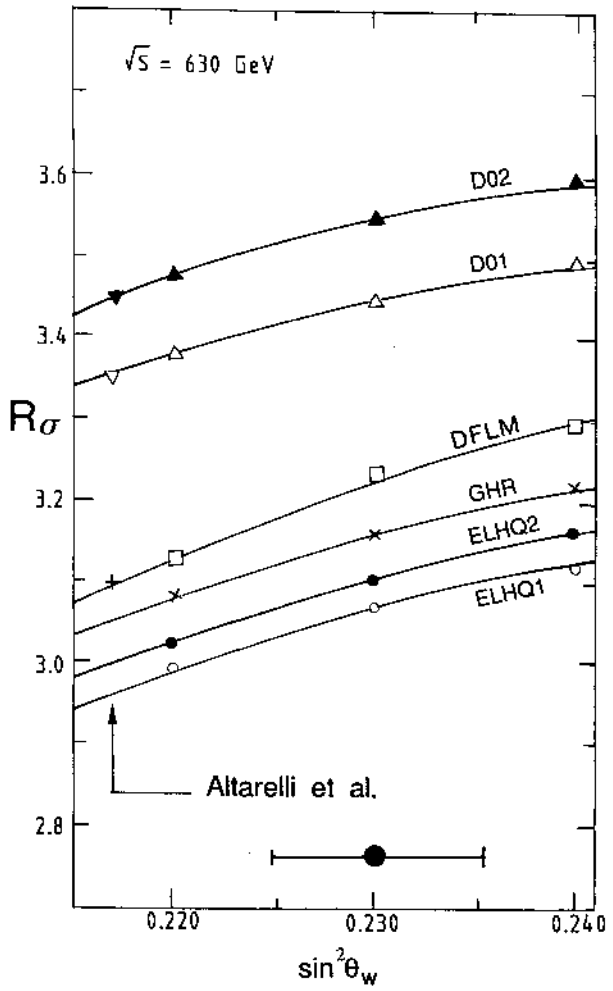
√s = 630 GeV
D02
D01
DFLM
GHR
ELHQ2
ELHQ1
Altarelli et al.
R_σ
sin²θ_W
3.6
3.4
3.2
3.0
2.8
0.220
0.230
0.240

Fig. 28

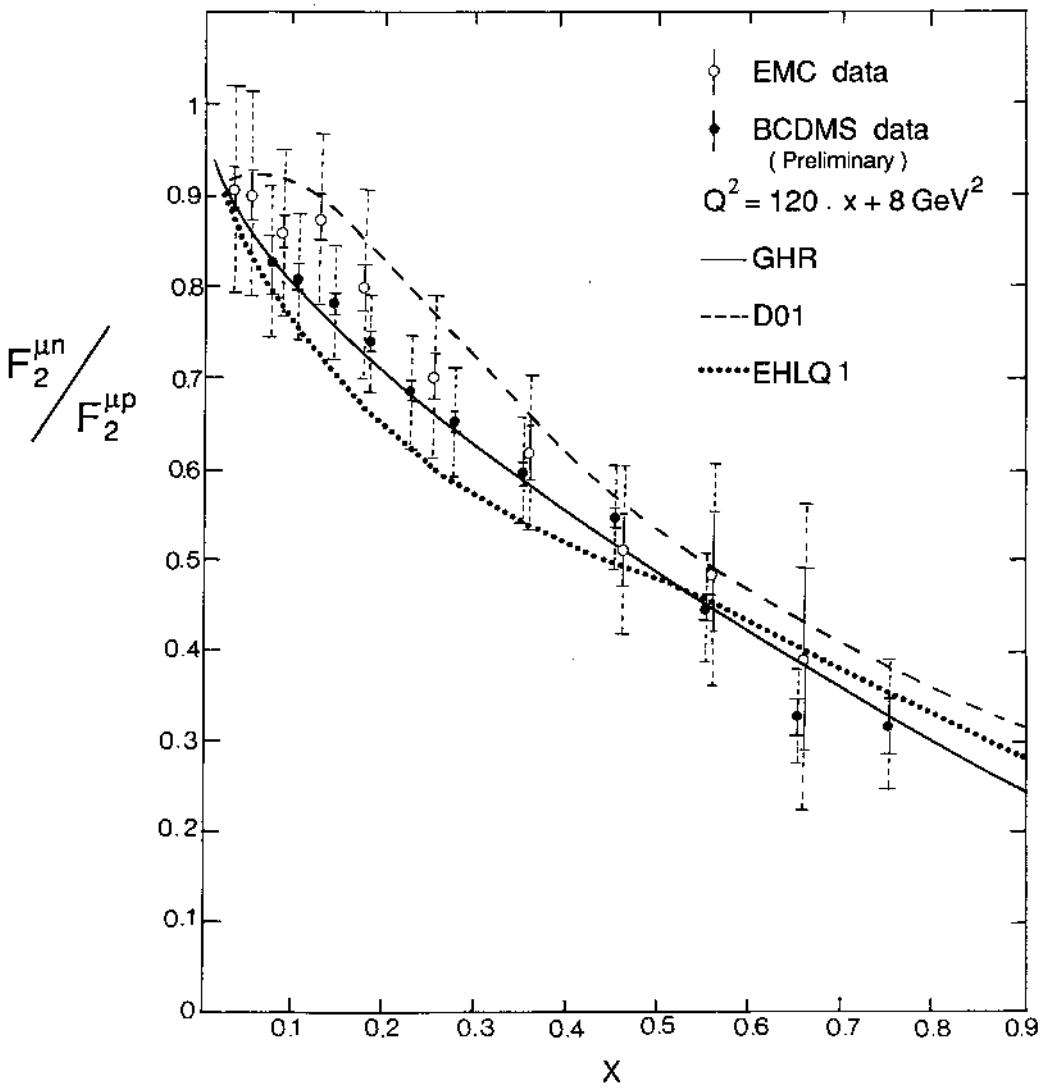
EMC data
BCDMS data
(Preliminary)
$Q^2 = 120 \cdot x + 8\ GeV^2$
GHR
D01
EHLQ 1
$F_2^{\mu n} / F_2^{\mu p}$
X
0
0.1
0.2
0.3
0.4
0.5
0.6
0.7
0.8
0.9
1

Fig. 29

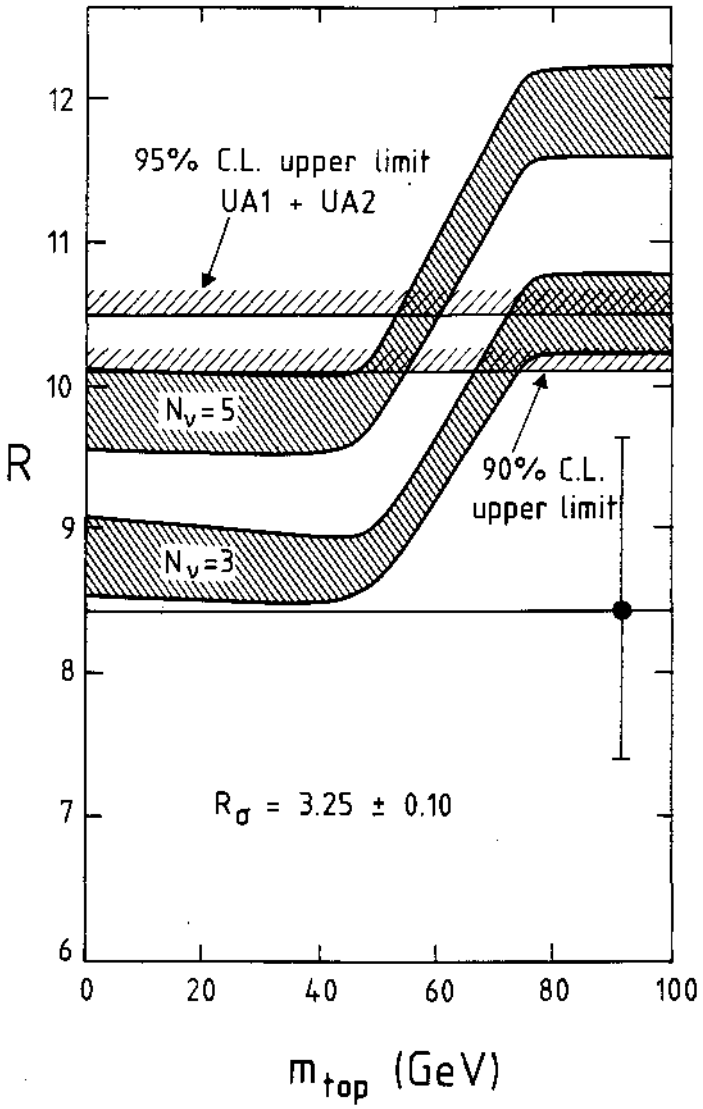
95% C.L. upper limit
UA1 + UA2
$N_\nu = 5$
$N_\nu = 3$
90% C.L.
upper limit
$R_\sigma = 3.25 \pm 0.10$
R
m_{top} (GeV)
12
11
10
9
8
7
6
0
20
40
60
80
100

Fig. 30

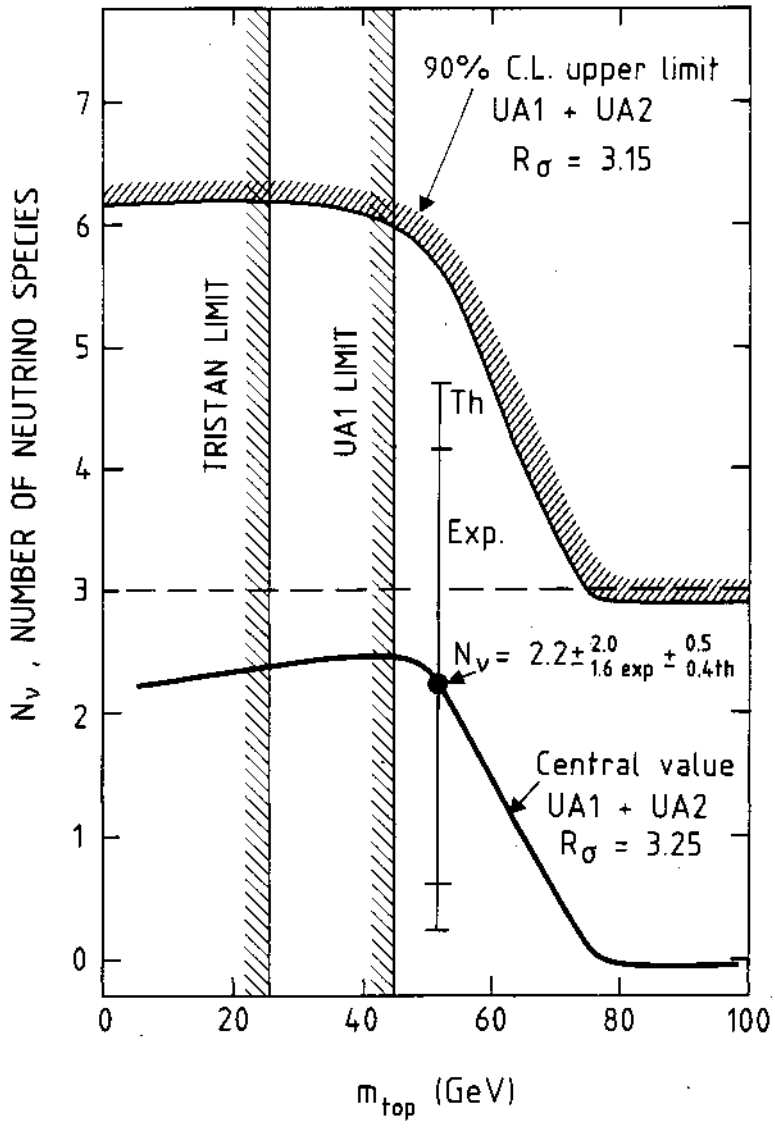
90% C.L. upper limit
UA1 + UA2
R_σ = 3.15
TRISTAN LIMIT
UA1 LIMIT
Th
Exp.
$N_\nu = 2.2 \pm^{2.0}_{1.6\ exp} \pm^{0.5}_{0.4th}$
Central value
UA1 + UA2
R_σ = 3.25
N_ν , NUMBER OF NEUTRINO SPECIES
m_{top} (GeV)
0
1
2
3
4
5
6
7
0
20
40
60
80
100

Fig. 31

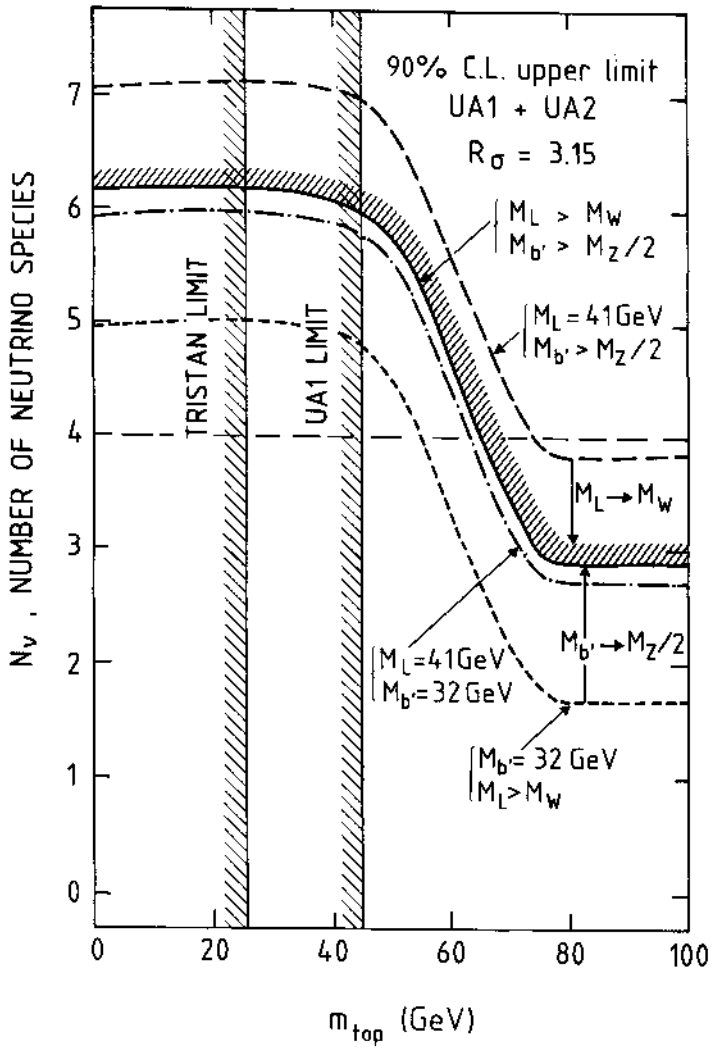
90% C.L. upper limit
UA1 + UA2
R_σ = 3.15
$M_L > M_W$
$M_{b'} > M_Z/2$
$M_L = 41$GeV
$M_{b'} > M_Z/2$
TRISTAN LIMIT
UA1 LIMIT
$M_L \to M_W$
$M_{b'} \to M_Z/2$
$M_L = 41$GeV
$M_{b'} = 32$ GeV
$M_{b'} = 32$ GeV
$M_L > M_W$
N_ν , NUMBER OF NEUTRINO SPECIES
m_{top} (GeV)

Fig. 32

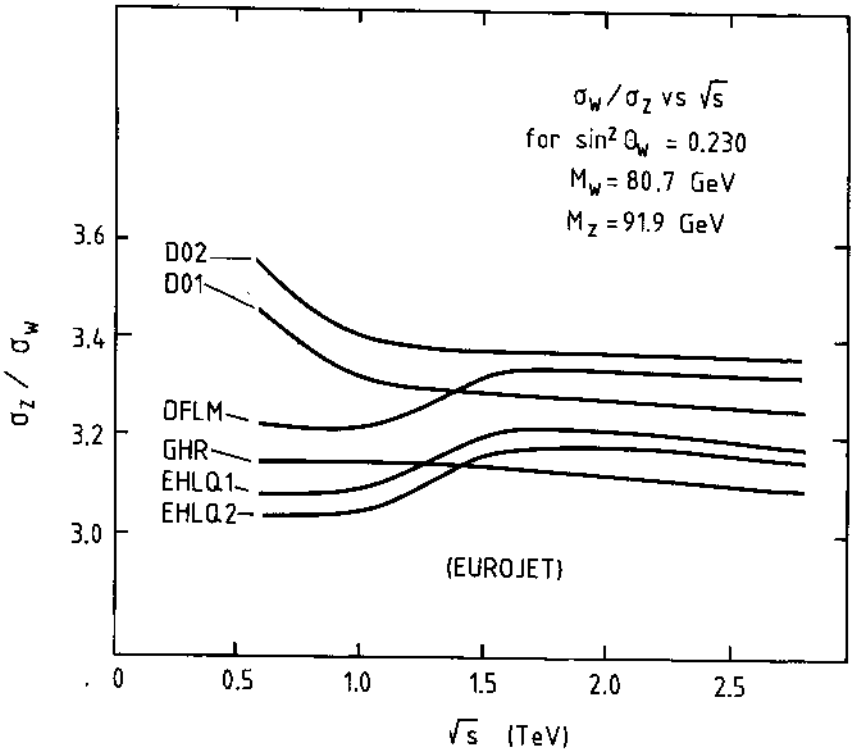
σ_W/σ_Z vs $\sqrt{s}$
for $\sin^2\theta_W$ = 0.230
M_W = 80.7 GeV
M_Z = 91.9 GeV
D02
D01
OFLM
GHR
EHLQ1
EHLQ2
(EUROJET)
σ_Z / σ_W
$\sqrt{s}$ (TeV)

Fig. 33

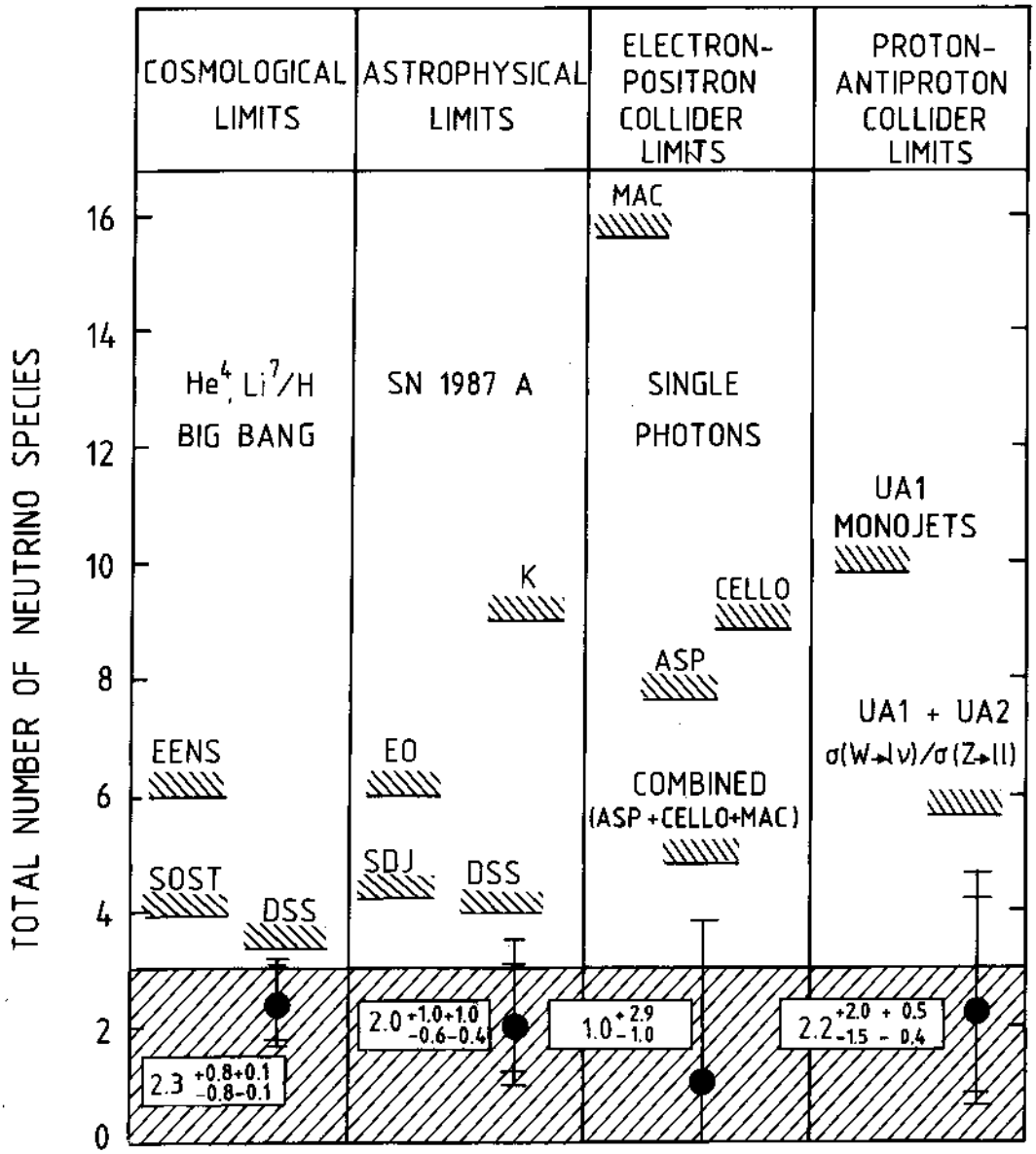
COSMOLOGICAL LIMITS
ASTROPHYSICAL LIMITS
ELECTRON-POSITRON COLLIDER LIMITS
PROTON-ANTIPROTON COLLIDER LIMITS
TOTAL NUMBER OF NEUTRINO SPECIES
16
14
12
10
8
6
4
2
0
He4, Li7/H BIG BANG
SN 1987 A
SINGLE PHOTONS
MAC
UA1 MONOJETS
K
CELLO
ASP
UA1 + UA2
σ(W→lν)/σ(Z→ll)
EENS
EO
COMBINED (ASP+CELLO+MAC)
SOST
SDJ
DSS
DSS
2.3 +0.8+0.1 -0.8-0.1
2.0 +1.0+1.0 -0.6-0.4
1.0 +2.9 -1.0
2.2 +2.0 + 0.5 -1.5 - 0.4

Fig. 34

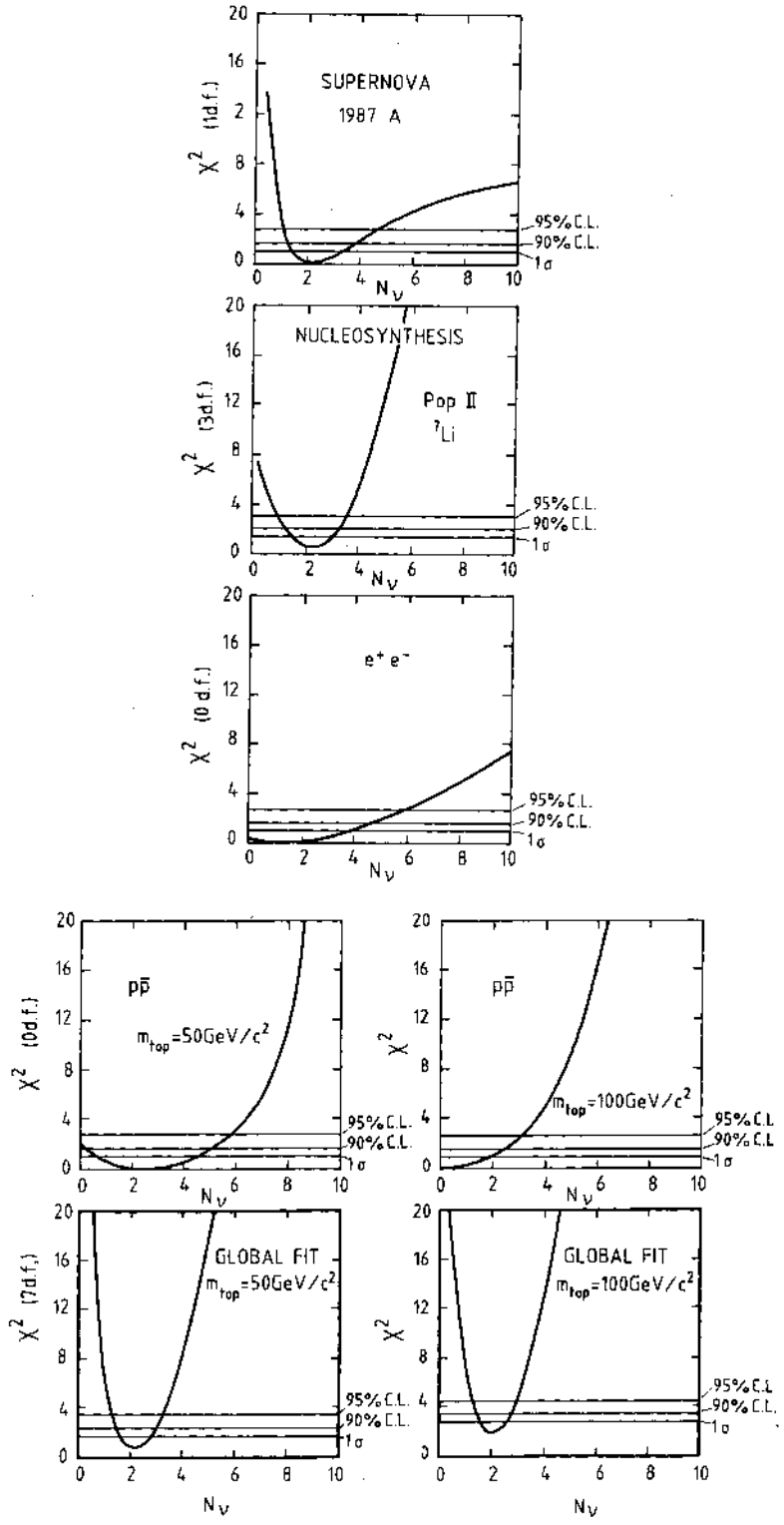
SUPERNOVA
1987 A
NUCLEOSYNTHESIS
Pop II
^{7}Li
e^+e^-
$p\bar{p}$
m_{top}=50GeV/c^2
m_{top}=100GeV/c^2
GLOBAL FIT
95% C.L.
90% C.L.
1σ
χ^2 (1d.f.)
χ^2 (3d.f.)
χ^2 (0d.f.)
χ^2 (7d.f.)
N_ν

Fig. 35